[AMERICAN JOURNAL OF SCIENCE, VOL. 293, SUMMER, 1993, P. 605–670]

American Journal of Science

SUMMER 1993

MINERAL-FLUID INTERACTIONS IN THE REYKJANES AND SVARTSENGI GEOTHERMAL SYSTEMS, ICELAND

STEVEN W. LONKER*, HJALTI FRANZSON**,
HREFNA KRISTMANNSDÓTTIR**

ABSTRACT. **Physical observations on features such as temperature, pressure, and formation permeability are integrated with alteration intensity, fluid and secondary mineral compositions, and textures to show the most important thermal, chemical, hydrodynamic, and kinetics factors that control the evolution of two Icelandic geothermal systems, the Reykjanes and Svartsengi systems. There is an increase in alteration intensity and the abundance of fracture and vesicle fillings, a decrease in the abundance of primary minerals, and more extensive compositional heterogeneity near many aquifers, which are defined by circulation losses and temperature and pressure profiles. Features such as resorption and overgrowth textures, absence of systematic element partitioning, metastability, and undersaturation/supersaturation are widespread and are indicative of mineral-mineral and mineral-fluid disequilibrium. The composition of chlorite, however, is more sensitive to changes in the physico-chemical conditions of the fluid compared to other secondary minerals probably due to larger values of $(4D_h k_\varphi / v^2)$, linear kinetic rate laws, or both, where D_h is the coefficient of hydrodynamic dispersion, k_φ is the reaction rate constant, and v is the fluid velocity. Chlorite grains in more permeable formations in one Reykjanes well show larger $Fe^{2+}/(Fe^{2+} + Mg)$ ratios and lower Si-contents compared to chlorite grains in less permeable formations. Chlorite geothermometry is used to map out the temperature patterns and extract information on permeability variations. Temperatures and fluid compositions derived from chlorite compositions indicate hotter, more reduced, lower pH fluids in the more permeable formations in the Reykjanes well. The correlation of temperatures derived from chlorite compositions with formation permeability in the Reykjanes well is indicative of more anisotropic permeability compared to the Svartsengi wells. Computer models and experimental studies show that overgrowths of chlorite on resorbed calcite, epidote, and quartz and the occurrence of chalcopyrite and Mg- and Si-rich chlorite in many Reykjanes samples are produced by seawater incursion, mixing of seawater and the acidic thermal brine, and seawater-basalt reaction. At lower seawater-rock ratios, the systems are restored to calcite (Svartsengi), epidote, quartz, and Fe^{2+}-Mg chlorite saturation. In many chlorite-filled vesicles, chlorite grains show a systematic rim-to-core increase in temperatures derived from chlorite compositions and grain size and a**

* Department of Geology, Australian National University, GPO Box 4, Canberra, A.C.T. 2601, Australia.
** Orkustofnun, Grensásvegur 9, 108 Reykjavík, Iceland

decrease in smectite content due to heating of cooler waters or late pulses of hot, reduced fluids. Oscillatory mineral deposition in vesicles probably formed by nonequilibrium processes involving diffusion and mineral precipitation. No systematic changes in epidote, garnet, and titanite compositions with formation permeability, temperature, or fluid composition were observed. Oxygen isotope and fluid inclusion studies indicate that some anhydrite, calcite, and quartz grains grew at an earlier stage when both systems were hotter and meteoric, possibly glacial-melt water. Both systems are cooling due to heat source decay, cooler water incursions, or both. The results of this study will be useful in testing experimental studies and computer models of seawater-basalt reaction and recognizing the thermal, chemical, kinetics, and hydrodynamic factors that control secondary alteration in submarine hydrothermal systems.

INTRODUCTION

Many studies have used a chemical equilibrium approach to show how fluid composition in active hydrothermal systems is controlled by reactions between the fluid and secondary minerals (Arnórsson, Gunnlaugsson, and Svavarsson, 1983a; Giggenbach, 1981). Fewer studies have used the mass transfer approach of Helgeson and coworkers (Helgeson and others, 1970) to show how factors such as reaction rates, porosity, mineral surface areas, fluid velocities, and mineral composition control chemical mass transport and the state of chemical equilibrium in hydrothermal systems (Bowers and Taylor, 1985; White, Chuma, and Goff, 1992). Textures, analytical data, and physical observations on features such as circulation loss and temperature and pressure profiles are used to extract information on spatial and temporal variations in temperature and fluid composition and the dependence of these variables on kinetic and hydrodynamic factors in two Icelandic geothermal systems. The physico-chemical and kinetics variables that produce textural complexity and compositional variability in thirty two samples from the production reservoirs will be used to interpret the evolution of the two hydrothermal systems.

In recent years, a considerable amount of literature has been devoted to the study of saline active and fossil hydrothermal systems, base metal massive sulfide deposits associated with mafic volcanics, geochemical fluxes at constructive plate margins, and experimental studies and computer codes modeling seawater-basalt reaction. Icelandic saline geothermal systems like the Reykjanes and Svartsengi systems share some features with submarine hydrothermal systems. The relationship of alteration minerals, mineral compositions, and textures with hydrology, fluid composition, and temperature in active saline hydrothermal systems can be used to recognize zones of upflow, lateral flow, less permeable formations, and areas of cooler water incursion in fossil saline hydrothermal systems.

Important differences do exist, however, between submarine hydrothermal systems and subaerial hydrothermal systems like Reykjanes and

Svartsengi. The initial fluid composition of submarine hydrothermal systems is a large reservoir of homogeneous seawater. Oxygen isotopes (Sveinbjörnsdóttir, 1983a; Sveinbjörnsdóttir, Coleman, and Yardley, 1986) and fluid inclusions (Franzson, 1990) indicate that the two Icelandic systems involved a high proportion of meteoric water, possibly glacial-melt water, during the early history. There is also a meteoric input to the top of these systems as well as cooler saline waters and hydrothermal brine. Other differences between Icelandic geothermal systems and submarine hydrothermal systems are discussed by Kristmannsdóttir (1983) and Stefánsson (1983).

Many variables control hydrothermal alteration including temperature, permeability, duration and amount of fluid flow, and fluid and rock composition (Browne, 1978). Temperature is considered to be an important factor controlling secondary alteration in the Icelandic geothermal systems. Depth-related variations in clay minerals, zeolites, and the appearance of epidote and actinolite are correlated with rock temperature for a specific rock (tholeiitic basalt) and fluid composition (Tómasson and Kristmannsdóttir, 1972; Kristmannsdóttir, 1975, 1976a,b, 1979; Kristmannsdóttir and Tómasson, 1978; Sveinbjörnsdóttir, 1992). These depth-related mineral zones, however, are not always clearly defined (Tómasson and Kristmannsdóttir, 1972). Several workers identified "lower temperature" mixed-layer phyllosilicates in the chlorite + epidote zone (Tómasson and Kristmannsdóttir, 1972; Kristmannsdóttir, 1976a, 1983; Sveinbjörnsdóttir, 1983a). Complex filling sequences in veins and amygdules have been recognized in the Svartsengi system (Franzson, 1983a,b). Kristmannsdóttir (1976a) and Pálmason and others (1979) believed that permeability differences in Icelandic systems controlled alteration intensity, but not alteration type. This paper will show that the alteration minerals, mineral compositions, and textures in the Reykjanes and Svartsengi systems do not record a simple increase of temperature with depth. First, a summary of the geology, fluid chemistry, hydrology, and thermal structure in the Reykjanes and Svartsengi systems is presented, which provides a framework for the present study.

GEOLOGY

The Reykjanes and Svartsengi systems are located on the Reykjanes Peninsula in southwestern Iceland, where the Mid-Atlantic Ridge emerges above sealevel (fig. 1). Along the subaerial extension of the spreading axis there is a narrow east-northeast-west-southwest microseismic zone below 2 km depth, which is interpreted as the plate boundary. The plate boundary in the upper 2 km of crust is represented by a right-stepping, en echelon array of northeast-southwest-trending volcanic fissure swarms, which are arranged approximately perpendicular to the spreading direction. There is a strong relationship of geothermal activity in the Reykjanes Peninsula with tectonic and magmatic anomalies, which occur at the intersection of the seismic zone with the fissure swarms (Arnórsson, 1978; Jakobsson, Jónsson, and Shido, 1978). The Reykjanes and Svart-

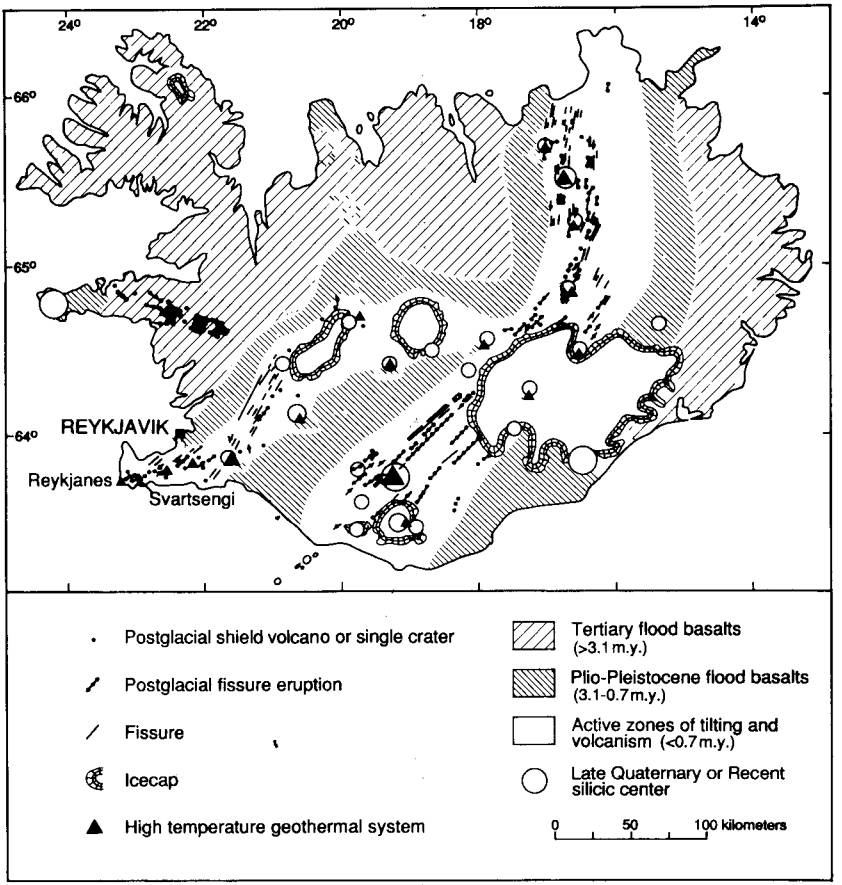

Fig. 1. Schematic geologic map of Iceland showing the major tectonic and volcanic features and the locations of the Reykjanes and Svartsengi geothermal systems. Diagram is modified from Saemundsson (1986).

sengi systems are situated within the Reykjanes and Grindavík swarms, respectively (Jakobsson, Jónsson, and Shido, 1978).

Stratigraphy

The surface geology and location of wells in the Reykjanes and Svartsengi systems are shown in figure 2A and B. Nine wells have been drilled into the Reykjanes system between 1956 and 1983. Twelve wells have been drilled into the Svartsengi system since 1972.

Most of the rocks on the surface of the Reykjanes Peninsula date from the last glacial and interglacial periods. The geologic maps in figure 2A and B show basaltic flows erupted subaerially since termination of the last glaciation and hyaloclastites formed during the last glacial period. The volcanic rocks of the swarms are products of eruption fissures and

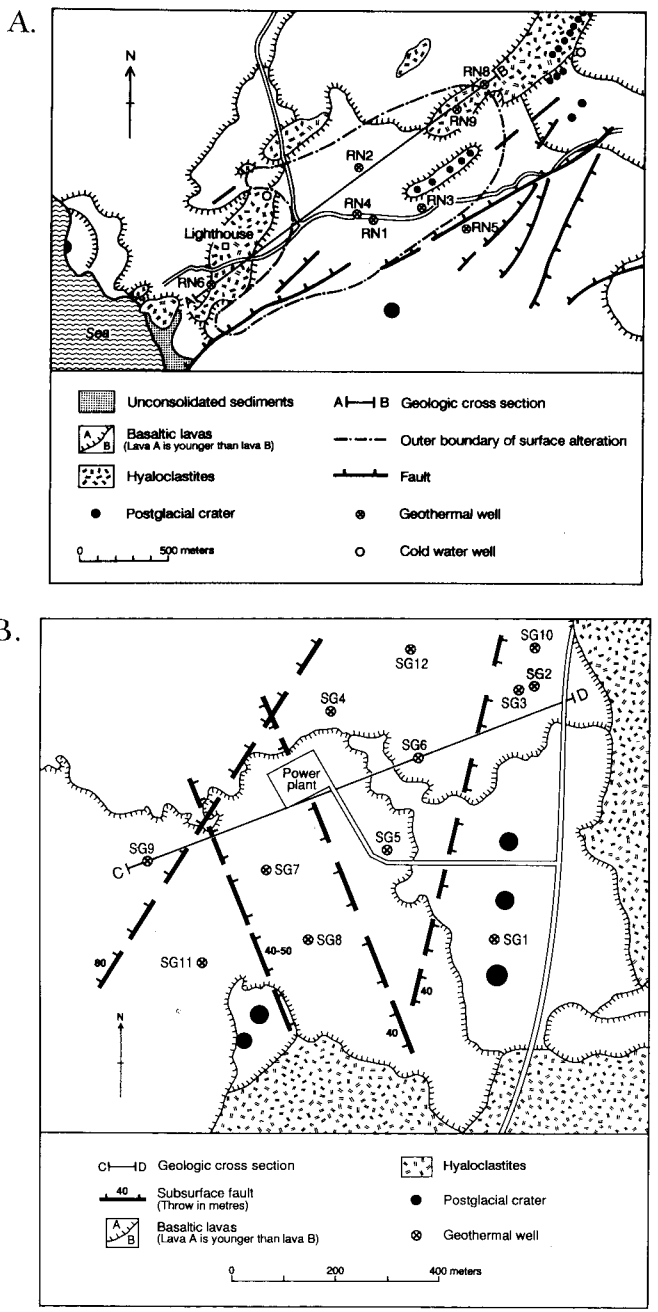

Fig. 2. Plan map view showing the location of geothermal wells, faults, and surface geology of the (A) Reykjanes and (B) Svartsengi geothermal systems. Surface geology is extracted from Jónsson (1978).

lava shield craters. Subglacial volcanics of the Reykjanes Peninsula piled up around erupting fissures producing northeast-southwest-trending ridges (Jakobsson, Jónsson, and Shido, 1978; Saemundsson, 1979, 1986).

Geologic cross sections of the extrusive volcanic units in the Reykjanes and Svartsengi systems are depicted in figure 3A and B. The upper 1000 m in the Reykjanes system are about two-thirds hyaloclastite tuffs and breccias and tuffaceous sediments and one-third basaltic lava (Björnsson and others, 1971; Tómasson, 1971; Tómasson and Kristmannsdóttir, 1972). The lower part of the Reykjanes section is dominated by subaerial basaltic lava (fig. 3A). Stratigraphic correlation of lava flows is difficult below 800 m depth in the Svartsengi system due to an increase in intrusions and faults with depth (Franzson, 1983a, 1990). Franzson (1983a, 1987), however, recognized at least four glacial and intervening interglacial periods in the Svartsengi stratigraphic extrusive succession with an age range from 500,000 yrs to Recent (fig. 3B).

Igneous intrusions are rarely intersected by the Reykjanes drillholes and probably become more common below 2500 m depth (Kristmannsdóttir, 1983). In the Svartsengi system, intrusions are found below 800 m depth (Franzson, 1983a, 1990). These intrusions are dominated by sills of fine-grained basalt and coarser-grained dolerite, which are generally less than 30 m thick (Franzson, 1983a).

Tectonic Features

The dominant tectonic features at the surface of the volcanic fissure swarms are northeast-southwest-trending faults and fractures, but north-south and north-northwest-south-southeast fractures and faults are also found. North-south to north-northwest-south-southeast-trending faults and fractures become more common with depth (Franzson, 1990). Prominent, but shallow graben structures occur in the Reykjanes and Svartsengi areas. Faulting in the Reykjanes Peninsula is a gradational process and takes place simultaneously with accumulation of lavas so there is an upward decrease in throw (fig. 3B).

FLUID CHEMISTRY

Three types of waters have been recognized in the western Reykjanes Peninsula: (1) cold meteoric water; (2) cold seawater; and (3) thermal water (Kristmannsdóttir, 1986). A thin lens of cold, compositionally homogeneous freshwater floats on cold seawater, which impregnates the underlying rocks. This freshwater lens thickens from practically zero in the Reykjanes thermal area to less than 30 m near the Svartsengi system (Sigurdsson, 1985). The freshwater lens, however, does not exist in the Svartsengi thermal area, where the thermal waters lie beneath the cold seawater. Compared to seawater, the Reykjanes and Svartsengi thermal waters are enriched in SiO_2^o, Ca^{2+}, and K^+ and depleted in SO_4^{2-} and Mg^{2+} due to base-exchange, hydrolysis, and redox reactions involving dissolved constituents and minerals in the rocks (Björnsson, Arnórsson, and Tómasson, 1970, 1972; Arnórsson, 1983).

The chloride concentration of the geothermal reservoir changes from 100 percent of the seawater concentration in the Reykjanes system to about 65 percent in the Svartsengi system (Arnórsson, 1978). Arnórsson (1978) explained the variation in chloride by a simple mixing model of meteoric groundwater with underlying seawater. In this interpretation, the Svartsengi thermal water is a mixture of about two-thirds seawater and one-third meteoric water. This interpretation implies negligible input of meteoric water into the Reykjanes system with no recycling of flashed water. The $\delta^{18}O$ values for Reykjanes thermal water are indeed close to the seawater value (Ólafsson and Riley, 1978).

Fluid inclusions, δD values for thermal water, and $\delta^{18}O$ values for alteration minerals, however, show a more complex origin for the Reykjanes and Svartsengi thermal waters. Oxygen isotope values for calcite and feldspar in Reykjanes well 8 indicate meteoric input in the uppermost 250 m, more marine influences at depth, and no major variations in fluid composition at greater depths (Sveinbjörnsdóttir, 1983a,b; Sveinbjörnsdóttir, Coleman, and Yardley, 1986). Ólafsson and Riley (1978) suggested on the basis of isotopic and chemical evidence that the Reykjanes thermal water formed by a mixture of locally derived meteoric water, probably rainwater (Gudmundsson, Hauksson, and Tómasson, 1981), with connate, high salinity seawater trapped interstitially in volcanic rocks during submarine eruption or post-depositional incursion followed by boiling at shallow levels. This interpretation would imply a balanced loss and gain of freshwater in the Reykjanes system, which is needed to maintain a chloride concentration close to the seawater concentration (Edmond, 1986). Quartz and bulk rock oxygen isotope values indicate that the deeper part of Reykjanes well 8 had been dominated by meteoric water, possibly glacial melt-water, during an earlier stage (Sveinbjörnsdóttir, 1983a,b; Sveinbjörnsdóttir, Coleman, and Yardley, 1986). Fluid inclusion data (quartz, anhydrite, calcite) from Svartsengi well 12 also indicate meteoric water in the early history of the system with increasing salinity with time (Franzson, 1990).

HYDROLOGY

As a result of high permeability, the groundwater table is low-lying in the western Reykjanes Peninsula (Arnórsson, 1978). The level of the groundwater table and the rock permeability control the extent of infiltration and degree of mixing of sea and meteoric waters (Arnórsson, Gunnlaugsson, and Svavarsson, 1983a). The amount of surface discharge in both systems is a matter of where the thermal reservoir is in relationship to the groundwater table. The Reykjanes system is dominated by strong upflow, which reaches the surface. The hot springs in the Reykjanes system discharge saline and steam-heated acid sulfate waters, which are produced from oxidation of sulfide to sulfate probably by cold seawater. The groundwater table is lower in the Svartsengi system, and surface discharge was nearly absent in the system prior to production.

In the Reykjanes system, heated saline waters ascend along tectonic features, boil, and cool in the upflow zone. Only a minor part of this fluid

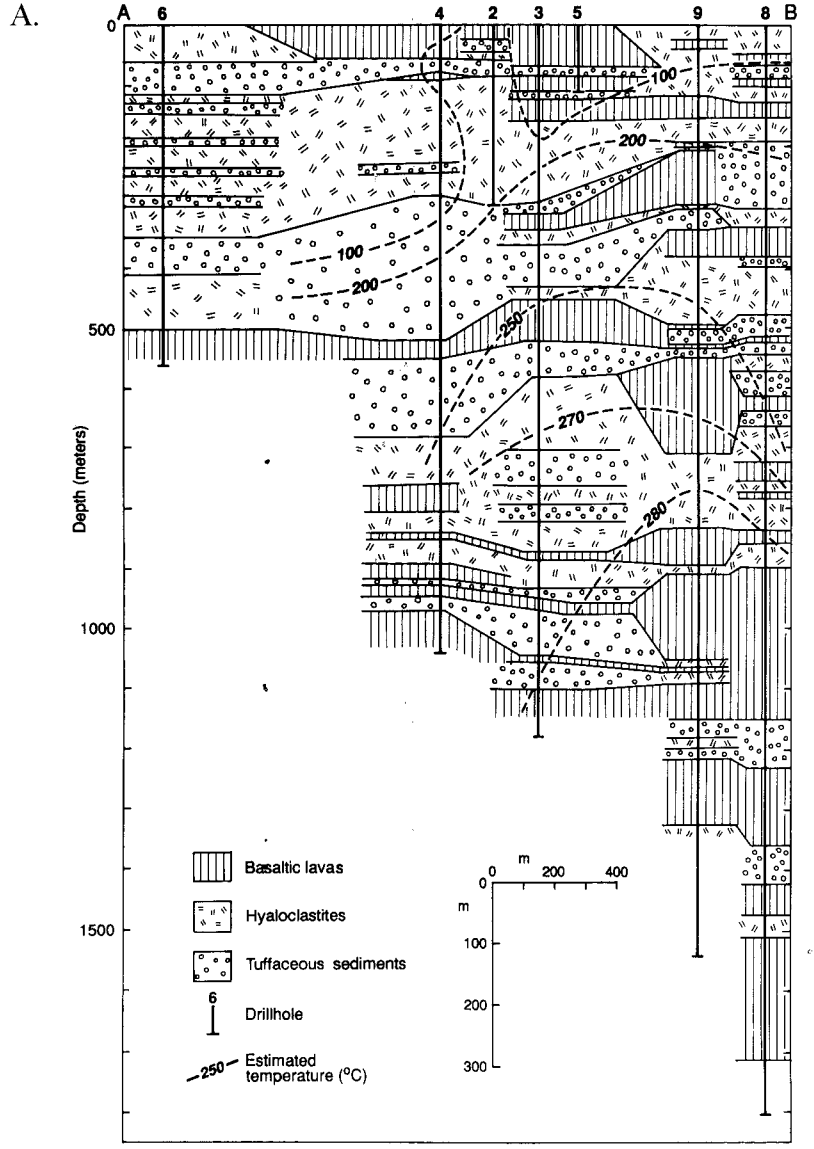

Fig. 3. Simplified geologic cross sections through the (A) Reykjanes and (B) Svartsengi geothermal systems showing the stratigraphy and isotherms. Locations of isotherms are approximate. Only the extrusive volcanics are depicted. Reykjanes and Svartsengi stratigraphic sections modified from Björnsson and others (1971) and Franzson (1983a, 1990), respectively. Section lines shown on figure 2A and B.

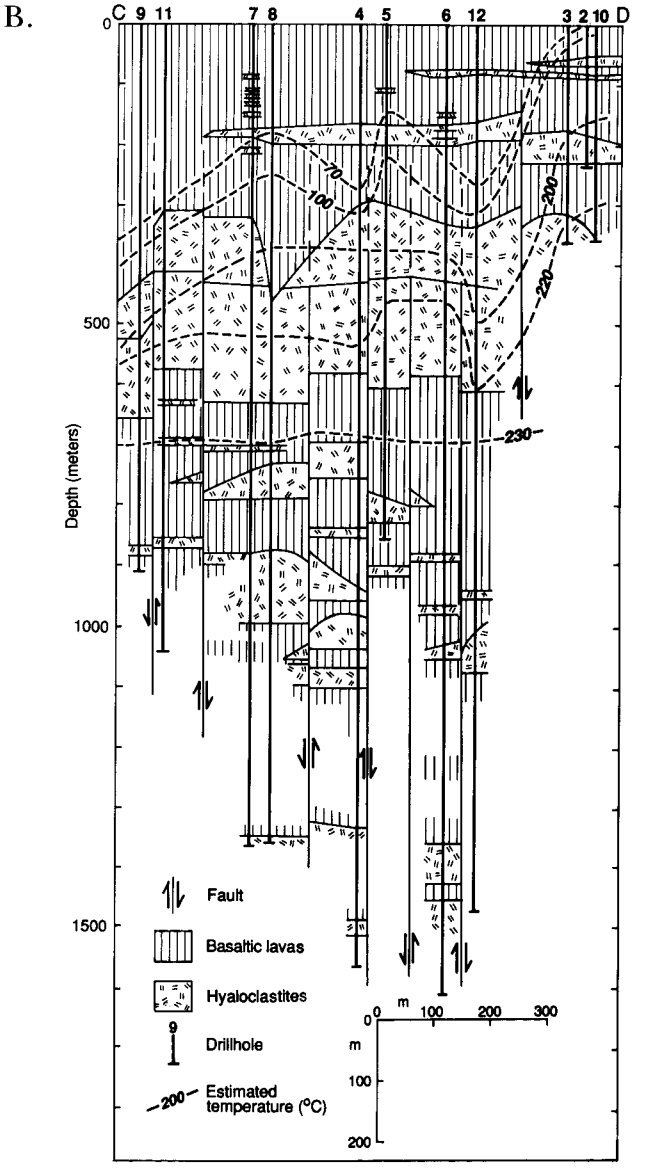

Fig. 3 (continued)

is discharged at the surface, and, presumably, most of the fluid flows into the hyaloclastites along the margins of the upflow zone (Björnsson, Arnórsson, and Tómasson, 1970, 1972) or is carried away by the groundwater. A 100 to 200 m thick layer of cold seawater overlies the southern

boundary of the thermal reservoir. Cold seawater also surrounds the periphery of the Reykjanes system (Björnsson, Arnórsson, and Tómasson, 1970, 1972; Tómasson and Kristmannsdóttir, 1972). Cap rock, which is formed by the precipitation of secondary minerals in pore spaces, separates the hydrothermal system from the surrounding cold seawater close to the surface and along the margins of the thermal area at shallow depths. Fracturing of the cap rock accompanied by cold seawater infiltration may occur following seismic activity (Tómasson and Kristmannsdóttir, 1972), thermal disturbances, or sealevel oscillations (Edmond, 1986). The flow of cold water down a hydrostatic gradient into the thermal system replaces water lost at the surface (Tómasson and Kristmannsdóttir, 1972) and condenses steam in the upflow zone (Arnórsson and Gunnlaugsson, 1985). Impermeable basalt at 900 m depth separates and caps a succession of thin, highly permeable scoriaceous contacts between basalt and hyaloclastite, shielding these rocks from direct infiltration by cold seawater. Although basaltic lavas have a lower primary porosity than hyaloclastites, most of the aquifers in the Reykjanes system are in the lava flows. Reykjanes well 8 intersects at least ten aquifers between 1000 and 1750 m depth. Above 900 m, lower density basalts and porous (20–30 percent porosity) hyaloclastites are not adequately capped and are subject to infiltration by cold seawater (Björnsson, Arnórsson, and Tómasson, 1970, 1972). The presence of an earlier high temperature alteration in Reykjanes well 6 may be indicative of a lateral shift of upflow toward the northeast possibly related to the invasion of cold seawater into the thermal reservoir (Björnsson, Arnórsson, and Tómasson, 1970, 1972).

Reservoir modeling of the Svartsengi system indicates that the thermal reservoir and underlying microseismic zone have high permeabilities of approx 8.39×10^{-13} m^2 and 1.18×10^{-13} m^2, respectively, compared to the surrounding area with a permeability of about 9.87×10^{-15} m^2 (Vatnaskil Consulting Engineers, 1989). A tracer study indicates a high fluid velocity of 5.5×10^{-4} ms^{-1} between Svartsengi wells 6 and 12 (Gudmundsson and others, 1984). There are three aquifer systems within the Svartsengi system: the groundwater system, major liquid-dominated aquifers, and a small steam-bearing chimney. The groundwater system flows laterally toward the southwest at depths less than 300 m gaining some heat as it flows above the steam chimney (Björnsson and Steingrímsson, 1991). Cooler seawater surrounds the periphery of the system beneath the freshwater lens (Arnórsson and others, 1975; Gudmundsson and Thórhallsson, 1986). The hydrostatic pressure within the thermal reservoir is lower than the surrounding seawater except near the surface (Björnsson and Steingrímsson, 1991). Despite the increasing pressure difference with depth, the fluid composition in the thermal reservoir has remained close to two-thirds seawater and one-third freshwater even though the reservoir is surrounded by seawater, indicating the presence of a physical (cap rock) barrier, a viscosity barrier, or both at the margin of the system. Above 300 m depth, the aquifers intersected by

the drillholes occur along surface fissures, horizontal stratigraphic contacts, and in the vesicular top and bottom of lava flows (Franzson, 1983a, 1990). Formations with low permeability occur beneath the groundwater system at 300 to 600 m depth, so there is little communication between the groundwater system and the thermal reservoir (Björnsson and Steingrímsson, 1991). The main aquifers below 800 m depth are found along fractures and near-horizontal intrusive contacts (Franzson, 1983a, 1990). A small, steam-bearing chimney extends from the thermal reservoir toward the surface around wells 2,3, and 10 (Björnsson and Steingrímsson, 1991).

THERMAL STRUCTURE

Resistivity measurements indicate that the Reykjanes thermal area is chimney-like with a diameter of approx 1 km down to about 600 m depth (Björnsson, Arnórsson, and Tómasson, 1970, 1972; Björnsson and others, 1971). There is apparently one main upflow zone in the Reykjanes system near well 9 (fig. 3A). An incursion of cooler seawater has produced a temperature inversion at shallow depths in the southwestern (well 6) part of the Reykjanes system (fig. 3A). The $\delta^{18}O$ values for quartz in Reykjanes well 8 indicate a cooling trend with time, meteoric waters at an earlier stage, or both (Sveinbjörnsdóttir, 1983a; Sveinbjörnsdóttir, Coleman, and Yardley, 1986).

Resistivity surveys show that the Svartsengi reservoir increases with depth, where the areal extent of the hot reservoir is 6 to 7 km^2 at 600 m depth (Gudmundsson and Thórhallsson, 1986). Measured temperatures are uniform below 600 m depth (230°-240°C, fig. 3B), indicative of high permeability and a well-mixed fluid. There is no evidence from the distribution of measured temperatures for channelized fluid flow along faults except in the steam chimney. There is a temperature inversion of less than 5°C between 700 and 900 m and between 1100 and 1360 m in well 12, which lies close to the margin of the system (fig. 2B) (Björnsson and Steingrímsson, 1991). A north-south upflow zone occurs close to well 4, where a thermal maximum of 243°C is reached (Björnsson and Steingrímsson, 1991). Fluid inclusion data from Svartsengi well 12 show a cooling trend with time (Franzson, 1990).

METHODS OF INVESTIGATION

Analytical Techniques

A detailed examination was carried out on hydrothermal minerals in drill cuttings from Reykjanes wells 8 (RN8, 1360-1714 m) and 9 (RN9, 1070-1352 m) and Svartsengi wells 4 (SG4, 1104-1462 m) and 12 (SG12, 1108-1488 m). These wells were selected because there is a large database on subsurface geology, downhole temperatures, circulation losses, aquifers, fluid composition, and petrographic, X-ray diffraction, and stable isotope studies of mineral alteration. Random sampling was conducted at deeper depths below the well casing to examine the relationship between downwell mineral distribution and aquifer locations and to avoid the

effects of near surface processes. Icelandic geothermal systems are drilled with oilfield-type rotary drilling rigs, so cores are rarely taken (Pálmason and others, 1979). The time that cuttings take to get to the surface is dependent on the type of circulation fluid, the flow rate, circulation loss, and the drillhole diameter. The stated depth intervals for cuttings used in the discussion of alteration minerals are uncorrected for these factors due to lack of logging data in RN8 and SG4. Logging data in RN9 and SG12 indicate that most of the cuttings in these wells are within 15 m of the true depth. This uncertainty in sample depth does not affect the conclusions reached in this paper. Anomalous samples are few and are recognized by internally inconsistent changes in minerals, mineral compositions, and rock type, so there was little mixing of cuttings between depth intervals. Below the production casing, the wells are drilled with water rather than bentonite, so contamination from bentonite is not a problem. This paper shows that these problems are not insurmountable and that spatial and temporal variations in alteration patterns can indeed be worked out in fine-grained ($\leq$2mm) drill cuttings by careful petrography.

Wood chips and other foreign matter were removed by handpicking, and the cuttings were impregnated with polyester, which preserves the original textures. Polished sections, which were prepared in kerosene because of the presence of water-soluble minerals, were examined in transmitted and reflected light. Six to ten chips in each thin section were selected for analytical work based on textures of paragenetic importance and maximum number of phases. Two to three analyses of each phase on different grains were obtained, and the locations were recorded on photomicrographs. Mineral analyses were obtained by wavelength dispersive X-ray analysis on a Cameca CAMEBAX electron microprobe located at the Research School of Earth Sciences (RSES), Australian National University (ANU). This instrument is also equipped to do energy dispersive X-ray analysis and backscattered electron imaging, which were used to examine compositional homogeneity and position the electron microprobe beam. Instrumental conditions were a 15 KV accelerating voltage (25 KV on sphalerite), a beam current of 10 nA and a defocused beam of 12 μm on calcite and feldspar, and a beam current of 20 nA (40 nA on sphalerite) and beam diameter of 5 μm on the other minerals. Data reduction was performed using a ZAF correction procedure. Textures and compositional zoning were examined at a 20 KV operating voltage using backscattered electron imaging coupled with energy dispersive X-ray analysis on a Cambridge S360 scanning electron microscope located at the Research School of Biological Sciences, ANU. Anatase and fine-grained oxides were identified with a Dilor Microdil 28 Laser Raman microprobe at the Bureau of Mineral Resources, Canberra.

Calculation of Initial Discharge Chemistry

The aqueous speciation in the total discharge was calculated from chemical analyses of water and steam collected under pressure at the well-head with a Webre separator. A single phase (that is, one-phase

liquid feed) calculation was performed at the reservoir temperature using the methods presented by Reed (1982) and Reed and Spycher (1984). Table 1 gives the mass action equations for the aqueous and gas phases in terms of the ionic components and sources of thermochemical data used in the computations. Table 2 shows some representative analyses of the total discharge in the Reykjanes and Svartsengi systems in terms of molalities of component species, pH, and gas pressures.

No direct measurements of discharge enthalpy were taken during the early history of Reykjanes well 8, so discharge enthalpy was calculated from silica temperatures, which showed a decrease from 1971 to 1974. This was interpreted by Arnórsson (1978), Arnórsson, Grönvold, and Sigurdsson (1978), and Sveinbjörnsdóttir (1983a) to mean that the fluids were flashing in the formation (that is, two-phase liquid + steam flow into the well), so they calculated the Reykjanes well 8 total discharge accordingly. The early discharge history of RN8 provides an explanation for the decrease in silica temperatures. The deeper aquifers are more permeable than the upper aquifers in RN8. In 1970 and 1971, the flow rates and drawdown in the upper aquifers were large, so the contribution of the upper aquifers decreased rapidly with time compared to the deeper and hotter aquifers, causing the silica temperatures to increase. From 1971 to 1974, there was a flow rate decrease and less drawdown of the aquifers, so there was a larger contribution from the upper aquifers and, thus, a decrease in silica temperatures (Gudmundsson, Hauksson, and Tómasson, 1981). Pressure logs (unpublished Orkustofnun data) indicate that there was a one-phase liquid flow into the well after the well had been closed and undisturbed from 1974 to 1977.

There is some uncertainty as to the accuracy of many of the water and steam analyses collected in the early 1970's. The RN8 samples used in this study were collected after 1978 and represent a mixture of waters discharged from several cooler aquifers with different compositions and temperatures. The RN8 reservoir temperature used in this study (270°C) is based on quartz geothermometry (T_{QTZ}) and the vapor-saturated temperature equivalent of the discharge enthalpy (T_H), which was measured in 1980. There is a close match of T_{QTZ} and T_H in RN8 in many analyses from the late 1970's and early 1980's (table 2; Gudmundsson, Hauksson, and Tómasson, 1981; Bjarnason, 1984), further indicating a one-phase liquid flow into the well.

Cooler parts of Reykjanes well 9 were cased off, so fluid samples from the deep, hot reservoir are a mixture of fluids from aquifers with similar temperatures around 295°C. There is good agreement among measured temperatures, quartz geothermometry temperatures, and the vapor-saturated temperature equivalent of the discharge enthalpy in many analyses of total discharge waters in RN9 (table 2; Bjarnason, 1984), indicating one-phase liquid flow into the well.

The cooler parts of the Svartsengi wells are cased off, so the deep, hot reservoir was sampled from a mixture of aquifers with similar temperatures around 240°C. The Svartsengi thermal waters are spatially homoge-

TABLE 1

Mass action equations for aqueous and gas phases written in terms of the ionic components and sources of thermochemical data

	Reactions	Sources of thermochemical data
(1)	$AlF^{2+} = Al^{3+} + F^-$	a
(2)	$AlF_2^+ = Al^{3+} + 2F^-$	a
(3)	$AlF_3^\circ = Al^{3+} + 3F^-$	a
(4)	$AlF_4^- = Al^{3+} + 4F^-$	a
(5)	$AlF_5^{2-} = Al^{3+} + 5F^-$	a
(6)	$AlF_6^{3-} = Al^{3+} + 6F^-$	a
(7)	$AlOH^{2+} = Al^{3+} + H_2O^\circ - H^+$	b
(8)	$Al(OH)_2^+ = Al^{3+} + 2H_2O^\circ - 2H^+$	b
(9)	$Al(OH)_4^- = Al^{3+} + 4H_2O^\circ - 4H^+$	b
(10)	$Al(SO_4)^+ = Al^{3+} + SO_4^{2-}$	a
(11)	$Al(SO_4)_2^- = Al^{3+} + 2SO_4^{2-}$	a
(12)	$CaCO_3^\circ = Ca^{2+} + HCO_3^- - H^+$	a,c
(13)	$CaHCO_3^+ = Ca^{2+} + HCO_3^-$	a
(14)	$CaOH^+ = Ca^{2+} + H_2O^\circ - H^+$	a,d
(15)	$CaSO_4^\circ = Ca^{2+} + SO_4^{2-}$	a
(16)	$CH_4^\circ(v) = HCO_3^- + H_2O^\circ - SO_4^{2-} + HS^-$	c,e,f
(17)	$CO_2^\circ(v) = HCO_3^- + H^+ - H_2O^\circ$	c,e,f
(18)	$CO_3^{2-} = HCO_3^- - H^+$	c
(19)	$Fe^{3+} = Fe^{2+} + 1/8SO_4^{2-} + 9/8H^+ - 1/8HS^- - 1/2H_2O^\circ$	c,f,g
(20)	$FeCl^{2+} = Fe^{2+} + 1/8SO_4^{2-} + 9/8H^+ - 1/8HS^- - 1/2H_2O^\circ + Cl^-$	a,c,f,g
(21)	$FeCl_2^+ = Fe^{2+} + 1/8SO_4^{2-} + 9/8H^+ - 1/8HS^- - 1/2H_2O^\circ + 2Cl^-$	a,c,f,g
(22)	$FeCl_3^\circ = Fe^{2+} + 1/8SO_4^{2-} + 9/8H^+ - 1/8HS^- - 1/2H_2O^\circ + 3Cl^-$	a,c,f,g
(23)	$FeCl_4^- = Fe^{2+} + 1/8SO_4^{2-} + 9/8H^+ - 1/8HS^- - 1/2H_2O^\circ + 4Cl^-$	a,c,f,g
(24)	$FeCl^+ = Fe^{2+} + Cl^-$	h,i
(25)	$FeCl_2^\circ = Fe^{2+} + 2Cl^-$	h,i
(26)	$FeOH^{2+} = Fe^{2+} + 1/8SO_4^{2-} + 1/8H^+ - 1/8HS^- + 1/2H_2O^\circ$	c,f,g,j
(27)	$Fe(OH)_2^+ = Fe^{2+} + 1/8SO_4^{2-} - 7/8H^+ - 1/8HS^- + 3/2H_2O^\circ$	a,c,f,g
(28)	$Fe(OH)_3^\circ = Fe^{2+} + 1/8SO_4^{2-} - 15/8H^+ - 1/8HS^- + 5/2H_2O^\circ$	c,f,g,k
(29)	$Fe(OH)_4^- = Fe^{2+} + 1/8SO_4^{2-} - 23/8H^+ - 1/8HS^- + 7/2H_2O^\circ$	c,f,g,k

TABLE 1

(Continued)

(30)	$FeOH^+ = Fe^{2+} + H_2O° - H^+$	l
(31)	$Fe(OH)_2° = Fe^{2+} + 2H_2O° - 2H^+$	l
(32)	$Fe(OH)_3^- = Fe^{2+} + 3H_2O° - 3H^+$	l
(33)	$Fe(OH)_4^{2-} = Fe^{2+} + 4H_2O° - 4H^+$	a,l
(34)	$FeSO_4^+ = Fe^{2+} + 9/8SO_4^{2-} + 9/8H^+ - 1/8HS^- - 1/2H_2O°$	a,c,f,g
(35)	$FeSO_4° = Fe^{2+} + SO_4^{2-}$	a
(36)	$H_2°(v) = H_2O° + 1/4HS^- - 1/4SO_4^{2-} - 1/4H^+$	c,e,f
(37)	$H_2BO_3^- = H_3BO_3° - H^+$	m
(38)	$HCl° = H^+ + Cl^-$	n
(39)	$H_2CO_3° = HCO_3^- + H^+$	o
(40)	$HF° = H^+ + F^-$	p
(41)	$H_2S° = HS^- + H^+$	c,q
(42)	$H_2S(v) = HS^- + H^+$	c,e
(43)	$HSO_4^- = SO_4^{2-} + H^+$	c
(44)	$H_2SO_4° = SO_4^{2-} + 2H^+$	a,c
(45)	$H_2SiO_4^{2-} = H_4SiO_4° - 2H^+$	a,r,s
(46)	$H_3SiO_4^- = H_4SiO_4° - H^+$	a,r,s
(47)	$KCl° = K^+ + Cl^-$	c,h,t
(48)	$KSO_4^- = K^+ + SO_4^{2-}$	j
(49)	$MgCO_3° = Mg^{2+} + HCO_3^- - H^+$	a,c
(50)	$MgHCO_3^+ = Mg^{2+} + HCO_3^-$	a
(51)	$MgOH^+ = Mg^{2+} + H_2O° - H^+$	a,d
(52)	$MgSO_4° = Mg^{2+} + SO_4^{2-}$	a
(53)	$NaCl° = Na^+ + Cl^-$	c,u
(54)	$NaH_3SiO_4° = H_4SiO_4° - H^+ + Na^+$	a,r,s
(55)	$NaSO_4^- = Na^+ + SO_4^{2-}$	t,v
(56)	$NH_3(v) = NH_4^+ - H^+$	c,q,w
(57)	$NH_4OH° = NH_4^+ + H_2O° - H^+$	a,d
(58)	$O_2°(v) = 1/2SO_4^{2-} - 1/2HS^- + 1/2H^+$	c,e
(59)	$OH^- = H_2O° - H^+$	d
(60)	$S^{2-} = HS^- - H^+$	a

a–Arnórsson, Sigurdsson, and Svavarsson (1982); b–Reed and Spycher (1984); c–Shock and Helgeson (1988); d–Sweeton, Mesmer, and Baes (1974); e–Helgeson and others (1978), f–Helgeson and Kirkham (1974); g–Shock and Helgeson (1989); h–Heinrich (1990); i–Heinrich and Seward (1990); j–Kharaka and others (1988); k–Tremaine and LeBlanc (1980); l–Sweeton and Baes (1970); m–Mesmer, Baes, and Sweeton (1971); n–Ruaya and Seward (1987); o–Read (1975); p–Truesdell and Singers (1971); q–Shock, Helgeson, and Sverjensky (1989); r–Seward (1974); s–Busey and Mesmer (1977); t–Ball, Nordstrom, and Jenne (1980); u–Helgeson, Kirkham, and Flowers (1981); v–Ohmoto and Lasaga (1982); w–Giggenbach (1980)

TABLE 2

Total molalities (log m_i, moles/kg) of component species, pH, and gas pressures (P_i, bars) in the Reykjanes and Svartsengi initial discharge calculated at the reservoir temperature (T°C). Abbreviations: T_H vapor-saturated temperature equivalent of the discharge enthalpy; T_{QTZ} quartz geothermometry temperature; n.a. not analyzed

	Reykjanes				Svartsengi				
well number	8	8	9	9	4	6	7	8	11
sample number	233	5	225	262	3008	132	180	136	182
date of sampling	9/20/83	1/20/87	9/14/83	10/24/83	5/28/79	10/7/82	7/19/83	10/8/82	7/20/83
source of data	d,e	e	e	d,e	f	g	g	g	g
Al^{3+}	-4.56	n.a.	n.a.	-4.52	-5.67	n.a.	n.a.	n.a.	n.a.
Ca^{2+}	-1.35	-1.39	-1.43	-1.40	-1.56	-1.64	-1.60	-1.60	-1.61
Cl^-	-0.24	-0.25	-0.29	-0.28	-0.41	-0.46	-0.44	-0.44	-0.44
$CO_2°$	-1.69	-1.69	-1.42	-1.47	-2.02	-1.91	-1.95	-1.93	-2.01
F^-	-5.04	-5.05	-5.09	-5.06	-5.16	-5.32	-5.22	-5.35	-5.22
Fe^{2+}	-5.77	n.a.	n.a.	-6.43	-5.60	n.a.	n.a.	n.a.	n.a.
$H_3BO_3°$	n.a.	n.a.	n.a.	n.a.	-3.18	n.a.	n.a.	n.a.	n.a.
$H_2S°$	-3.16	-3.14	-2.83	-2.92	-3.79	-3.83	-3.74	-3.73	-3.69
K^+	-1.40	-1.42	-1.43	-1.43	-1.58	-1.55	-1.56	-1.53	-1.58
Mg^{2+}	-4.45	-4.16	-4.46	-4.40	-4.26	-4.40	-4.56	-4.45	-4.53
Na^+	-0.33	-0.35	-0.38	-0.39	-0.54	-0.57	-0.55	-0.54	-0.54
NH_4^+	n.a.	n.a.	n.a.	n.a.	-4.49	n.a.	n.a.	n.a.	n.a.
$SiO_2°$	-2.01	-1.99	-1.93	-1.99	-2.14	-2.15	-2.16	-2.15	-2.16
SO_4^{2-}	-3.63	-3.66	-3.70	-3.86	-3.46	-3.57	-3.59	-3.46	-3.57
P_{CO_2}	1.56	1.60	2.59	2.30	0.83	1.11	1.01	1.05	0.87
P_{H_2S}	0.02	0.02	0.04	0.03	0.55E-2	0.51E-2	0.63E-2	0.63E-2	0.70E-2
P_{H_2}	0.44E-2	0.68E-2	0.05	0.01	0.29E-2	0.01	0.16E-2	0.90E-2	0.40E-2
pH/T°C	5.18/270°	5.18/270°	5.00/295°	4.88/295°	5.57/240°	5.38/240°	5.30/240°	5.38/240°	5.46/240°
T_H[a]	273	273	292	292	240	240	240	240	240
T_{QTZ}[b]	278	285	309	284	239	241	239	241	239
T_{QTZ}[c]	273	279	294	278	237	239	237	239	237

a–discharge enthalpy from unpublished Orkustofnun data (1980), vapor-saturated temperature equivalent of enthalpy from Keenan and others (1978); b–Fournier (1985); c–Arnórsson, Gunnlaugsson, and Svavarsson (1983b); d–unpublished Orkustofnun data; e–Bjarnason (1987); f–Arnórsson, Gunnlaugsson, and Svavarsson (1983a); g–Bjarnason (1988)

neous in fluid composition, and there has not been much change with time in fluid chemistry in wells 7,8,9, and 11, indicating good fluid mixing and high permeability (Bjarnason, 1988). There is no chemical data for well 12 due to freshwater injection (1984-1988) and intermittent freshwater dilution from well 5 (1988-1991). Pre-1984 fluid analyses

from Svartsengi well 6 probably apply also to well 12 because a tracer study and freshwater dilution in well 6 indicate that a fault(s) or fracture(s) connect the two wells (Gudmundsson and others, 1984).

MINERALOGY

Figure 5A to D shows the sampled depths, downhole distribution of primary and secondary minerals, stratigraphy, measured temperatures after post-drilling stabilization, aquifers, and circulation losses in Reykjanes wells 8 and 9 and Svartsengi wells 4 and 12. All the samples are from the production reservoirs. The stratigraphic sections in figure 5A to D are correct for the stated depth. Cutting samples used in this alteration study, however, are uncorrected for depth, so some samples (RN9, 1352 m; SG12, 1108 m; SG12, 1290 m; SG12, 1392 m; SG12, 1488 m) fall within areas designated as "No Cuttings." Aquifers are defined by major circulation losses during drilling, disturbances in temperature profiles in static wells, constant pressure with time, and geological criteria like increases in alteration intensity and abundance of fracture and vesicle fillings relative to less permeable formations. Figure 5D shows that aquifers at 1165, 1195, and 1216 m depth in SG12 occur where there is only minor circulation loss. Geological and thermal criteria were used by Franzson (1983b) to identify these aquifers.

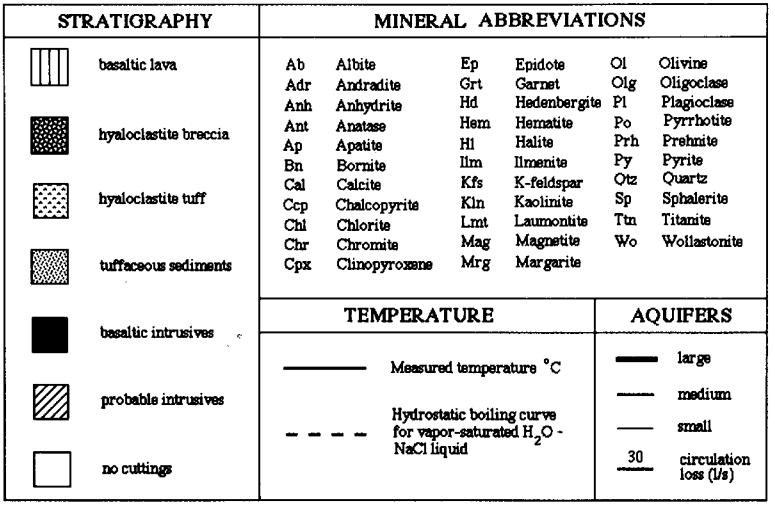

Fig. 4. Key to abbreviations and symbols used in figures and text. Sources of data: stratigraphy, circulation losses, aquifers (RN8–Björnsson, Árnórsson, and Tómasson, 1970, 1972; Björnsson and others, 1971; RN9–Franzson and others, 1983; SG4–Arnórsson and others, 1975; Franzson, 1990; unpublished Orkustofnun data; SG12–Franzson, 1983b, 1990); measured temperature profiles (RN8, RN9–unpublished Orkustofnun data; SG4, SG12–Björnsson and Steingrímsson, 1991), and hydrostatic boiling curves (Bjarnason, 1985).

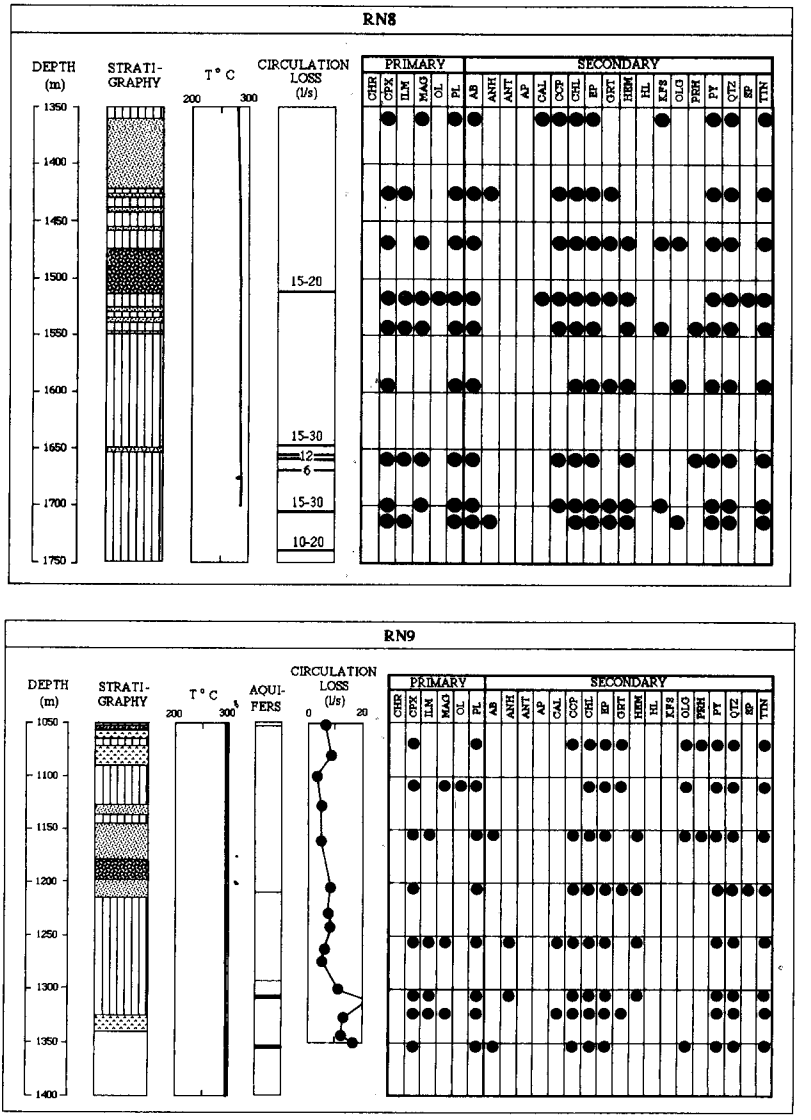

Fig. 5. Distribution of primary and secondary minerals, stratigraphy, measured temperatures, aquifers, and circulation losses as a function of depth in wells (A) RN8, (B) RN9, (C) SG4, and (D) SG12. Only the extrusive volcanics are depicted in the stratigraphic columns. No intrusive rocks were found in the sampled depth intervals in RN8 and RN9. Only the circulation losses are depicted in RN8. Disturbances in temperature profiles indicate a continuous aquifer below 1646 m in RN8 (Björnsson and others, 1971). There are no data on circulation loss at 1450 m in SG4.

C.

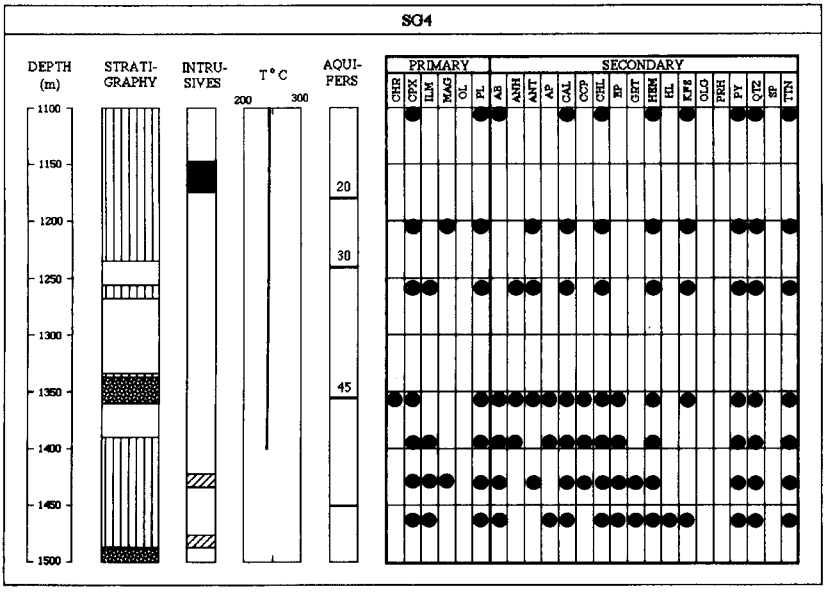

D.

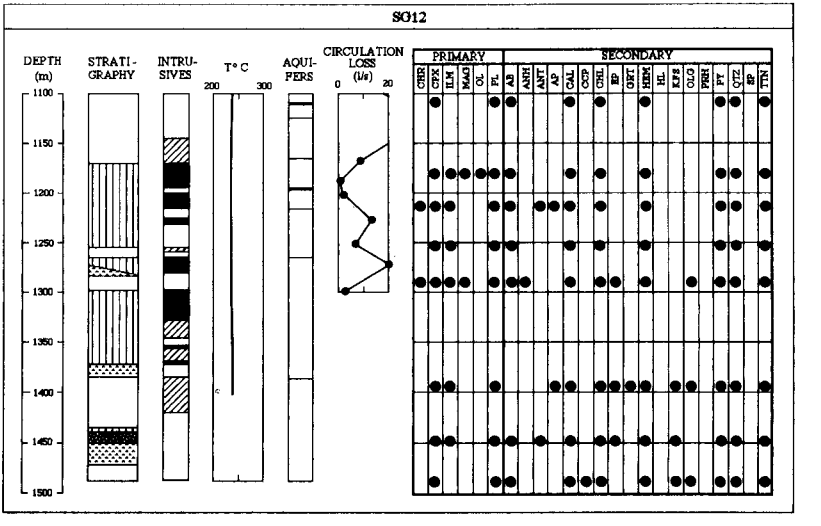

Fig. 5 (continued)

Primary Mineralogy

The degree of preservation of primary textures is a function of formation permeability and the type, abundance, and grain size of primary minerals. Glass is completely replaced even in less permeable

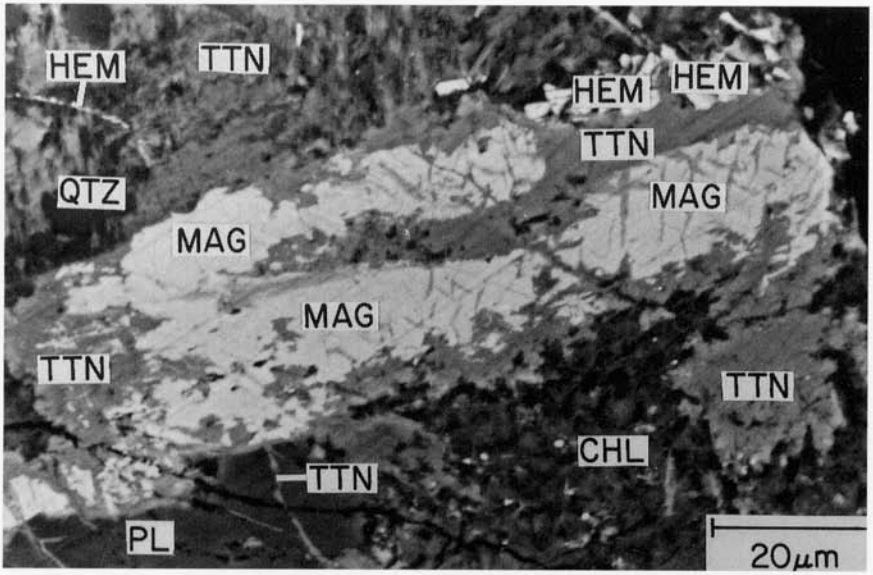

Fig. 6. Backscattered scanning electron image of magnetite mantled by titanite and hematite from Svartsengi well 4, 1430 m depth. Black area in upper right hand corner is epoxy.

formations by colloform and concentric bands of chlorite, garnet, and titanite, and irregular aggregates of calcite. Olivine is uncommon, replaced by chlorite, and occurs only in less permeable formations in RN9 and SG12. Chromite has a sporadic distribution in permeable (SG4, SG12) and less permeable (SG12) formations. Primary plagioclase (An90-An50) and clinopyroxene ($Fe^{2+}/(Fe^{2+} + Mg) = 0.10$ to 0.78) are present in all samples. Patches and veinlets of albite, calcite, chlorite, epidote, and K-feldspar replace primary plagioclase. Clinopyroxene is altered to chlorite, garnet, hematite, and titanite. Some altered clinopyroxenes have lower Ca contents, higher Fe/Mg ratios, and lower oxide totals than unaltered clinopyroxene, probably due to fine-grained intergrowths with secondary minerals. Unaltered and partially altered ilmenite ($X_{FeTiO_3} = 0.7$ to 0.9) and magnetite ($X_{Fe_3O_4} = 0.70$ to 0.98) also occur in many samples. Ragnarsdóttir, Walther, and Arnórsson (1984) reported only secondary magnetite occurring as "xenoblastic patches in the chlorite" at 1430 m depth in SG4. Textures show that these magnetite grains are partially or completely mantled by titanite and hematite, indicating a probable primary origin (fig. 6). Exsolution and oxidation of titanomagnetite during subsolidus cooling would produce a Ti-poor (nearly pure magnetite below 500°C) and an ulvöspinel-rich phase. The ulvöspinel-rich titanomagnetite undergoes solvus exsolution to ilmenite and hematite (Steinthorsson and others, 1992). In altered samples,

hematite, titanite, and, less commonly, anatase occur along grain boundaries, in crosscutting fractures, and in the centers of many ilmenite, Ti-poor magnetite, and titanomagnetite grains. The primary feldspars, pyroxenes, and Fe-Ti oxides are compositionally heterogeneous on the scale of a drill cutting in many samples due to compositional zoning (plagioclase and clinopyroxene) and fine-grained intergrowths with secondary minerals. It cannot be ascertained whether some of the isolated, fine-grained crystals of apatite are primary.

Secondary Mineralogy

The secondary minerals observed in the samples include albite, anatase (Svartsengi), anhydrite, apatite (Svartsengi), calcite, chalcopyrite, chlorite, epidote, garnet, halite (Svartsengi), hematite, K-feldspar, oligoclase, prehnite (Reykjanes), pyrite, quartz, sphalerite (Reykjanes), and titanite. No discrete grains of actinolitic amphibole were found.

The secondary minerals occur as open space fillings in vesicles, fractures, and in the groundmass as well as replacement of primary minerals and glass. It could not be ascertained whether secondary minerals filling open spaces formed from direct precipitation from the fluid, complete replacement (solid state or dissolution/precipitation) from preexisting minerals, or both. The paragenesis of secondary minerals is determined from pore and fracture filling sequences (youngest in core), crosscutting relationships, dissolution (cavity linings and overgrowths on corroded grains) and replacement (replacement along cleavage traces) features, and inclusion sequences. The determination of mineral deposition sequences in a drill cutting is made difficult by the presence of multiple generations of secondary minerals, crosscutting veins filling vesicles, small sample size, and finely intergrown minerals. There is an increase in the abundance of complex vesicle and fracture fillings near aquifers relative to less permeable formations in wells RN8 (1700 m, 1714 m) and SG4 (1430 m, 1462 m). No systematic differences in paragenesis as a function of formation permeability could be determined.

Chlorite.—Chlorite fills open spaces in vesicles and fractures and replaces the glassy groundmass and primary clinopyroxene, olivine, and plagioclase. Chlorite occurs in fine grained (< 10 μm), porous masses of well defined, but poorly oriented crystals (fig. 7A) and in fan-shaped aggregates. Hematite, titanite, or both occur as pore fillings in masses of chlorite crystals (fig. 7A). Quartz lines the walls of some chlorite-filled vesicles. In many of the samples, chlorite mantles corroded grains of calcite, epidote, and quartz. These textures indicate that chlorite mineralization is late and postdates calcite, epidote, and quartz. Chlorite-rich layers alternate with garnet-, quartz-, or titanite-rich layers in some vesicles (fig. 7B). Vesicles filled with chlorite may show an increase in chlorite crystallinity (crystallite size) from rim to core (fig. 7B), and one vesicle in SG12 at 1252 m even shows the reverse trend. In some vesicles, an irregular, well-defined boundary separates poorly crystalline chlo-

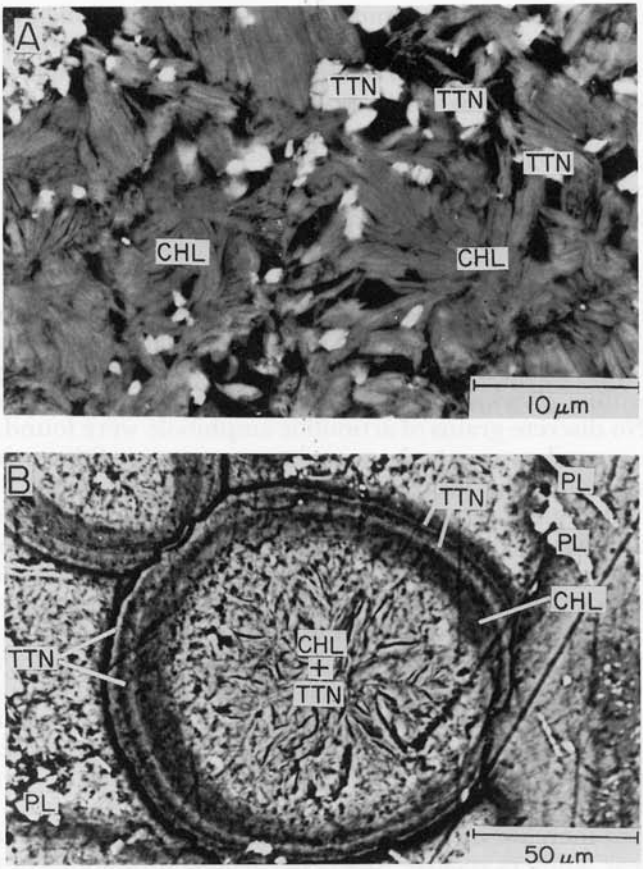

Fig. 7. Backscattered scanning electron images of (A) porous aggregate of well-defined crystals of chlorite and titanite from SG12, 1392 m depth and (B) vesicle filling from RN8, 1714 m depth showing successive deposition of titanite and fine-grained chlorite followed by more coarsely crystalline chlorite with titanite.

rites, which have higher Mg, Si, and Ca contents, from crystalline chlorites. However, no systematic changes in chlorite crystallinity (crystallite size) as a function of depth were observed.

Representative chemical analyses of chlorite are given in table 3. Chlorite analyses must be carefully selected to avoid contamination. Only analyses with a sum of the interlayer cations (ΣXII) less than 0.10 are used in this paper. Chlorite composition is variable even on the scale of a drill cutting (fig. 8A-D). Chlorite compositions in RN8 and RN9 show a linear correlation of $Fe^{2+}/(Fe^{2+} + Mg)$ with tetrahedral Al (Al^{IV}), which is probably related to the exchanges $FeMg_{-1}$ and $Al_2Mg_{-1}Si_{-1}$ (fig. 8A,B). There is a relationship of chlorite composition with formation permeabil-

TABLE 3

Representative chlorite analyses

	145	432	618	701	821	823	884	960
SiO_2	29.51	29.82	27.56	29.90	33.02	32.64	27.90	29.67
Al_2O_3	16.72	16.32	17.65	17.05	14.93	15.42	18.91	16.84
TiO_2	0.00	0.00	0.04	0.00	0.00	0.00	0.00	0.03
FeO*	21.46	21.25	26.76	20.45	17.47	17.08	22.26	20.74
MnO	0.50	0.40	0.44	0.35	0.31	0.29	0.28	0.22
MgO	19.58	19.73	15.08	20.20	21.50	22.11	19.39	20.35
CaO	0.12	0.33	0.43	0.35	0.76	0.64	0.09	0.20
Na_2O	0.10	0.00	0.03	0.03	0.06	0.03	0.10	0.04
K_2O	0.05	0.00	0.02	0.01	0.02	0.00	0.01	0.04
F	0.00	0.00	0.08	0.00	0.00	0.08	0.00	0.00
Cl	0.01	0.02	0.00	0.01	0.01	0.01	0.07	0.00
	88.05	87.87	88.09	88.35	88.08	88.30	89.01	88.13
-(O=F)	0.00	0.00	0.03	0.00	0.00	0.03	0.00	0.00
-(O=Cl)	0.00	0.00	0.00	0.00	0.00	0.00	0.02	0.00
Total	88.05	87.87	88.06	88.35	88.08	88.27	88.99	88.13
				Formulas based on 14 oxygens				
Si	3.0275	3.0614	2.9205	3.0363	3.2962	3.2469	2.8471	3.0253
AlIV	0.9725	0.9386	1.0795	0.9637	0.7038	0.7531	1.1529	0.9747
AlVI	1.0485	1.0358	1.1248	1.0765	1.0531	1.0550	1.1214	1.0487
Ti	0.0000	0.0000	0.0032	0.0000	0.0000	0.0000	0.0000	0.0025
Fe^{2+}	1.8412	1.8250	2.3714	1.7367	1.4583	1.4204	1.9001	1.7687
Mn	0.0438	0.0349	0.0396	0.0300	0.0258	0.0246	0.0239	0.0194
Mg	2.9944	3.0197	2.3811	3.0579	3.1998	3.2785	2.9499	3.0929
ΣVI	5.9279	5.9154	5.9201	5.9011	5.7370	5.7785	5.9953	5.9322
Ca	0.0134	0.0359	0.0492	0.0384	0.0816	0.0679	0.0098	0.0217
Na	0.0193	0.0000	0.0071	0.0064	0.0113	0.0052	0.0196	0.0077
K	0.0064	0.0000	0.0026	0.0017	0.0022	0.0000	0.0019	0.0054
ΣXII	0.0391	0.0359	0.0589	0.0465	0.0951	0.0731	0.0313	0.0348
F	0.0000	0.0000	0.0255	0.0000	0.0000	0.0244	0.0000	0.0000
Cl	0.0025	0.0028	0.0000	0.0013	0.0022	0.0025	0.0114	0.0000

* All Fe as FeO

Sample numbers: 145 (SG4, 1462 m, area 11); 432 (SG12, 1252 m, area 4); 618 (SG12, 1488 m, area 8); 701 (RN8, 1468 m, area 1); 821 (late chlorite, RN9, 1352m, area 3); 823 (early chlorite, RN9, 1352 m, area 3); 884 (SG4, 1358 m, area 2); 960 (RN8, 1700 m, area 3)

ity in several wells. In RN9, higher $Fe^{2+}/(Fe^{2+} + Mg)$ ratios and lower Si contents are associated with aquifers and high circulation loss (fig. 9B). There are no samples below 1352 m in RN9, so compositional patterns near this large aquifer could not be ascertained. The relationship of chlorite composition with formation permeability is not as well-defined in the other wells. In RN8, there is a gradational increase in the $Fe^{2+}/(Fe^{2+} + Mg)$ ratio and decrease in Si content to a depth of 1660 m. Similar trends were described in RN8 by Sveinjörnsdóttir (1983a, 1992). Chlorite grains with lower Si contents occur in more permeable formations at 1660 and 1700 m depth (fig. 9A). There is little change in chlorite

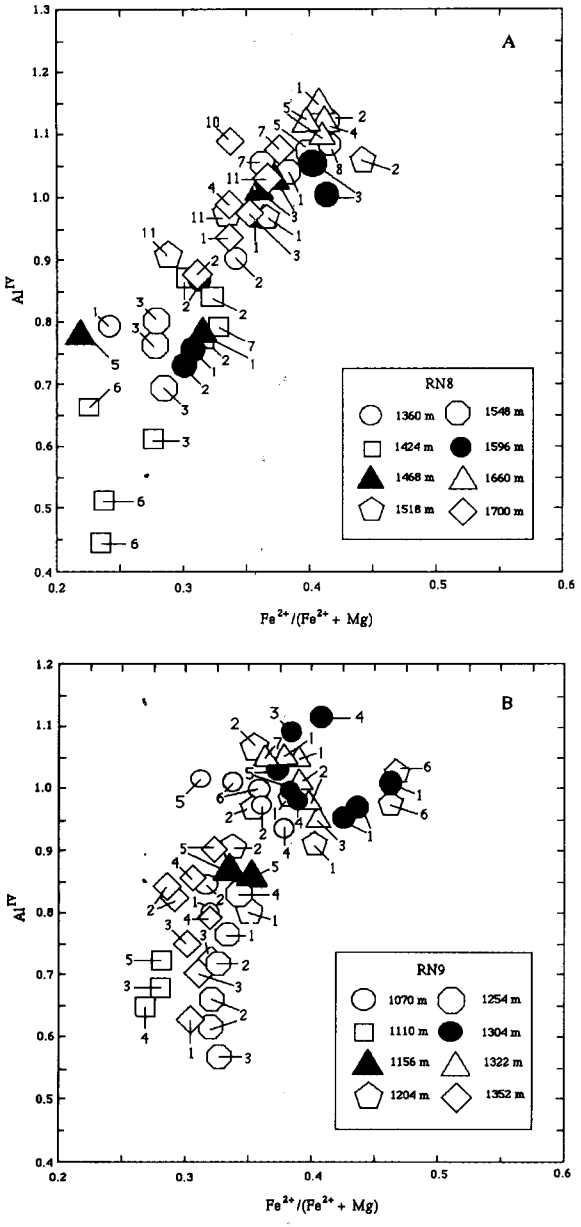

Fig. 8. Plot of tetrahedral Al (Al^{IV}) versus $Fe^{2+}/(Fe^{2+} + Mg)$ ratio in chlorites from (A) RN8, (B) RN9, (C) SG4, and (D) SG12.

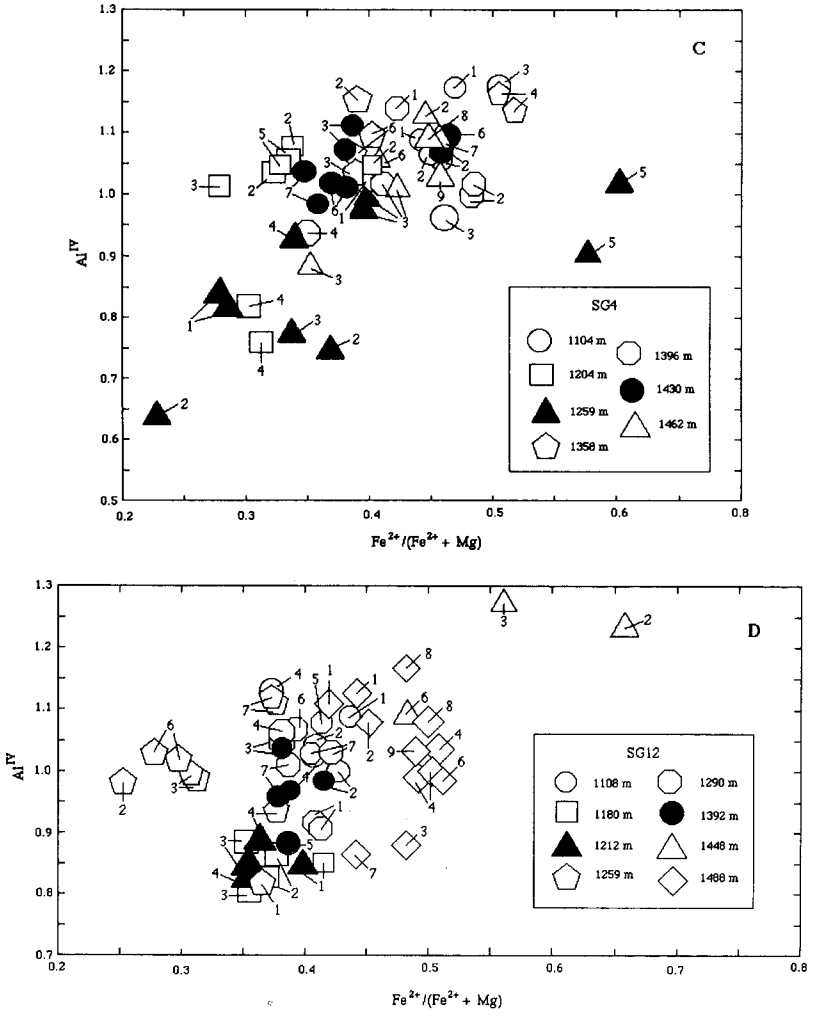

Fig. 8 (continued)

composition with depth in SG4 (fig. 9C). The correlation of chlorite composition with formation permeability is the reverse in more permeable formations near 1180 and 1212 m in SG12, where chlorite grains show an increase in the Si and Ca contents (fig. 9D).

No correlation of chlorite composition with mineral association or host rock lithology was observed. Moreover, many samples showed similar chlorite compositions in veins, vesicles, and in the groundmass within a cutting. Only at 1352 m depth in RN9 were there multiple generations of chlorite with distinctly different compositions (table 3).

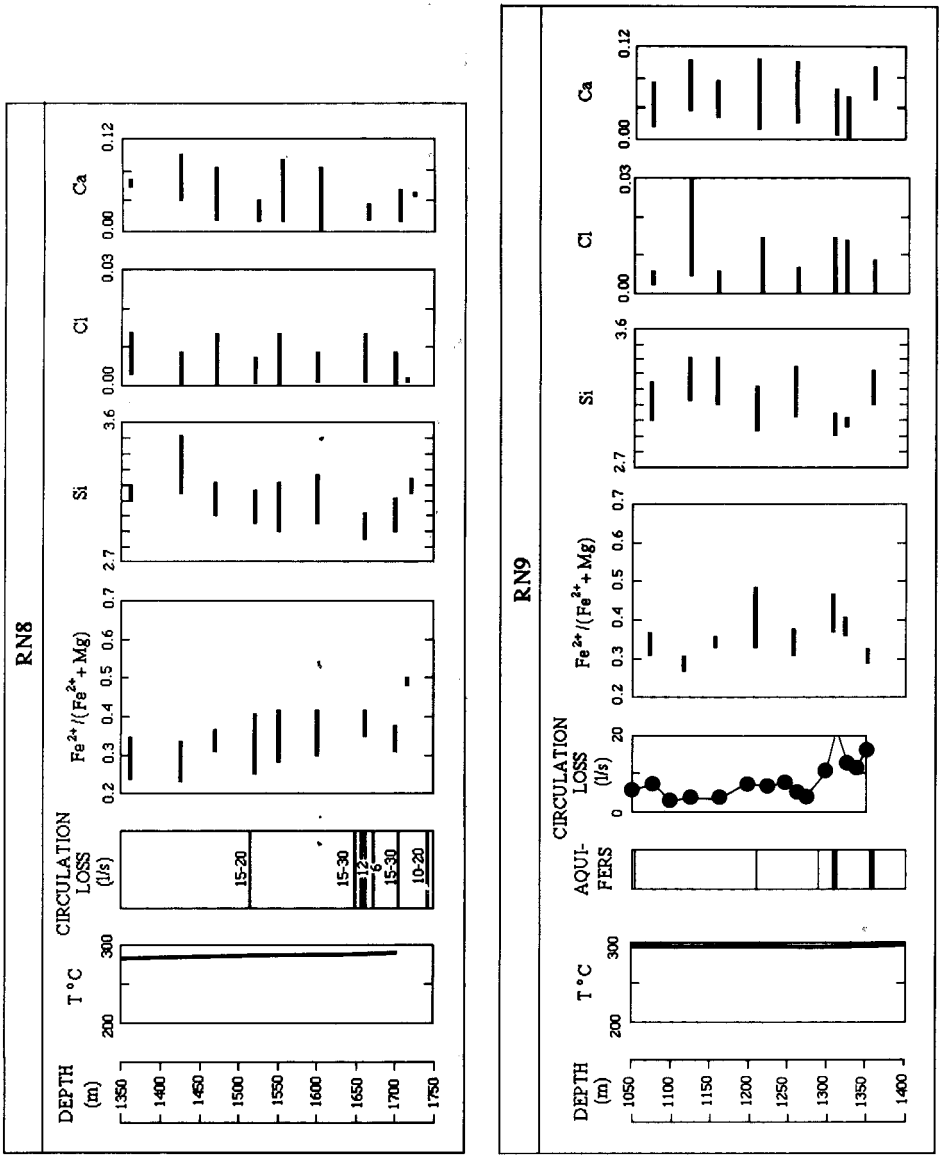
A.
RN8
DEPTH (m)
T °C
CIRCULATION LOSS (l/s)
$Fe^{2+}/(Fe^{2+}+Mg)$
Si
Cl
Ca
15-20
15-30
12
15-30
10-20
B.
RN9
DEPTH (m)
T °C
AQUI-FERS
CIRCULATION LOSS (l/s)
$Fe^{2+}/(Fe^{2+}+Mg)$
Si
Cl
Ca

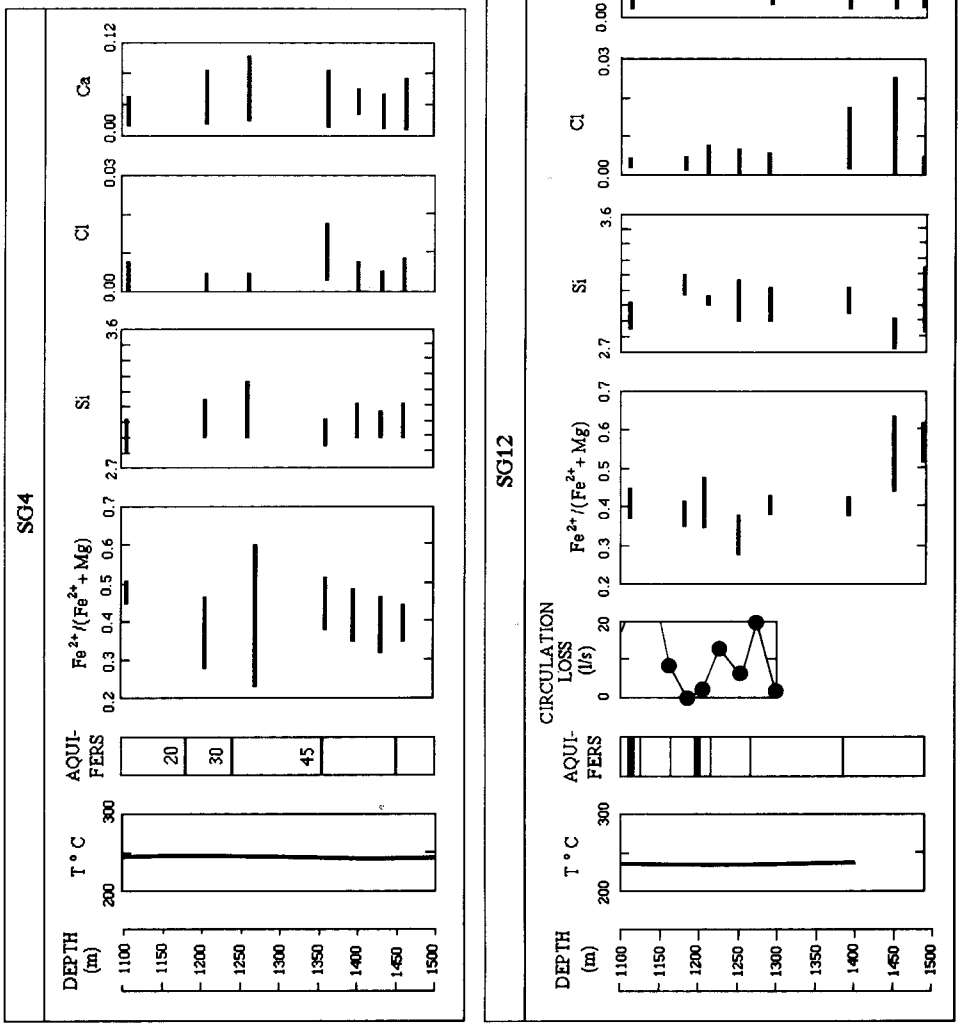

Fig. 9. Measured temperatures, aquifers, circulation losses, and chlorite mineral chemistry as a function of depth in wells (A) RN8, (B) RN9, (C) SG4, and (D) SG12.

Epidote.—Epidote occurs most commonly as larger (< 0.8 mm) xenoblastic crystals and smaller (25-250 μm) fan-shaped aggregates of columnar crystals which fill open spaces and replace primary plagioclase. Some epidote grains are intergrown with euhedral pyrite; other epidote grains contain quartz inclusions or are intergrown with quartz. In many samples, epidote is mantled with chlorite (fig. 10) or occurs as resorbed grains in chlorite. The surfaces of these epidote grains are usually irregular and embayed, suggesting dissolution (fig. 10). Chlorite-epidote relations are ambiguous at 1462 m in SG12, probably due to the presence of multiple generations of secondary minerals. Franzson (1983b) noted an increase in the abundance of epidote in several aquifers in SG12. Epidote, however, is absent from the major aquifer at 1195 m and is scarce (< 5 percent) in the smaller aquifer at 1216 m in SG12 (Franzson, 1983b). Epidote is also scarce in dense intrusions in SG12, where porosity and permeability are low.

Representative epidote analyses are given in table 4. Charge balance calculations indicate that the iron is in the trivalent state. The analyzed epidotes are Fe^{3+}-rich ($X_{Ca_2Fe_3Si_3O_{12}(OH)}$ = 0.19 to 0.44). Indeed, some of the epidotes in this paper (table 4) and in earlier studies (Sveinbjörnsdóttir, 1983a, 1992; Ragnarsdóttir, Walther, and Arnórsson, 1984) exceed the "compositional limit" of one Fe^{3+} per formula unit ($X_{Ca_2Fe_3Si_3O_{12}(OH)}$ = 0.33) (Bird and Helgeson, 1980). No rare earth elements were detected in the

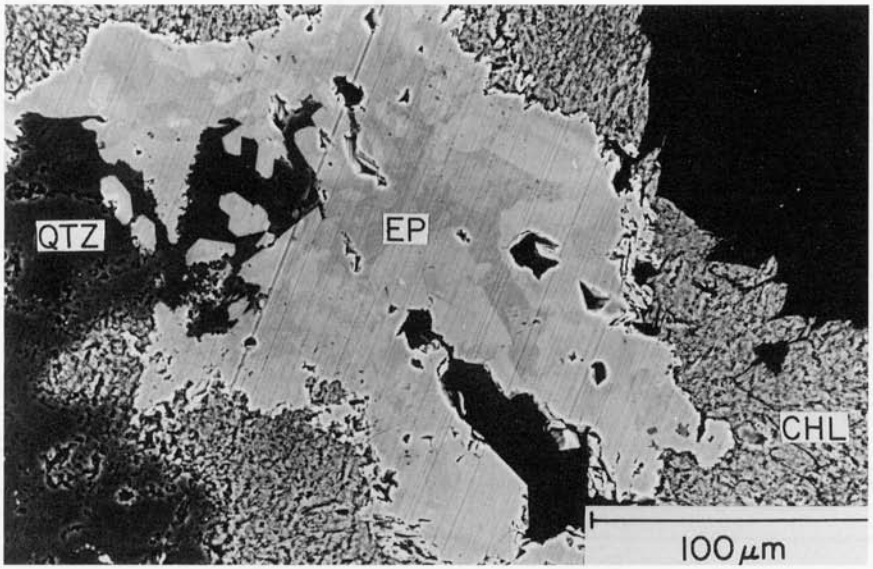

Fig. 10. Backscattered scanning electron image of compositional zoning in epidote mantled by chlorite from SG4, 1462 m depth. Darker areas in epidote are Al-rich and lighter areas are Fe^{3+}-rich. Black areas in upper right hand corner and within epidote are epoxy.

TABLE 4

Representative epidote analyses

	132	292	502	558	815	911	968	1148
SiO_2	37.88	37.58	38.33	36.87	37.32	37.01	37.58	37.68
Al_2O_3	21.49	22.03	22.92	21.56	19.93	21.98	22.97	24.65
TiO_2	0.11	0.05	0.11	0.00	0.05	0.18	0.00	0.13
Cr_2O_3	0.00	0.00	0.00	0.06	0.00	0.00	0.00	0.03
Fe_2O_3*	16.41	15.42	14.66	16.72	18.10	16.40	14.25	13.07
MnO	0.06	0.27	0.11	0.08	0.13	0.06	0.07	0.15
MgO	0.00	0.07	0.00	0.03	0.05	0.00	0.00	0.08
CaO	23.34	23.06	23.26	23.07	23.09	23.13	23.25	23.75
Total	99.29	98.48	99.39	98.39	98.67	98.76	98.12	99.54
				Formulas based on 8 cations				
Si	3.0101	3.0003	3.0224	2.9579	3.0046	2.9548	2.9966	2.9448
AlIV	0.0000	0.0000	0.0000	0.0421	0.0000	0.0452	0.0034	0.0552
AlVI	2.0126	2.0729	2.1301	1.9965	1.8911	2.0231	2.1553	2.2153
Ti	0.0066	0.0030	0.0065	0.0000	0.0030	0.0108	0.0000	0.0076
Cr	0.0000	0.0000	0.0000	0.0038	0.0000	0.0000	0.0000	0.0019
Fe^{3+}	0.9795	0.9247	0.8685	1.0077	1.0948	0.9835	0.8536	0.7673
ΣVI	2.9987	3.0006	3.0051	3.0080	2.9889	3.0174	3.0089	2.9921
Mn	0.0040	0.0183	0.0073	0.0054	0.0089	0.0041	0.0047	0.0099
Mg	0.0000	0.0083	0.0000	0.0036	0.0060	0.0000	0.0000	0.0093
Ca	1.9871	1.9725	1.9651	1.9830	1.9917	1.9786	1.9864	1.9887
ΣVII	1.9912	1.9991	1.9725	1.9920	2.0066	1.9826	1.9911	2.0079

* All Fe as Fe_2O_3

Sample numbers: 132 (SG4, 1462 m, area 7); 292 (RN8, 1548 m, area 8); 502 (SG12, 1392 m, area 2); 558 (SG12, 1448 m, area 4); 815 (RN9, 1352 m, area 3); 911 (SG4, 1396 m, area 1); 968 (RN8, 1700 m, area 5); 1148 (RN9, 1322 m, area 5)

epidotes. Epidote vesicle, vein, and pseudomorph compositions are similar. No systematic changes of epidote composition with depth or aquifer location were observed in most of the samples. Compositional heterogeneity (Fe^{3+}-content) in epidote, however, is more extensive in many of the more permeable formations in RN9, SG4, and SG12.

Some epidote grains are compositionally homogeneous, whereas others are compositionally heterogeneous and may even show complex zoning patterns (fig. 10). In several samples, epidote grains replacing plagioclase are zoned with Al-rich rims. Epidote grains mantled with hematite, however, may have an Al-rich core and a Fe^{3+}-rich rim.

Garnet.—Garnet occurs in many of the Reykjanes samples and in the Svartsengi samples below 1358 m depth. Garnet has not been previously reported in the Reykjanes and Svartsengi systems. Garnet (<2 μm-0.5 mm diam) occurs as open space fillings, pore fillings in masses of chlorite crystals, veinlets and vug linings in sodic feldspar, inclusions in albite, and as a replacement of clinopyroxene and glass. Garnet lines the walls in some chlorite-filled vesicles indicating early garnet deposition. Vesicles at 1714 m in RN8 contain complex sequences of chlorite- and garnet-rich

layers (fig. 11A,B). Epidote-garnet sequences are ambiguous. Garnet crystals engulfed in a mass of chlorite crystals mantle corroded epidote grains at 1204 m in RN9, and garnet rims corroded epidote at 1430 m in SG4. Garnet deposition precedes epidote at 1462 m in SG4, where resorbed garnet is overgrown by epidote.

Representative garnet analyses are given in table 5. Most of the analyzed garnets plot at intermediate compositions on the andradite-grossular join with less than 5 mole percent almandine + pyrope + spessartine. Garnets at 1462 m depth in SG4, however, are nearly pure andradite (table 5). Many analyses have totals between 98 and 99 wt percent, suggesting the presence of a hydrogarnet components (table 5).

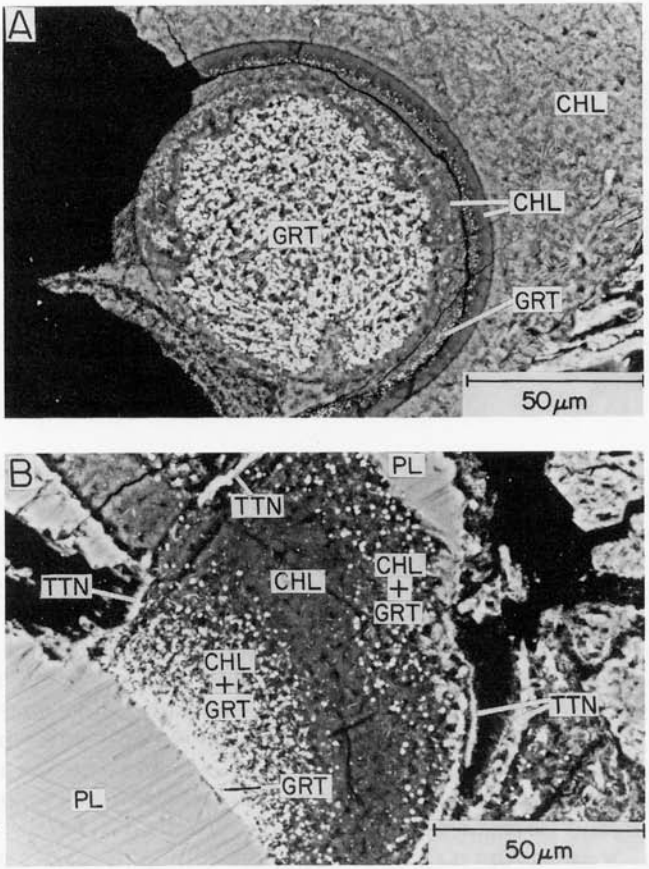

Fig. 11. Backscattered scanning electron images of vesicle fillings from RN8, 1714 m depth showing reversals in chlorite-garnet sequences. Rim-to-core sequences are (A) poorly crystalline chlorite to poorly crystalline chlorite + garnet to crystalline chlorite + garnet to garnet and (B) titanite to chlorite + garnet to chlorite.

TABLE 5

Representative garnet analyses

	129	356	528	649	698	787	993	1133
SiO_2	34.46	36.22	35.86	36.34	37.39	37.92	36.95	36.21
Al_2O_3	0.35	8.34	8.70	9.52	11.19	14.07	11.81	9.95
TiO_2	0.00	0.62	1.09	0.32	0.66	0.39	0.47	0.47
Cr_2O_3	0.00	0.12	0.00	0.00	0.06	0.12	0.05	0.00
Fe_2O_3	31.26	18.83	18.26	18.74	15.27	11.47	13.78	17.26
FeO	0.22	0.81	0.30	0.52	1.12	1.46	1.53	1.03
MnO	0.09	0.62	0.34	0.37	0.40	0.35	0.87	0.35
MgO	0.00	0.19	0.25	0.36	1.68	3.09	0.00	0.27
CaO	31.93	32.87	33.40	32.95	31.67	29.78	32.94	32.68
Total	98.31	98.62	98.20	99.12	99.44	98.65	98.40	98.22
			Formulas based on 12 oxygens and 8 cations*					
Si	2.9687	2.9726	2.9464	2.9519	2.9788	2.9845	2.9877	2.9605
AlIV	0.0313	0.0274	0.0536	0.0481	0.0212	0.0155	0.0123	0.0395
AlVI	0.0042	0.7793	0.7889	0.8633	1.0295	1.2897	1.1132	0.9192
Ti	0.0000	0.0383	0.0673	0.0195	0.0395	0.0231	0.0286	0.0289
Cr	0.0000	0.0078	0.0000	0.0000	0.0038	0.0075	0.0032	0.0000
Fe^{3+}	2.0264	1.1629	1.1290	1.1452	0.9157	0.6791	0.8383	1.0621
ΣVI	2.0305	1.9883	1.9853	2.0281	1.9885	1.9994	1.9833	2.0102
Fe^{2+}	0.0161	0.0554	0.0205	0.0355	0.0744	0.0963	0.1036	0.0702
Mn	0.0066	0.0431	0.0237	0.0255	0.0270	0.0233	0.0596	0.0242
Mg	0.0000	0.0232	0.0306	0.0436	0.1995	0.3625	0.0000	0.0329
Ca	2.9472	2.8904	2.9403	2.8677	2.7033	2.5113	2.8537	2.8627
ΣVIII	2.9699	3.0121	3.0151	2.9722	3.0042	2.9934	3.0169	2.9900

* Formula normalization to 12 oxygens with adjustment of Fe^{2+}/Fe^{3+} ratio until cation total sums 8 (Papike, 1987)

Sample numbers: 129 (SG4, 1462 m, area 7); 356 (RN8, 1714 m, area 4); 528 (SG12, 1392 m, area 5); 649 (SG4, 1430 m, area 3); 698 (RN8, 1468 m, area 1); 787 (RN9, 1110 m, area 3); 993 (RN8, 1700 m, area 10); 1133 (RN9, 1322 m, area 3)

No systematic changes in garnet composition with depth or formation permeability were observed.

No compositional zoning was observed in most of the analyzed garnet grains. An andradite-grossular garnet at 1392 m depth in SG12, however, is zoned with alternating layers of Mg-poor (1 mole percent pyrope) and Mg-rich (12-14 mole percent pyrope) compositions.

Prehnite.—Prehnite is uncommon and occurs as sheaflike aggregates in open space fillings in RN8 and RN9. Most of the analyzed prehnites are Fe^{3+}-rich. High Fe^{3+} and low Fe^{3+} prehnite occur as fracture fillings in different cuttings at 1156 m in RN9 and crosscut earlier albite veins (table 6).

Feldspars.—Albite ($X_{NaAlSi_3O_8}$ = 0.90 to 0.98), oligoclase ($X_{NaAlSi_3O_8}$ = 0.85 to 0.89), and K-feldspar ($X_{KAlSi_3O_8}$ = 0.91 to 0.98) occur in the groundmass, as open space fillings and as a replacement of primary plagioclase. K-feldspar occurs in most samples in RN8, SG4, and below 1392 m in SG12 but is absent in RN9. K-feldspar predates albite as inferred from crosscutting relationships, albite overgrowths, and inclusion sequences. Many K-feldspar and some albite grains replacing pri-

TABLE 6

Representative prehnite analyses

	151	180	275
SiO_2	42.87	43.58	43.33
Al_2O_3	20.60	23.31	21.06
Fe_2O_3*	5.30	1.49	5.07
MgO	0.00	0.00	0.09
CaO	26.13	26.26	25.96
Na_2O	0.00	0.10	0.00
Total	94.90	94.74	95.51
	Formulas based on 11 oxygens		
Si	3.0202	3.0258	3.0248
AlIV	0.9798	0.9742	0.9752
AlVI	0.7307	0.9332	0.7576
Fe^{3+}	0.2810	0.0778	0.2662
Mg	0.0000	0.0000	0.0094
ΣVI	1.0117	1.0110	1.0332
Ca	1.9724	1.9535	1.9417
Na	0.0000	0.0135	0.0000
Σ	1.9724	1.9669	1.9417

* All Fe as Fe_2O_3

Sample numbers: 151 (RN9, 1156 m, area 6); 180 (RN9, 1156 m, area 7); 275 (RN8, 1548 m, area 4)

mary plagioclase are embayed and corroded, indicative of dissolution. No systematic changes were observed in feldspar composition with depth or formation permeability. Primary plagioclase, however, is more extensively altered to albite in most aquifers.

Calcite.—Calcite occurs as open space fillings and as a replacement of the glassy groundmass and primary clinopyroxene and plagioclase. Calcite occurs in sparse amounts (<5 volume percent) in only a few samples in RN8 and RN9. In contrast, calcite is found in all samples in SG4 and SG12 and is particularly abundant (up to 30 volume percent) in the larger aquifers. Many calcite grains are mantled by chlorite or occur as resorbed grains in chlorite. These calcite grains have irregular and embayed surfaces probably formed by dissolution. Some vesicles contain intergrowths of calcite with anhydrite, quartz, or both. Quartz lines the walls of some calcite-filled vesicles. Chlorite-calcite and epidote-calcite relations are ambiguous at 1462 m in SG4, probably due to the presence of multiple generations of secondary minerals.

Minor elements in the analyzed calcite grains are Fe^{2+} (X_{FeCO_3} = 0.00 to 0.06) and Mn (X_{MnCO_3} = 0.00 to 0.06). No systematic changes of calcite composition with depth or aquifer location were observed. One calcite grain at 1252 m in SG12 is compositionally zoned with a rim of alternat-

ing Mn- and Fe^{2+}-rich (X_{MnCO_3} = 0.03 to 0.04, X_{FeCO_3} = 0.01 to 0.06) and -poor (X_{MnCO_3} < 0.01, X_{FeCO_3} < 0.01) layers with a broad, homogeneous core of nearly pure $CaCO_3$.

Titanite.—Titanite is found in all samples and occurs as a pore filling in aggregates of chlorite or garnet crystals, overgrowths on garnet and epidote, vug linings, intergrowths with anatase, hematite, or both, and as a replacement of clinopyroxene, plagioclase, Fe-Ti oxides, and glass. Open-space fillings of chlorite + titanite (fig. 7A) and hematite + titanite (fig. 12A) are common. In some samples, titanite mantles chlorite (fig. 12B). Some vesicles contain alternating layers of titanite, chlorite (fig. 7B), and garnet.

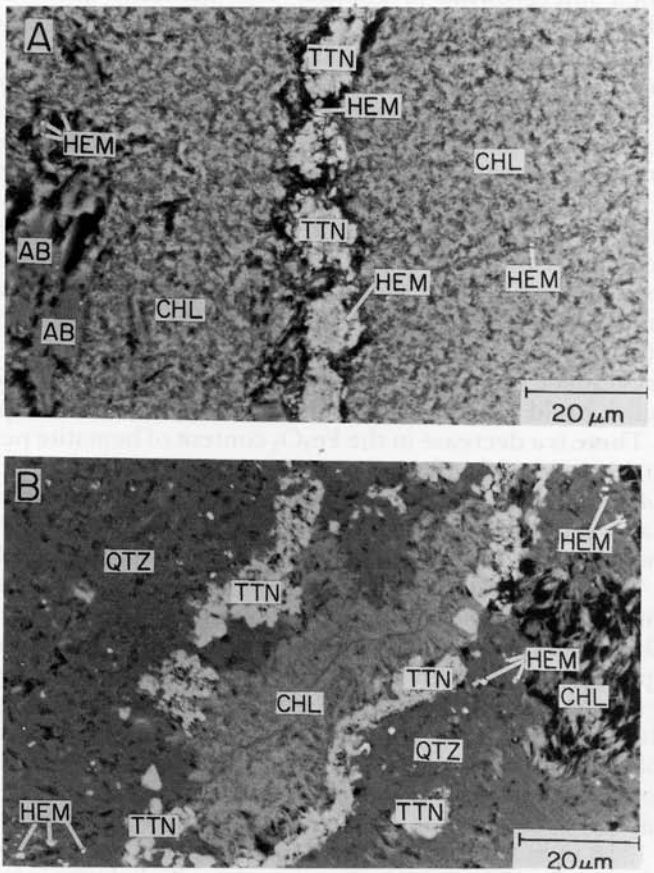

Fig. 12. Backscattered scanning electron images of (A) fracture filled with hematite + titanite crosscutting chlorite + hematite from SG4, 1430 m depth, and (B) titanite mantling hematite-free chlorite from SG4, 1462 m depth. Note the dissolution textures in albite (fig. 12A). It is not known whether these dissolution features formed during primary plagioclase replacement or after albite deposition.

No systematic correlation was observed between titanite composition and mode of occurrence, mineral association, rock type, formation permeability, or depth. Compositional zoning was not detected in the analyzed titanites. Compositional heterogeneity (Ti,Al) is more extensive in several of the more permeable formations in RN8 and RN9. The antipathetic variation of Al, Fe^{3+}, and F with Ti in the analyzed titanites is probably related to the exchange $Ti^{4+} + 0^{2-} = (Al^{3+},Fe^{3+}) + (OH^-, F^-)$.

Anatase.—Anatase (0.12-2.16 wt percent V_2O_3) occurs as a pore filling in masses of chlorite crystals, as intergrowths with titanite, and as a replacement of primary Fe-Ti oxides. Only the Svartsengi samples contain anatase. Anatase occurs in most samples in SG4 but has a sporadic distribution in SG12. Chemical analysis of anatase is a problem due to fine-grained intergrowths of anatase with hematite and titanite. No relationship of anatase composition with formation permeability could be ascertained due to the paucity of analyses.

Hematite.—Hematite occurs as a pore filling in aggregates of chlorite crystals, intergrowths with titanite (fig. 12A), and as a replacement of clinopyroxene, glass, and Fe-Ti oxides. In the Svartsengi samples, hematite is common, particularly in many of the aquifers where alteration of primary Fe-Ti oxides is more extensive and along the margins of intrusions. Ragnarsdóttir, Walther, and Arnórsson (1984), however, did not report hematite from 1430 m in SG4. Hematite is not as abundant in the Reykjanes samples. In most samples, hematite postdates (overgrowths, wall lining of dissolution cavities, crosscutting fractures) or is contemporaneous (intergrowths) with titanite.

No systematic correlation of hematite composition with formation permeability could be determined in most wells due to the paucity of analyses. There is a decrease in the Fe_2O_3 content of hematite near a large aquifer at 1360 m in SG4 (fig. 13).

Sulfides.—Pyrite is the most abundant sulfide and occurs in all samples as a groundmass mineral, as an open space filling, as an intergrowth with epidote, and, less commonly, within masses of chlorite crystals. The abundance of pyrite increases in several of the major aquifers in SG12 (Franzson, 1983a,b) and in other wells.

Chalcopyrite occurs as a pore filling in aggregates of chlorite crystals, blebs in pyrite, intergrowths with epidote, and irregularly shaped blebs in sphalerite. Most samples from RN8 and RN9 contain chalcopyrite. In the Svartsengi wells, however, chalcopyrite occurs only toward the base of SG4 (1358-1430 m) and SG12 (1488 m) (fig. 5A-D). In SG4, chalcopyrite mantles and crosscuts pyrite at 1430 m but is included in pyrite at 1462 m.

Sphalerite is uncommon and occurs only in the aquifers in RN8 and RN9. At 1518 m in RN8, sphalerite is embayed and partially overgrown with epidote and occurs as inclusions in garnet. Sphalerite is intergrown with epidote at 1204 m in RN9. This sphalerite is compositionally zoned with a chalcopyrite-bearing Fe-rich rim ($Fe/(Fe + Zn) = 0.052$ to 0.064) and a chalcopyrite-free core ($Fe/(Fe + Zn) = 0.042$ to 0.051).

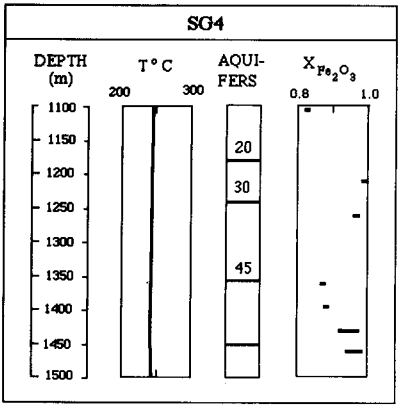

Fig. 13. Measured temperatures, aquifers, circulation losses, and mole fraction of Fe_2O_3 in hematite as a function of depth in SG4.

Quartz.—Quartz is found in all samples and occurs in the groundmass, open space fillings, wall lining in anhydrite-, calcite-, and chlorite-filled vesicles, intergrowths with anhydrite, calcite, and epidote, and inclusions in epidote. In many samples, grains of resorbed quartz occur in chlorite. Continuous, alternating layers of quartz with chlorite are also found in some vesicles.

Other minerals.—Anhydrite occurs sporadically in the Reykjanes and Svartsengi samples as an open space filling, intergrowths with calcite, chlorite, or quartz, and as elongated, isolated crystals up to 1 mm in length. Quartz lines the walls of some anhydrite-filled vesicles. No minor elements were detected in anhydrite during analysis.

Apatite is found below 1358 m in SG4 and near two aquifers in SG12, where it occurs as a pore space filling in masses of chlorite crystals, fracture filling, intergrowths with hematite and titanite, and as a replacement of primary plagioclase. Analyses indicate that the apatites are fluorine-rich ($X_{Ca_5(PO_4)_3F}$ = 0.65 to 0.95).

Halite is found only at 1462 m in SG4, where it occurs in a groundmass of chlorite and mantles titanite. The titanite contains cavities, and its grain surface is diffuse and embayed, indicative of dissolution (fig. 14).

DEPARTURES FROM EQUILIBRIUM

Disequilibrium between the fluid and secondary minerals may be due to kinetic factors that affect the rate of mass transfer of aqueous species from primary and secondary minerals (mineral surface area, porosity, mineral composition, catalysts or inhibitors to mineral reaction), hydrodynamic factors (fluid velocity, permeability), or perturbations in temperature and fluid composition. The irreversible mass trans-

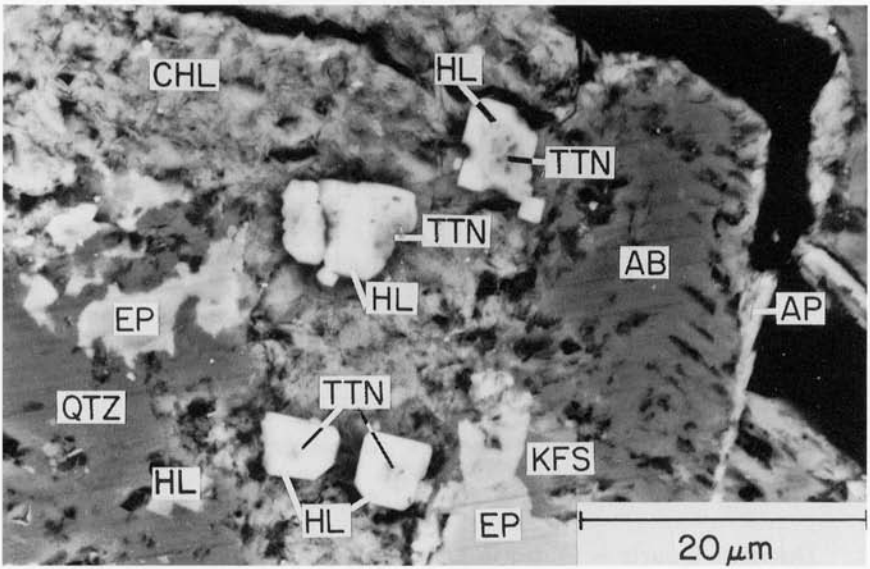

Fig. 14. Backscattered scanning electron image of halite mantling resorbed titanite from SG4, 1462 m depth. Black area in upper right hand corner is epoxy.

fer of species i from primary mineral r to the aqueous fluid is given by the equation (Lasaga, 1984);

$$\frac{dc_i}{dt} = q_i(t) + \frac{1}{\phi} R_{diss} = q_i(t) + \frac{A_r}{\phi} k_{diss} \prod_j a_j^m \left(1 - \frac{Q_i}{K_{eq}}\right)^n \qquad (1)$$

where dc_i/dt is the change in the concentration of species i ($molm^{-3}$) with time (s), $q_i(t)$ incorporates the external sources and sinks which add or subtract $molm^{-3}$ of i per unit time, ϕ is the porosity, R_{diss} is the dissolution rate law for primary mineral r ($molm^{-3}s^{-1}$), A_r is the reactive surface area of mineral r per unit volume of rock (m^2m^{-3}), k_{diss} is the overall dissolution rate constant for primary mineral r ($molm^{-2}s^{-1}$), a_j^m is the activity of species j raised to some power m, Q_i is the ion activity quotient for the mineral-fluid reaction, K_{eq} is the equilibrium ion activity quotient, and n is a real number (not necessarily an integer). The rate constant (k_{diss}) is considered to be consistent with transition state theory for elementary reactions and contains all the rate constants of the elementary reactions in the overall reaction (Lasaga 1981a,b). The term Πa_j^m incorporates the concentrations of surface-active solutes like H^+ which behave as catalysts or inhibitors to the mineral reaction.

As the solution approaches equilibrium, the concentrations of aqueous species are controlled by equilibrium with secondary phases (φ). The

net mass transfer rate of aqueous species i is given by the equation:

$$\frac{dc_i}{dt} = q_i(t) - \frac{1}{\phi} R_i = q_i(t) + \frac{1}{\phi} (R_{diss} - R_{ppt}) \quad (2)$$

where R_i is the sum of the reaction rate laws for all mineral-fluid reactions that involve i (dissolution minus precipitation of secondary mineral φ). The reaction rate is negative for dissolution (R_{diss}) and positive for precipitation (R_{ppt}).

The influence of fluid velocity (v) on mineral-fluid equilibrium can be evaluated by incorporating v into the chemical mass transport equation. In the one dimensional case, chemical mass transport of species i is given by the equation (Steefel and Van Capellen, 1990):

$$\frac{\partial(\phi c_i)}{\partial t} = - \frac{\partial(\phi v_x c_i)}{\partial x} + \frac{\partial}{\partial x}\left[D_h \frac{\partial(\phi c_i)}{\partial x} \right] - R_i \quad (3)$$

where v_x is the fluid velocity in direction x (ms^{-1}) and D_h (m^2s^{-1}) is the coefficient of hydrodynamic dispersion (sum of coefficients of mechanical dispersion and molecular diffusion). The average fluid velocity ($\bar{v}$) for one-dimensional laminar flow of a fluid of constant density between two parallel walls of a fracture is given by the equation (Helgeson, 1992):

$$\bar{v} = -\left(\frac{\rho g k}{\mu}\right) \frac{dh}{d\bar{x}} = -\left(\frac{\rho g b^2}{12\mu}\right) \frac{dh}{d\bar{x}} \quad (4)$$

where ρ is the fluid density (kgm^{-3}), g is the gravitational acceleration (9.8 ms^{-2}), k is the permeability of the material within the fracture (m^2), μ is the fluid viscosity ($kgm^{-1}s^{-1}$), $\bar{x}$ is the distance along the direction of flow in the open fracture (m), and b is the fracture width (m). The hydraulic head (h) is defined as

$$h = z + \frac{P_f}{\rho g} \quad (5)$$

where z is the elevation (m) where the hydraulic head is calculated and P_f is the fluid pressure ($kgm^{-1}s^{-2}$).

The solution of eq (3) at constant surface area, porosity, hydrodynamic dispersion, and fluid velocity with linear (n = 1 in eq 1) kinetics and a fixed position for a reaction front at τ is given by the equation (Lichtner, 1988):

$$c(x) = c_{eq} - (c_{eq} - c_\tau)\exp[-\gamma(x - \tau)] \quad (6)$$

where c(x) is the concentration of i in the fluid at position x, c_{eq} is the concentration of i in the fluid in equilibrium with mineral φ, c_τ is the

concentration of i in the fluid at the reaction front, and γ is defined as

$$\gamma = \begin{cases} \dfrac{k_\varphi}{v} & (D_h = 0,\ v \neq 0) \quad (7A) \\ \left(\dfrac{k_\varphi}{D_h}\right)^{1/2} & (D_h \neq 0,\ v = 0) \quad (7B) \\ \dfrac{v}{2D_h}\left[\left(1 + \dfrac{4D_h k_\varphi}{v^2}\right)^{1/2} - 1\right] & (D_h \neq 0,\ v \neq 0) \quad (7C) \end{cases}$$

The reaction front separates a region occupied by the mineral from a region where the mineral has completely dissolved. The reaction rate constant k_φ (s^{-1}) is defined as

$$k_\varphi = \frac{A_\varphi k_{diss}}{\phi c_{eq}} \tag{8}$$

where A_φ is the surface area of secondary mineral φ per unit volume of rock (m^2m^{-3}).

The minimum distance (x_{min}) that species i in the fluid reaches equilibrium with mineral φ (linear kinetics and constant A_φ, ϕ, D_h, and v) is given by:

$$x_{min} = -\gamma^{-1} \ln\left(1 - \frac{c(x)}{c_{eq}}\right) \tag{9}$$

Eq (9) is derived from eq (6) by setting the position of reaction front τ at $x = 0$ and assuming that $c_\tau/c_{eq} << 1$ (Kerrick, Lasaga, and Raeburn, 1991). There is a more rapid approach to mineral-fluid equilibrium and a shorter duration of reaction with larger reaction rate constants (k_φ) and hydrodynamic dispersion coefficients (D_h) or smaller fluid velocities (v) compared to cases with small k_φ and D_h and large v. This result is not surprising since the higher the fluid velocity and permeability, the shorter the time that the fluid is in contact with the reacting rock.

For non-linear kinetics ($n \neq 1$ in eq 1), the solution of eq (3) at constant A_φ, ϕ, and v and negligible D_h shows that no matter how large the value of k_φ, there is always a constant deviation from mineral-fluid equilibrium and a long duration of reaction depending on the values of n and v/k_φ and the elimination of reactant(s) (Kerrick, Lasaga, and Raeburn, 1991). There is a more rapid approach to mineral-fluid equilibrium and a shorter duration of reaction for linear ($n = 1$) kinetics (Kerrick, Lasaga, and Raeburn, 1991).

Thus, departures from equilibrium provide an important means of measuring the effects of reaction kinetics and hydrodynamic factors. The approach used in this paper is to examine first the state of equilibrium between coexisting mineral phases with textures, distribution of exchangeable elements, and mineral stability at the reservoir temperature. Depar-

tures from mineral-fluid equilibrium will next be assessed by computing saturation indices (Q_i/K_{eq}) of secondary minerals with the analyzed fluid compositions. At equilibrium, $Q_i/K_{eq} = 1$ (saturation). The Q_i/K_{eq} ratio exceeds 1 for supersaturated minerals and is less than 1 for undersaturated minerals (Reed and Spycher, 1984). The saturation indices of aluminosilicate minerals were not considered due to inaccuracy in the low concentrations of aqueous Al in the fluids and uncertainties in the stability constants for the aqueous aluminum complexes. Instead, the state of chlorite-fluid equilibrium is examined with the Fe^{2+}-Mg mineral-fluid exchange reaction.

Departures From Phase Equilibrium

Textures.—For grains of the same mineral in the same drill cutting, a departure from textural equilibrium is indicated by the following: (1) grains of the same mineral are not the same size in similar surroundings; (2) contacts between grains of the same mineral are not always planar; and (3) grains of the same mineral may indent each other. For grains of different minerals in the same drill cutting, a departure from textural equilibrium is defined by the absence of a consistent indentation or inclusion order.

There is no evidence in the samples for progressive textural changes such as a grain size increase with depth (temperature). Some vesicles, however, show evidence of progressive changes in chlorite crystallinity (crystallite size) from rim to core. At least one vesicle (SG12, 1252 m) even exhibits a decrease in crystallinity from rim to core. Textures such as vesicle and fracture fillings, overgrowths, mineral inclusions, and dissolution and replacement features are indicative of a complex history of varying temperature and salinity, kinetic factors that affect mass transfer rates, or both.

Element partitioning.—For coexisting minerals in the same drill cutting, the systematic distribution of exchangeable elements can be used to assess stable or metastable equilibrium. Figure 15 shows the temperature dependence of Fe^{3+} and Al partitioning between epidote and garnet as well as epidote and garnet compositions in the same drill cutting. None of the epidote and garnet grains in the same drill cutting was deposited at the same temperature. Most of the garnet compositions show little variation in $Fe^{3+}/(Fe^{3+} + Al)$ ratio and plot at intermediate compositions, whereas many epidote compositions are heterogeneous on the scale of a drill cutting. Garnets at 1462 m in SG4 are nearly pure andradite and do not plot with the other samples.

Phase stability.—Figure 16A to C shows the calculated compositional limits of the Ca-Fe^{3+}-Al minerals and plagioclase at the reservoir temperatures compared with analyzed compositions from the aquifers deep below the well casing. The compositional data near the large aquifer at 1354 m in RN9 are not considered because of the absence of data below 1352 m. The compositional limits of the Ca-Fe^{3+}-Al minerals were calculated with the thermochemical data and activity models in tables 7

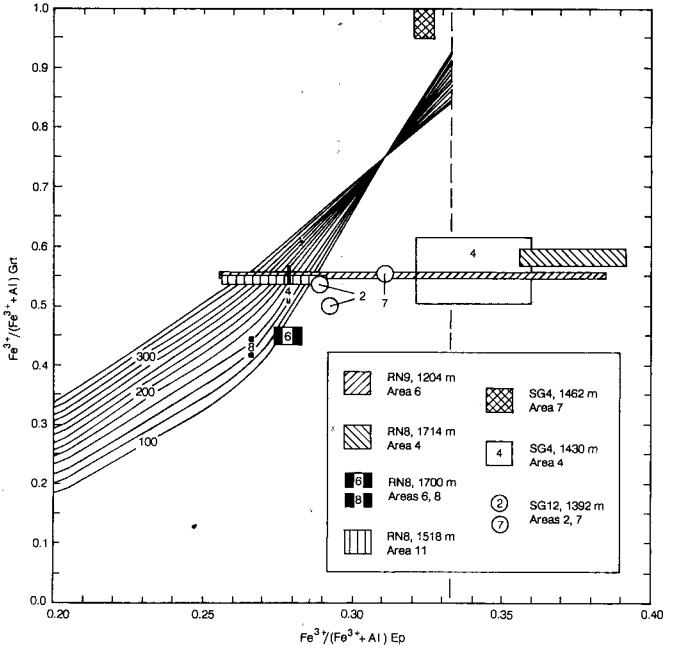

Fig. 15. Plot of the $Fe^{3+}/(Fe^{3+} + Al)$ ratio in epidote versus the $Fe^{3+}/(Fe^{3+} + Al)$ ratio in garnet contoured as a function of temperature. Isotherms are calculated with the thermochemical data in table 7 and the activity models in table 8. Dashed line shows the "compositional limit" of one Fe^{3+} atom per formula unit. Also shown is the range of epidote and garnet compositions within a drill cutting. Most areas contain one drill cutting. Two areas (SG4, 1430 m, area 4; SG12, 1392 m, area 2) contain two drill cuttings with epidote and garnet.

and 8 by simultaneous solution of logK expressions for intercrystalline Fe^{3+}-Al exchange reactions (Ep-Grt, Ep-Prh), intracrystalline Fe^{3+}-Al exchange in epidote, and hydrolysis reactions (Ep-Grt, Ep-Prh, Ep-Pl, Prh-Pl, Grt-Pl). The two phase assemblage prehnite + garnet is not stable at the reservoir temperatures. The calculations were carried out at the reservoir temperature until $\log(a_{Ca^{2+}}/a_{H^+}^2)$ converged to the average value in the reservoir fluid. Table 2 shows there is little variation in total Ca^{2+} molality in RN8, RN9, and Svartsengi reservoir waters. The compositions of analyzed epidote and sodic feldspar grains overlap with the calculated compositions and are stable at the reservoir temperatures and $\log(a_{Ca^{2+}}/a_{H^+}^2)$ ratios (fig. 16A-C). With the exception of andradite-rich garnet at 1462 m depth in SG4 (fig. 16C), the analyzed garnet and prehnite compositions do not overlap with the calculated compositions and are not stable at the reservoir temperatures and $\log(a_{Ca^{2+}}/a_{H^+}^2)$ ratios. Calculation of anatase/titanite stability indicates that titanite is the stable Ti mineral at the reservoir temperatures and $\log(a_{Ca^{2+}}/a_{H^+}^2)$ ratios. Addi-

tional evidence for phase disequilibrium includes such features as the presence of primary minerals even in the most extensively altered samples, compositional heterogeneity on the scale of a drill cutting, and compositional zoning in epidote and garnet.

Departures From Mineral-Fluid Equilibrium

Saturation indices and the phase diagrams in this section were computed with the thermochemical data and activity models in tables 7 and 8, respectively.

Anhydrite and quartz.—Studies by Arnórsson and coworkers (Arnórsson, 1978; Arnórsson, Grönvold, and Sigurdsson, 1978; Pálmason and others, 1979; Arnórsson, Gunnlaugsson, and Svavarsson, 1983a; Gíslason and Arnórsson, 1990) and Reed and Spycher (1984) have shown that the Reykjanes and Svartsengi reservoir waters are saturated with anhydrite and quartz.

Calcite.—Calcite solubility is more sensitive than other minerals to small errors in gas add-back and pH, so there may be some uncertainty in the degree of calcite super- or undersaturation. The Svartsengi reservoir waters are saturated (SG 6,7,8,11) or slightly supersaturated (SG4) with respect to calcite (fig. 17). Calcite scale has been deposited in Svartsengi wells since production began (Kristmannsdóttir, 1989; Líndal, 1989), so the Svartsengi waters are calcite saturated. Reykjanes reservoir waters are slightly supersaturated (RN8) or undersaturated with calcite (RN8,9) (fig. 17). No calcite scale has been deposited in RN8 and RN9 since production began (Kristmannsdóttir, 1989; Líndal, 1989), so the Reykjanes reservoir waters are really calcite undersaturated. Calcite undersaturation is probably due to the increase in calcite solubility with increasing salinity (Ellis, 1963) as well as anhydrite precipitation at elevated temperatures, which results in a lowering of the Ca^{2+} concentration in the thermal brine. Arnórsson (1978), Arnórsson, Grönvold, and Sigurdsson (1978), and Arnórsson, Gunnlaugsson, and Svavarsson (1983a) found that their calculated $CaCO_3$ activity product for the Reykjanes reservoir (RN8) was calcite-supersaturated. Reed and Spycher (1984), however, used a RN8 gas and water analysis taken from Arnórsson, Gunnlaugsson, and Svavarsson (1983a) and found calcite undersaturation. This inconsistency may be due to uncertainties with thermochemical data (Reed and Spycher, 1984), two phase (liquid + steam) calculated used by Arnórsson and coworkers which overestimates pH, or both.

Al-K-Na minerals.—Sveinbjörnsdóttir (1983a) and Ragnarsdóttir, Walther, and Arnórsson (1984) plotted the RN8 and SG4 initial discharge compositions, respectively, on $\log(a_{Na^+}/a_{H^+})$ versus $\log(a_{K^+}/a_{H^+})$ diagrams. The reservoir compositions fall close to the metastable extension of the albite + K-feldspar boundary within the illite stability field. This illite stability field is affected by other activities (Al^{3+}, Fe^{2+}, Fe^{3+}, and Mg^{2+}), so saturation indices are used to test for mineral-fluid equilibrium. Saturation indices show that the reservoir waters from RN8, RN9, SG4, SG6, SG7, SG8, and SG11 are saturated with albite, illite, and

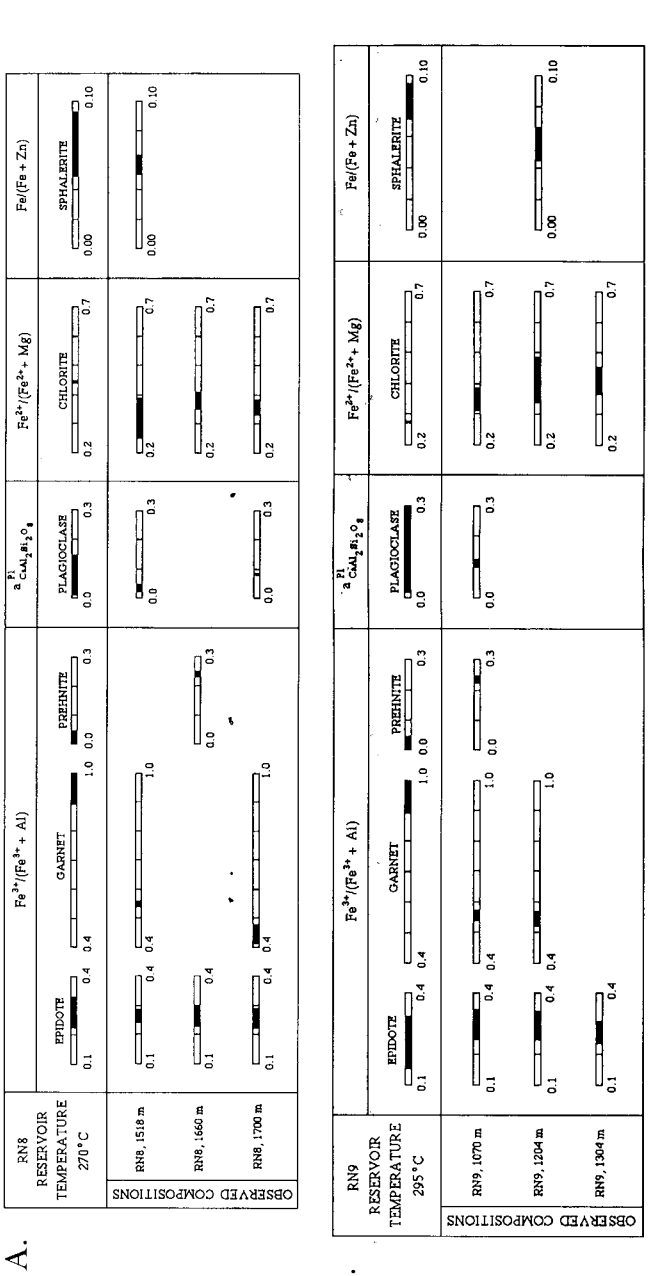

Fig. 16. Comparison of compositional limits of solid solution minerals at the reservoir temperatures with observed mineral compositions in samples near the aquifers (locations in fig. 5A–D). Calculation procedures of compositional limits of solid solution minerals are described in the text. (A) 270°C (RN8); (B) 295°C (RN9); and (C) 240°C (SG4 and SG12).

C.

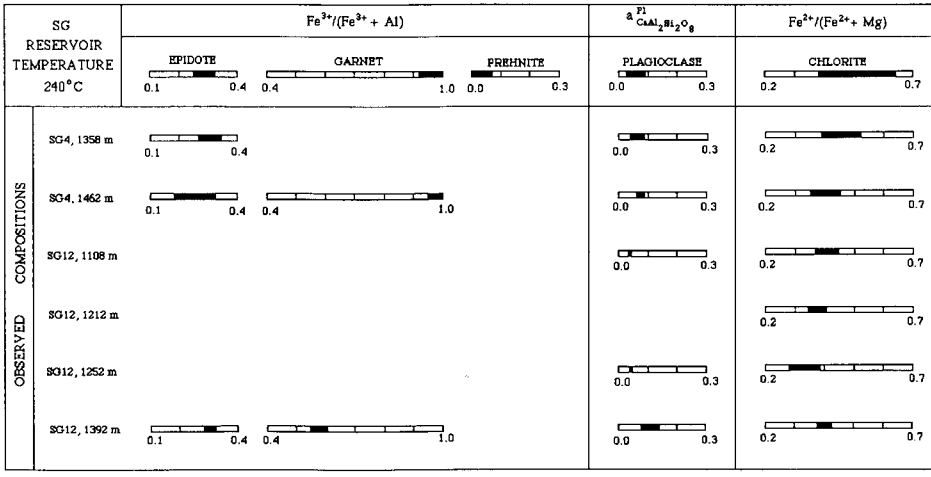

Fig. 16 (continued)

K-feldspar. Reed and Spycher (1984) also found that the RN8 reservoir fluid is saturated with albite, illite, and K-feldspar. No K-micas, however, were observed in this study in any of the Reykjanes and Svartsengi wells.

Chlorite.—The composition of chlorite coexisting with the reservoir fluid is calculated from measured values of $\log(a_{Fe^{2+}}/a_{Mg^{2+}})$ in the reservoir fluid and the logK expression for Fe^{2+}-Mg exchange between coexisting chlorite and fluid. None of the analyzed Reykjanes chlorite compositions overlaps with the chlorite compositions coexisting with the reservoir fluid (fig. 16A,B). The analyzed Svartsengi chlorite compositions overlap with the chlorite compositions coexisting with the reservoir fluid indicating that there is probably chlorite-fluid equilibrium (fig. 16C).

Fe-bearing minerals.—The predicted stabilities of iron-bearing minerals in Icelandic geothermal systems were initially investigated by Gunnlaugsson and Arnórsson (1982), who suggested that the fluids in the high temperature systems were in equilibrium with pyrite + anhydrite. Arnórsson and Gunnlaugsson (1985) found that anhydrite was not part of the mineral assemblage due to an absence of redox equilibrium between sulfide and sulfate. They proposed that pyrite + magnetite + epidote + prehnite or pyrite + epidote + prehnite + chlorite controlled H_2S and H_2 concentrations in the high temperature saline waters. It has been shown that the observed prehnite compositions are not stable at the Reykjanes reservoir temperatures and $\log(a_{Ca^{2+}}/a^2_{H^+})$ ratios.

Initial discharge compositions in the Reykjanes and Svartsengi systems are plotted on $\log(f_{H_2S})$ versus $\log(f_{H_2})$ diagrams (fig. 18A-C). The total discharge compositions for RN8 lie close to the intersection of the

TABLE 7

Sources of thermochemical data

Phases		Sources of Data
Minerals	albite, anhydrite, andradite, anorthite, calcite	a
	clinochlore, clinozoisite, epidote, grossular	
	hedenbergite, grossular, hedenbergite, hematite	
	K-feldspar, magnetite, prehnite, pyrite, quartz	
	wollastonite	
	anatase	b
	daphnite	c
	illite	d
	Fe^{3+}-prehnite	e
	titanite	f
Aqueous species	Al^{3+}, Ca^{2+}, Fe^{2+}, Fe^{3+}, H^+, K^+, Na^+, Mg^{2+}	g
Neutral inorganic species	$CO_2°$, $H_2°$, $H_2S°$, $SiO_2°$	h
	$H_2O°$	i
Vapor Phases	$CO_2°(v)$, $H_2°(v)$, $H_2S°(v)$	a

a–Helgeson and others (1978); b–Robie, Hemingway, and Fisher (1978); c–$H^\circ_{f,298.15}$ extracted from James, Turnock, and Fawcett (1976), $S^\circ_{298.15}$ and heat capacity from Walshe (1986); d–Reed and Spycher (1990); e–Rose and Bird (1987); f–Holland and Powell (1985); g–Shock and Helgeson (1988,–1989); h–Shock, Helgeson, and Sverjensky (1989); i–Helgeson and Kirkham (1974)

magnetite + pyrite, epidote + pyrite + chlorite, and epidote + magnetite + chlorite boundaries (fig. 18A). Reed and Spycher (1984) predicted that the RN8 reservoir fluid was saturated with chlorite, epidote, and pyrite at the reservoir temperature. Most of the RN9 reservoir waters plot in the epidote + magnetite field (fig. 18B). Activities of daphnite are reduced in the Reykjanes chlorites, which would expand the Fe^{2+}-chlorite field at the expense of the epidote + magnetite field in figure 18A and B. The Svartsengi reservoir waters plot close to the intersection of the hematite, Fe^{2+}-chlorite, and pyrite fields (fig. 18C). Some compositions from SG4 and 6 are saturated with hematite (fig. 18C).

In contrast to the present study, Ragnarsdóttir, Walther, and Arnórsson (1984) omitted the Fe^{2+}-chlorite field on a $\log(f_{H_2S})$ versus $\log(f_{H_2})$ diagram, so their SG4 reservoir composition plotted near the magne-

TABLE 8

Activity-composition relations for the components of silicate solid solutions

Mineral	Activity-Composition Relation
chlorite	$a_{Mg_5Al_2Si_3O_{10}(OH)_8,Chl} = 141.56(X_{Mg}^{VI})^5(X_{Al}^{VI})(X_{Al}^{IV})(X_{Si}^{IV})^3$
	$a_{Fe_5Al_2Si_3O_{10}(OH)_8,Chl} = 141.56(X_{Fe^{2+}}^{VI})^5(X_{Al}^{VI})(X_{Al}^{IV})(X_{Si}^{IV})^3$
	$a_{Mg_6Si_4O_{10}(OH)_8,Chl} = (X_{Mg}^{VI})^6(X_{Si}^{IV})^4$
	$a_{Al_4Si_4O_{10}(OH)_8,Chl} = 45.56(X_{Vac}^{VI})^2(X_{Al}^{VI})^4(X_{Si}^{IV})^4$
epidote[a]	
	$a_{Ca_2Al_3Si_3O_{12}(OH),Ep} = (X_{Ca}^{VII})^2(X_{Al}^{M(1)})(X_{Al}^{M(2)})(X_{Al}^{M(3)})(X_{Si}^{IV})^3(X_{OH})$
	$a_{Ca_2FeAl_2Si_3O_{12}(OH),Ep} = k(X_{Ca}^{VII})^2[(X_{Al}^{M(1)})(X_{Fe^{3+}}^{M(3)})]^{(1+\sigma)/2}[(X_{Al}^{M(3)})(X_{Fe^{3+}}^{M(1)})]^{(1-\sigma)/2}(X_{Si}^{IV})^3(X_{OH}$
garnet	
	$a_{Ca_3Al_2Si_3O_{12},Grt} = (X_{Ca}^{VIII})^3(X_{Al}^{VI})^2$
	$a_{Ca_3Fe_2Si_3O_{12},Grt} = (X_{Ca}^{VIII})^3(X_{Fe^{3+}}^{VI})^2$
	$a_{Fe_3Al_2Si_3O_{12},Grt} = (X_{Fe^{2+}}^{VIII})^3(X_{Al}^{VI})^2$
	$a_{Mg_3Al_2Si_3O_{12},Grt} = (X_{Mg}^{VIII})^3(X_{Al}^{VI})^2$
	$a_{Mn_3Al_2Si_3O_{12},Grt} = (X_{Mn}^{VIII})^3(X_{Al}^{VI})^2$
K-feldspar	
	$a_{KAlSi_3O_8,Kfs} = X_{KAlSi_3O_8}$
	$a_{NaAlSi_3O_8,Kfs} = X_{NaAlSi_3O_8}$
plagioclase	
	$a_{NaAlSi_3O_8,Pl} = X_{NaAlSi_3O_8}$
	$a_{CaAl_2Si_2O_8,Pl} = X_{CaAl_2Si_2O_8}$
	$a_{KAlSi_3O_8,Pl} = X_{KAlSi_3O_8}$
prehnite	
	$a_{Ca_2Al_2Si_3O_{10}(OH)_2,Prh} = X_{Al}^{VI}$
	$a_{Ca_2FeAlSi_3O_{10}(OH)_2,Prh} = X_{Fe^{3+}}^{VI}$

a The ordering parameter σ and the constant k are defined by equations and data given in Bird ar Helgeson (1980).

tite + pyrite boundary. They did not observe hematite at 1430 m in SG4 and identified all magnetite as secondary. The results in this study also differ from Heinrich and Seward (1990), who plotted two analyses labeled "Reykjanes" from Arnórsson, Gunnlaugsson, and Svavarsson (1983a) on the K-feldspar + muscovite + albite + quartz + pyrite + pyrrhotite + magnetite curve as a function of log[Fe_t] and [Cl_t]. One of these analyses, however, is from SG4, the other from RN8. Moreover,

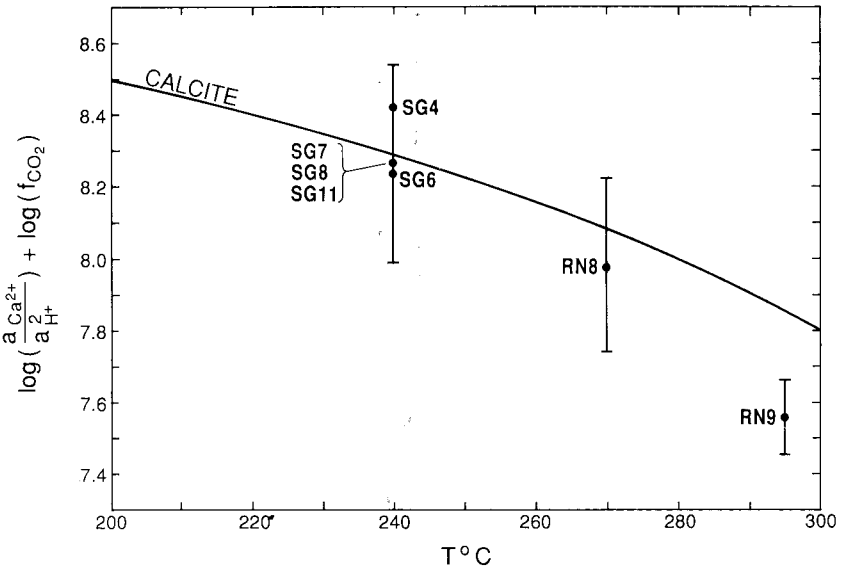

Fig. 17. $\text{Log}(a_{Ca^{2+}}/a^2_{H^+}) + \log(f_{CO_2})$ versus temperature (°C) showing the calcite saturation curve and initial discharge compositions in RN8 and RN9 and SG 4, 6, 7, 8, and 11. The brackets show the range in total discharge compositions, and the solid circle gives the average total discharge composition for each well.

muscovite and pyrrhotite do not even occur in the studied systems, and magnetite has a complex history of exsolution-oxidation and subsequent replacement by alteration minerals.

Sphalerite.—The saturation index of sphalerite could not be calculated due to the absence of analytical data on aqueous Zn^{2+}. Instead, the composition of sphalerite coexisting with the reservoir fluid is extracted from figure 18A and B and is compared with the analyzed compositions in figure 16A and B. The analyzed sphalerite composition from a RN8 aquifer is probably in equilibrium with the reservoir fluid (fig. 16A). Sphalerite from a RN9 aquifer, however, has a lower Fe-content than the sphalerite composition coexisting with the reservoir fluid (fig. 16B).

Summary.—The most important result of this section is that mineral-mineral and mineral-fluid disequilibrium is extensive in most of the Reykjanes and Svartsengi samples. Some minerals (epidote, sodic plagioclase, titanite) are stable at the reservoir temperatures and $\log(a_{Ca^{2+}}/a^2_{H^+})$ ratios. Other minerals (anhydrite, quartz, sphalerite in RN8, calcite and chlorite in Svartsengi) are in equilibrium with the reservoir fluid indicating local equilibrium among several phases during certain periods of time. In contrast to the present study, Sveinbjörnsdóttir (1983a, 1992) and Ragnarsdóttir, Walther, and Arnórsson (1984) found that the secondary minerals approached equilibrium with the reservoir fluids in RN8

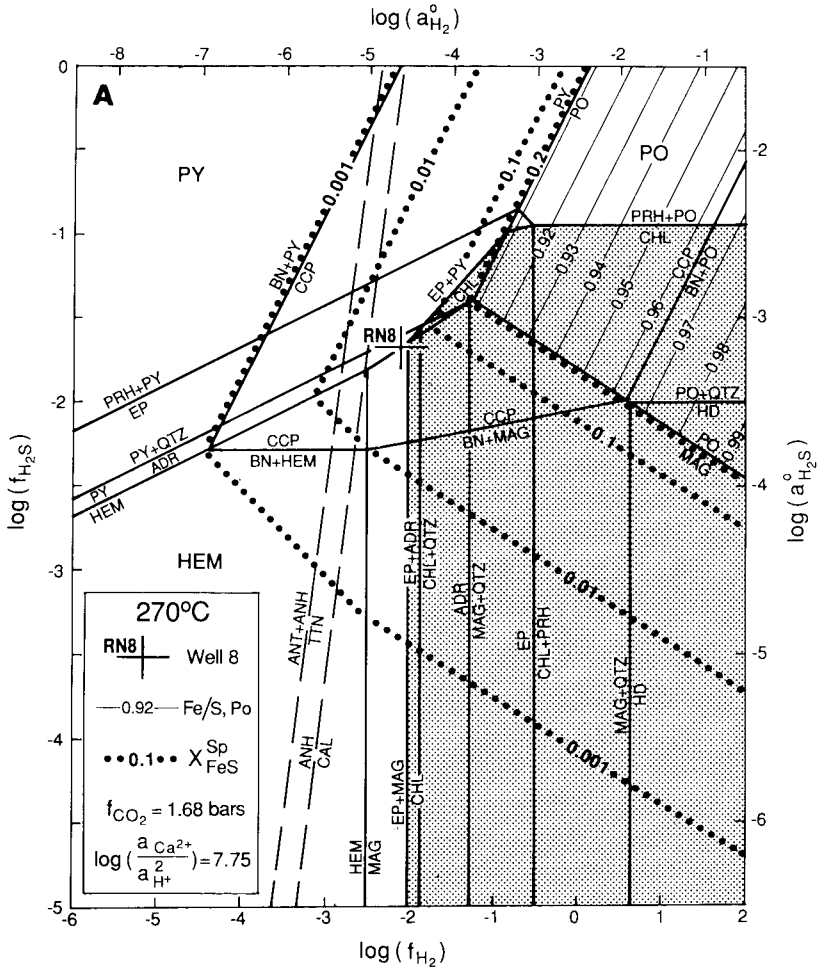

Fig. 18. Log(f_{H_2S}) versus log(f_{H_2}) showing range of initial discharge compositions and phase relations for pure endmembers at (A) 270°C, log ($a_{Ca^{2+}}/a^{2}_{H^+}$) = 7.75 (RN8); (B) 295°C, log ($a_{Ca^{2+}}/a^{2}_{H^+}$) = 7.17 (RN9); and (C) 240°C, log ($a_{Ca^{2+}}/a^{2}_{H^+}$) = 8.3 (SG 4, 6, 7, 8, 11). The stippled area shows the stability field for Fe^{2+}-chlorite. The pyrrhotite + pyrite equilibrium boundary at 240°C is from Barton, Bethke, and Roeder (1977) and at higher temperatures from Toulmin and Barton (1964). Isopleths of Fe/S (atomic) in pyrrhotite and X_{FeS} in sphalerite are from Barker and Parks (1986) and Scott and Barnes (1971), respectively. The chalcopyrite + bornite + pyrite equilibrium curve is from Schneeberg (1973).

and SG4 (1430 m), respectively. Sveinbjörnsdóttir (1983a, 1992) concluded that chlorite and epidote were in equilibrium based on the Al distribution, which is surprising given the complexity of the solid solutions and textural evidence for epidote dissolution and chlorite overgrowth. Reasons for disequilibrium will be explored in the next section.

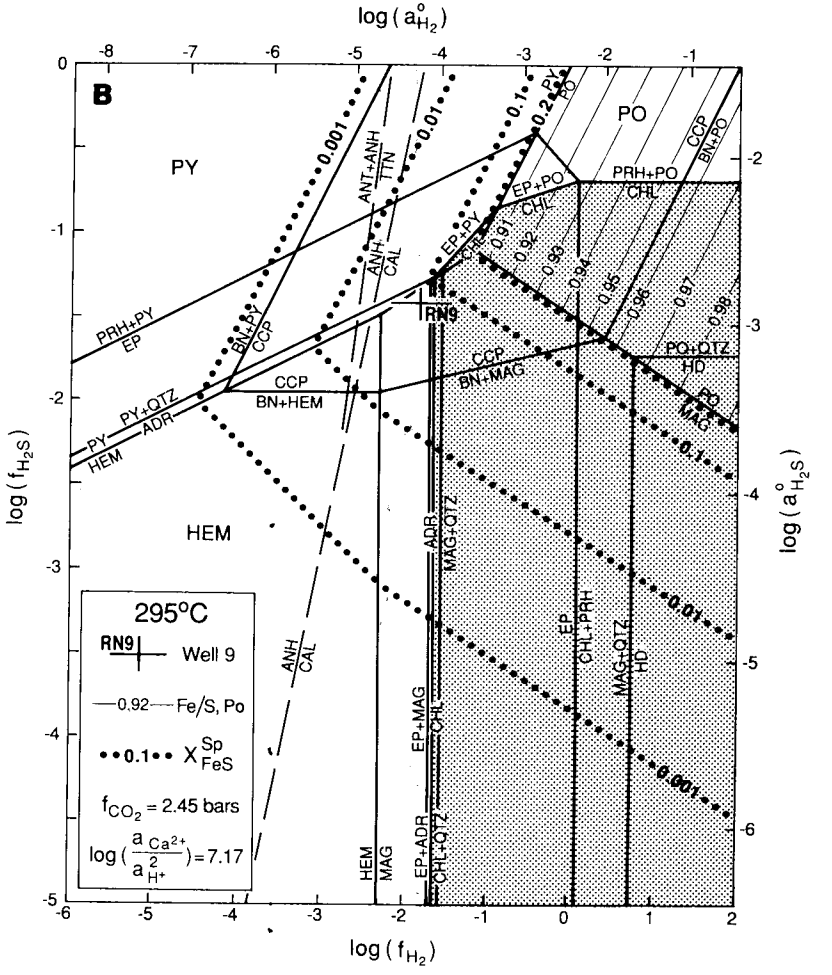

Fig. 18 (continued)

Hematite occurs in several Reykjanes aquifers and is particularly abundant in many SG4 and SG12 aquifers. Hematite, titanite, or both replace Ti-poor and titanomagnetite in many samples. Clearly, there has been a shift of the Reykjanes and Svartsengi waters into the hematite stability field.

There is no unequivocal mineralogical and textural evidence in support of a shift of the reservoir waters out of the feldspar stability field and into the illite stability field. No illite was observed, and there is uncertainty regarding the origin of dissolution textures in the secondary feldspars. Feldspar dissolution may have occurred during replacement of

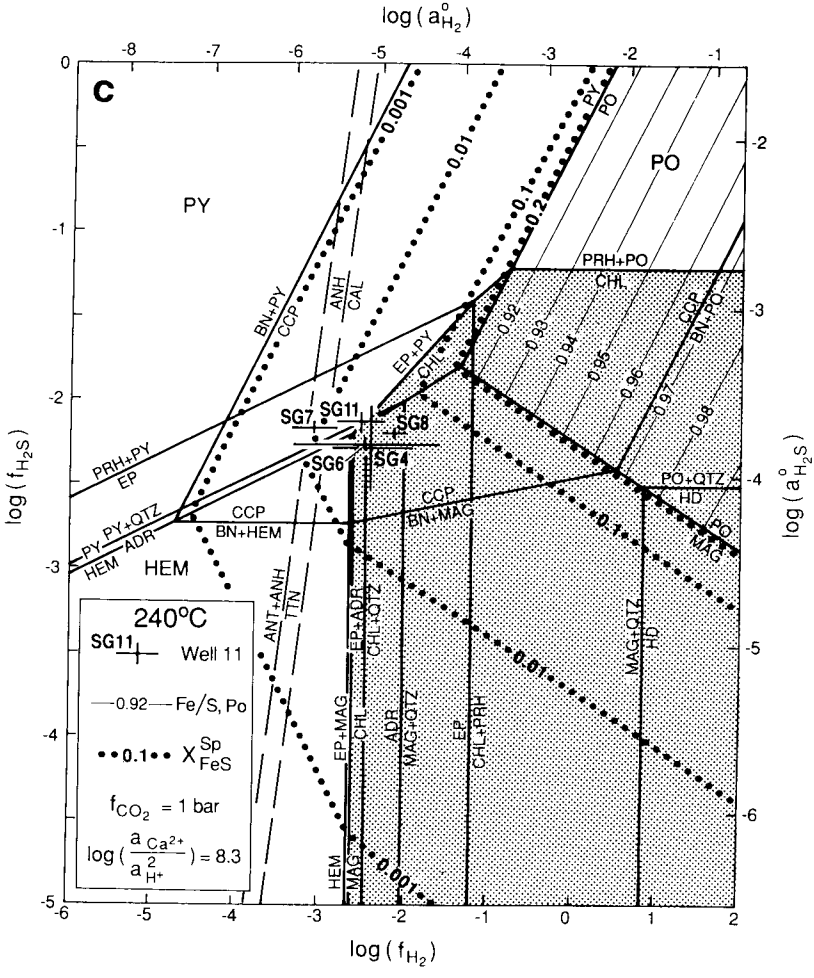

Fig. 18 (continued)

primary plagioclase, after secondary feldspar precipitation during a shift out of the feldspar stability field, or both. The inconsistency of observed and reservoir Al-K-Na minerals may reflect poor thermochemical data for illite, spatial-temporal heterogeneity in fluid composition and temperature, or a kinetics control.

FLUID FLOW

The key to understanding the evolution of the geothermal systems is the identification of the physico-chemical and kinetics variables that produce complexities in parageneses and fluctuations in mineral compo-

sition even on the scale of a drill cutting. Clearly, not all trends in mineral composition with formation permeability are consistent and systematic. Evidence for widespread phase and mineral-fluid disequilibrium has been presented. Some compositional heterogeneity is related to mixing of drill cuttings within the 5 to 10 m depth interval producing some loss in spatial and temporal control of samples. Other textures and compositional variations may be due to nonequilibrium processes. This section will show which textures and compositional trends reflect variations in the physico-chemical conditions of fluid-rock interaction. Geothermometry is used to examine if thermal gradients are maintained at a steady state during alteration.

Many of the sampled aquifers in RN8 and RN9 lie near hyaloclastite-basalt contacts (fig. 5A and B). Some of the hyaloclastite units are too thin to depict in the stratigraphic columns in figure 5A and B. Most of the sampled aquifers in SG4 and SG12 occur along intrusive contacts (fig. 5C and D; Franzson, 1983a,b). No geologic structures occur near the following aquifers: 1705 and 1741 m in RN8; 1289, 1310, and 1354 m in RN9; 1240 and 1360 m in SG4; and 1109 and 1216 m in SG12.

Hotter Aquifers

The degree of preservation of primary textures, abundance of fracture and vesicle fillings, quantity and type of secondary minerals, and mineral compositions show changes near many of the aquifers. Difficulties do arise, however, when examining compositional changes in cuttings where aquifers are closely spaced (below 1646 m in RN8). Olivine and glass are completely altered, and there is an increase in the alteration intensity of primary plagioclase and Fe-Ti oxides near many aquifers. Chlorite compositions have higher $(Fe^{2+}/(Fe^{2+} + Mg)$ ratios and lower Si contents near most aquifers in RN9. This relationship of chlorite composition with formation permeability is not as well-defined in other wells. Moreover, there is compositional heterogeneity in chlorite, epidote, hematite, and titanite, and an increase in the abundance of calcite, epidote, hematite, and pyrite near many of the aquifers compared to less permeable formations.

Chlorite is paragenetically late in many of the samples, so that any geothermometer using chlorite composition should provide temperatures characteristic of the more recent history of the two geothermal systems. The chlorites in the Svartsengi wells are probably in chemical equilibrium with the reservoir fluid. Figure 19A to D shows temperatures calculated with the chlorite geothermometer of Jowett (1991), which relates measured down-hole temperatures from wells in the Salton Sea, California and Los Azufres, Mexico geothermal systems with tetrahedral Al (Al^{IV}) and $Fe^{2+}/(Fe^{2+} + Mg)$ in chlorite. There are, however, uncertainties with this geothermometer, so that the relative changes in temperature are important and not the actual estimates of temperature. These uncertainties include temperature calibration, mineral assemblage, the effect of interlayered smectite in the calibration samples, and the role of

Fe^{3+} in chlorite. The extent of Fe^{3+} substitution and the substitution mechanism in the calibration and analyzed samples are unknown. Ten percent substitution of Fe^{3+} for tetrahedral Al could reduce the temperature estimate by 30°C. Nevertheless, it will be shown that there is a correlation of temperatures derived from chlorite compositions with a measured temperature inversion in SG12, with the location of hotter aquifers in RN9, and with grain size and smectite content in chlorite-filled vesicles. These temperatures derived from chlorite compositions are probably equilibrium temperatures. Other chlorite compositions could be metastable producing nonequilibrium temperatures. These nonequilibrium temperatures derived from chlorite compositions may even be in excess of 300°C exceeding the measured temperatures and even falling on the hydrostatic boiling curve.

The temperatures derived from chlorite compositions near the more permeable formations at 1660 m in RN8 and at 1052, 1210, 1289, and 1309 m in RN9 are higher relative to less permeable formations stratigraphically above and below (fig. 19A and B). The pattern of temperatures derived from chlorite compositions near the more permeable formations at the base of RN8 (1742 m) and RN9 (1354 m) could not be ascertained because there are no samples from greater depths. The correlation of temperatures derived from chlorite compositions with formation permeability in RN9 is indicative of anisotropic permeability and a poorly mixed fluid. In many Reykjanes samples, there is a large range in temperatures derived from chlorite compositions (100°-320°C) as well as compositional heterogeneity in chlorite grains on the scale of a drill cutting.

Most of the temperatures derived from chlorite compositions in SG4 and SG12 fall in a temperature range of 200° to 300°C (fig. 19C and D). There are, however, lower chlorite temperatures in SG4 at 1204 and 1259 m. The smaller chlorite temperature distribution in most Svartsengi samples compared to the Reykjanes samples is not surprising since the range in tetrahedral Al is smaller in most Svartsengi chlorite grains (0.8-1.2) compared to Reykjanes chlorite grains (0.4-1.2) (fig. 8A-D). It is the Al^{IV} content that shows a systematic correlation with temperature in the chlorite geothermometer. Chlorite compositions from 1204 and 1259 m in SG4 overlap the Mg- and Si-rich Reykjanes chlorite compositions and may have precipitated at lower temperatures, represent metastable compositions, or both. The spatial distribution of temperatures derived from chlorite compositions in most Svartsengi samples suggests chlorite precipitation over a narrower temperature range and, thus, more isotropic permeability than the Reykjanes samples.

The $FeMg_{-1}$ and $Al_2Si_{-1}Mg_{-1}$ components in chlorite increase with decreasing pH and H_2S/H_2 ratio (Lonker and others, 1990). Many chlorite grains in RN9 aquifers show an increase in $FeMg_{-1}$ and $Al_2Si_{-1}Mg_{-1}$ compared to the samples stratigraphically above and below. Hematite grains show a decrease in Fe_2O_3-content near the large aquifer at 1360 m in SG4. These observations indicate the presence of a more

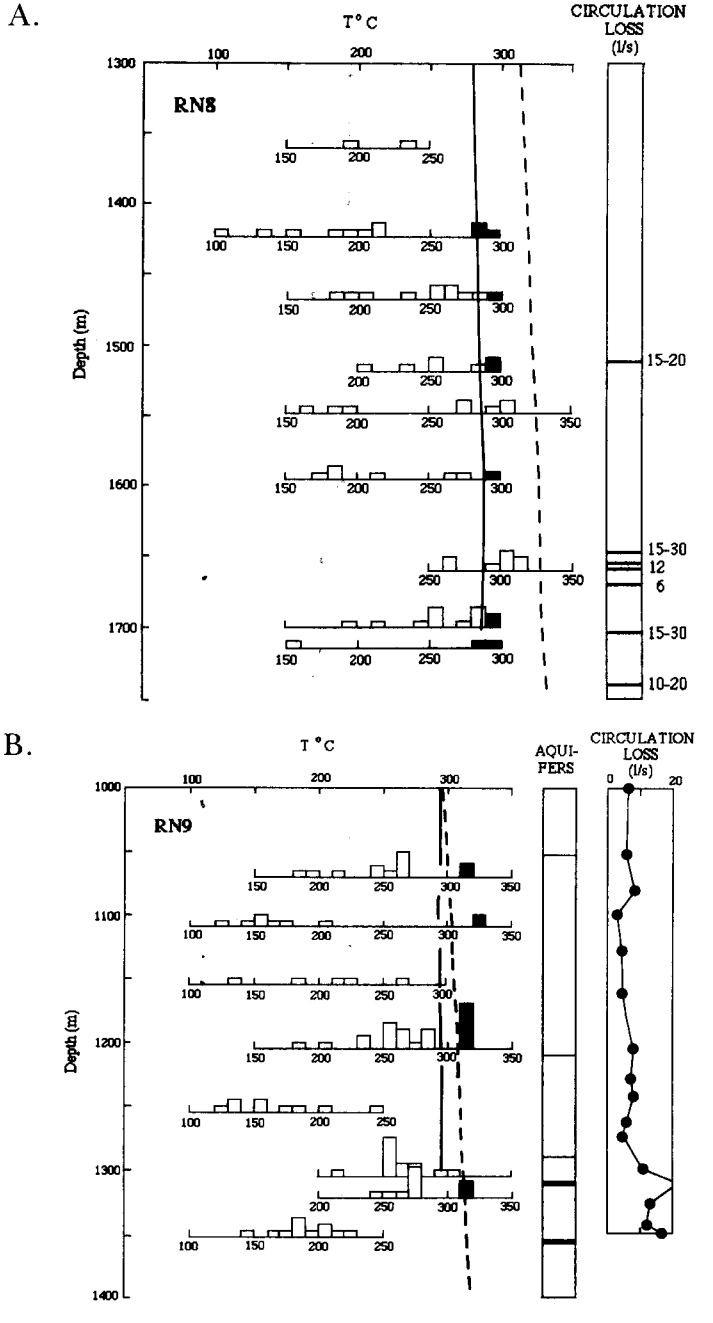

Fig. 19. Plots of T°C versus depth (meters) showing the measured temperatures (solid line), hydrostatic boiling curve for H_2O-NaCl liquid (dashed line), aquifers and circulation losses, temperatures calculated from the empirical chlorite geothermometer of Jowett (1991) (open boxes), and minimum stability temperatures for analyzed garnet compositions (solid boxes). (A) RN8, (B) RN9, (C) SG4, and (D) SG12.

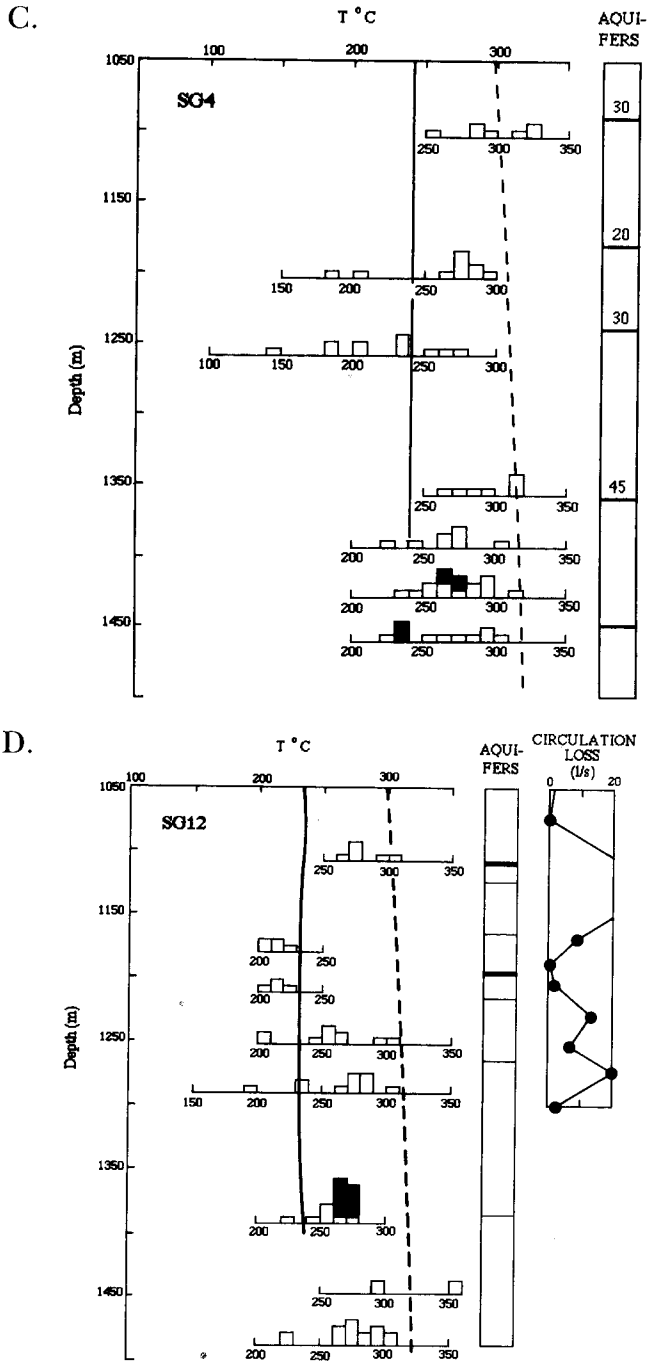

Fig. 19 (continued)

reduced, lower-pH fluid in the aquifers. Thus, the absence of chlorite-fluid equilibrium in RN9 is probably due to spatial/temporal heterogeneity in fluid composition, temperature, or both. Figure 19A and B show that the measured temperatures in RN8 and RN9 are close to the hydrostatic boiling curve. Calculations using the program CHILLER (Reed, 1982) reveal that isoenthalpic boiling and subsequent cooling of the RN8 (sample number 233) and RN9 (sample number 262) reservoir compositions produce increases in pH and H_2S/H_2, early chlorite and calcite precipitation, K-feldspar and quartz saturation, later calcite undersaturation and quartz supersaturation, and a decrease in $FeMg_{-1}$ in chlorite. Boiling probably did not occur in the Reykjanes aquifers for K-feldspar and calcite are absent or scarce (<5 volume percent) in samples near the more permeable formations (fig. 5A and B). The low abundance of K-feldspar is probably related to bulk composition. Moreover, some calcite and quartz grains in the Reykjanes samples are resorbed and overgrown by Mg-rich chlorite. A high salinity brine may have been produced by localized boiling along an intrusive contact at 1462 m in SG4 (fig. 5C), where halite mantles titanite (fig. 14).

In the more permeable formations, there is extensive alteration of primary minerals, an abundance of secondary minerals, an increase in fracture and vesicle fillings, and compositional heterogeneity in solid solution minerals. These observations indicate an increase in chemical reaction rates and a long history of self-sealing, fracturing, and fluid discharge in the more permeable formations.

Cooler Aquifers

Temperatures derived from chlorite compositions decrease in the vicinity of a major aquifer at 1195 m and smaller aquifers at 1165 and 1216 m in SG12 (fig. 19D). Trends in chlorite composition and epidote abundance are the opposite in this depth interval. Chlorite grains have a larger Si and Ca content relative to chlorite in less permeable formations stratigraphically above. There is also a scarcity of epidote in this depth interval. These aquifers also have features in common with other aquifers such as an increase in alteration intensity of primary plagioclase and Fe-Ti oxides as well as an increase in the abundance of calcite and pyrite. Epidote would probably not be stable in a cooler water incursion which explains the low abundance of epidote. Moreover, the larger Ca and Si contents in the chlorite are probably indicative of a larger trioctahedral smectite content lending further support to a cooler water incursion. No fine-grained intergrowths of these chlorites with Ca-bearing minerals were observed with scanning electron microscopy. Finally, the measured temperatures show a temperature inversion in SG12 of less than 5°C between 1100 and 1360 m (Björnsson and Steingrímsson, 1991). These cooler water incursions probably flowed along the contact of a dolerite intrusion since the sample at 1212 m is only 2 m from an intrusive contact (Franzson, 1983b). No evidence of contact metamorphism was observed.

Mixed layer smectite/chlorite has been identified with X-ray diffraction at 1704 and 1708 m in RN8 (Kristmannsdóttir, 1971, 1976b; Svein-

björnsdóttir, 1983a), close to a permeable formation at 1705 m. The trends in secondary mineral compositions and chlorite temperatures, however, do not support a temperature inversion near this aquifer. Other occurrences of mixed layer phyllosilicates in the chlorite + epidote zone could be related to incomplete transformation of smectite-to-chlorite in less permeable formations.

Fluid Incursions

The distribution of some secondary minerals and mineral compositions indicates that waters with different temperatures and salinities have percolated through fractures in less permeable formations as well as in aquifers. Anhydrite forms during the initial stages of seawater-basalt reaction (Mottl, Holland, and Corr, 1979) and during heating of cold seawater (Tómasson and Kristmannsdóttir, 1972). Precipitation of anhydrite also occurs in meteoric waters (Krafla and Nesjavillir geothermal systems, Iceland), but the source of SO_4^{2-} is unknown. Fluid inclusions indicate that some of the anhydrites in SG12 (834 m, 1314 m) were deposited from waters that are less saline and hotter (up to 15°C) compared to the present reservoir composition and temperature (Franzson, 1990).

Several observations indicate that the Reykjanes waters have a more complex history of changing temperatures and salinities than the Svartsengi waters. Most of the Reykjanes chlorites have precipitated over a larger temperature range than the Svartsengi chlorites. Reykjanes well 8 chlorites are more Mg-rich than chlorites in equilibrium with the reservoir composition. The Mg-rich chlorites in RN8 and in RN9 precipitated at lower temperatures (fig. 19A and B). Experimental studies (Mottl, 1983) and computer modeling (Reed, 1983) show that in the early stages of seawater-basalt interaction, Mg^{2+} is removed from seawater producing H^+ and Mg-rich chlorite. Magnesium-rich chlorite is also precipitated during mixing of seawater with the acidic thermal brine, which raises pH and $m_{SO_4^{2-}}$. Seawater incursions were probably more extensive in RN8 than RN9 due to permeability differences and distance from the upflow zone.

Sulfur isotopic studies in the Reykjanes (RN2, 3, 8) and Svartsengi (SG4) fluids, pyrites, and anhydrites indicate marine sulfate reduction in the deepest and hottest parts of the systems (Sakai and others, 1980; Torssander, 1986) by the reaction

$$8Fe^{2+} + 10H^+ + SO_4^{2-} = 8Fe^{3+} + 4H_2O^\circ + H_2S^\circ \qquad (10)$$

Sulfate reduction to sulfide oxidizes Fe^{2+} in primary minerals and glass to Fe^{3+}, which goes into epidote, intergrown in some samples with sulfides, and hematite. Mixing with oxidized sulfur and leached sulfur from basaltic rocks alters the $\delta^{34}S$ values, which become lighter toward the surface (Sakai and others, 1980; Torssander, 1986). Chalcopyrite occurs in most Reykjanes samples but is found only near the base of the two Svartsengi wells (fig. 5A-D). Evidence has been presented for extensive

seawater incursions in RN8 and, to a lesser extent, in RN9. The widespread distribution of chalcopyrite in the RN8 and RN9 is probably related to seawater addition into the acidic, thermal brine causing cooling, a decrease of a_{Cl^-}, and an increase in pH resulting in chalcopyrite precipitation.

Pyrite and hematite abundances show large increases relative to less permeable formations in many Svartsengi and in some Reykjanes aquifers and along the margins of intrusions. The Reykjanes and most Svartsengi reservoir waters are, however, undersaturated with hematite (fig. 18A-C). This inconsistency is probably a result of spatial/temporal variations in fluid composition, temperature, or both, caused by mixing of cooler, oxidized waters with the hot, reduced thermal waters, cooling in the upflow zone, and seawater sulfate reduction. Intergrowths of hematite and titanite are common and constrain the fluid composition to the hematite + titanite stability field in a $\log(f_{H_2S})$ versus $\log(f_{H_2})$ diagram (fig. 18A-C). Anatase is not in equilibrium at the Svartsengi reservoir temperature and $\log(a_{Ca^{2+}}/a^2_{H^+})$ ratio, and its presence in some samples may indicate lower temperatures, lower $\log(a_{Ca^{2+}}/a^2_{H^+})$, or both relative to the reservoir temperature and composition. Areas with a scarcity of hematite and pyrite may be due to any number of factors: fewer incursions of cooler, oxidized waters; lower permeabilities; or heating of waters.

Fossil Aquifers

Fossil aquifers show no circulation losses and no changes in temperature logs due to fluid loss or gain but do show mineralogical and compositional evidence for extensive water-rock reaction. There is at least one fossil aquifer within a hyaloclastite formation possibly near a small basaltic intrusion at 1448 m in SG12 (Franzson, 1983b). The large $Fe^{2+}/(Fe^{2+} + Mg)$ ratios and Cl content and small Si content in chlorite (fig. 9D), small Fe_2O_3 content in hematite, and high temperatures derived from chlorite compositions (fig. 19D) compared to less permeable formations stratigraphically above and below indicate the presence of a hot, reduced, lower-pH brine that was probably substantially evolved from seawater. Abundant calcite, pyrite, and epidote also occur near 1448 m.

MINERALOGICAL EVOLUTION

Vesicles

Chlorite compositions in chlorite-filled vesicles are depicted as a function of crystallinity (crystallite size), Ca content, and temperatures derived from chlorite compositions in figure 20. Poorly crystalline chlorites, some of which have higher Ca contents (smectite), form at lower temperatures (5°-40°C) than crystalline chlorites. The occurrence in some vesicles of an irregular boundary layer between poorly crystalline and crystalline chlorite may indicate that the lower temperature phyllosil-

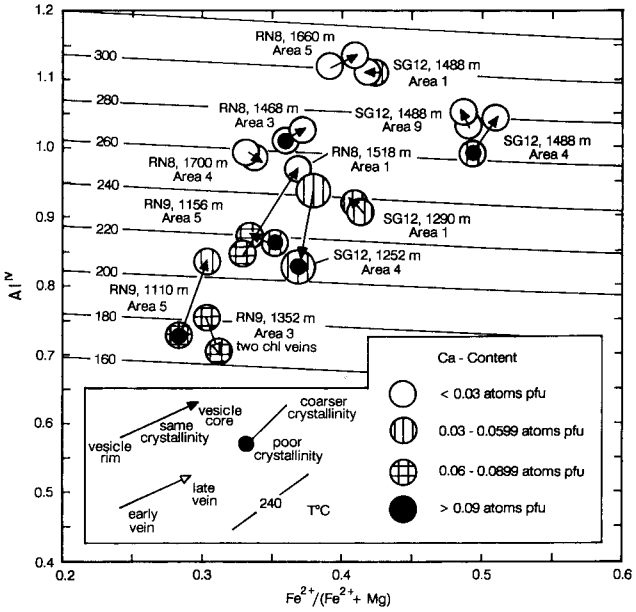

Fig. 20. Plot of tetrahedral Al (Al^{IV}) versus the $Fe^{2+}/(Fe^{2+} + Mg)$ ratio in chlorite contoured as a function of temperature. Temperatures calculated with the empirical chlorite geothermometer of Jowett (1991). Chlorite rim and core compositions in vesicles and chlorite vein compositions are also depicted as a function of crystallinity and Ca content.

icates were dissolved or were replaced by higher temperature chlorite. Many vesicle filling sequences in the lower temperature range in figure 20 record a heating trend, whereas other vesicles particularly in the higher temperature range filled under near isothermal conditions. Only one vesicle (SG12, 1252 m, area 4) recorded a cooling trend from the crystalline rim to the poorly crystalline core possibly from a later incursion of cooler water or an early pulse of hotter, thermal fluid. Chlorite-filled vesicles are more common in the Reykjanes samples, where the heating trends may be due to heating of cooler waters or late pulses of hot, reduced thermal fluids.

In some vesicles, chlorite-rich layers alternate with garnet-, quartz-, and titanite-rich layers (figs. 7B, 11A). Oscillatory deposition can form by geochemical self-organization, which forms in geochemical systems far removed from equilibrium (Ortoleva and others, 1987). Recurrent banding can be produced during hydrolytic devitrification of glass by diffusion of H^+, alkalis, and other ions followed by precipitation of secondary minerals in the alkali-depleted layer of glass. Banding growth ceases when water access is hindered by a permeability reduction (Magonthier, Petit, and Dran, 1992).

Overgrowths

The occurrence of early K-feldspar mantled by albite in RN8, SG4, and at the base of SG12 indicates a path of increasing temperature, (a_{Na^+}/a_{K^+}), or both (Browne, 1978; Giggenbach, 1984). Such a path could occur by heating of cooler waters or late pulses of hot, thermal fluids.

Several common textures in the Reykjanes and Svartsengi systems are probably produced by incursions of waters with different salinities and temperatures. Resorbed calcite, epidote, and quartz are separated from overgrowths of chlorite by an irregular, embayed boundary (fig. 10). Such textures are indicative of an increase in calcite, epidote, and quartz solubility, followed by a decrease in chlorite solubility. Calculations using the program CHILLER (Reed, 1982) reveal that seawater from Surtsey, Iceland (sample number 88-0101) is saturated with calcite at temperatures less than 246°C, undersaturated with calcite at higher temperatures, and saturated with clinochlore and undersaturated with daphnite, epidote, and quartz from 22° to 295°C. Seawater-basalt reaction at high water-rock ratios produces Ca^{2+} loss to seawater, Mg^{2+} uptake into chlorite, quartz undersaturation, and a decrease in pH (Mottl, 1983; Reed, 1983). Dissolution of calcite or epidote, which consumes H^+ and releases Ca^{2+}, followed by chlorite precipitation, which consumes Mg^{2+} and produces H^+, probably occurs during seawater incursion and seawater-basalt reaction at high seawater-rock ratios. Saline waters dissolve calcite at higher temperatures; less saline waters at lower temperatures. Calcite, epidote, and quartz undersaturation and Mg-rich chlorite saturation occur locally with large seawater-rock ratios, until the systems are restored to calcite (Svartsengi), epidote, quartz, and Fe^{2+}-Mg chlorite saturation at lower seawater-rock ratios.

Veins

Vein chlorite compositions at 1352 m in RN9 are depicted in figure 20. These compositions show a cooling trend with time with a sequence (early to late) of quartz, chlorite, titanite, chlorite. High Fe^{3+} and low Fe^{3+} prehnite occur as fracture fillings in different cuttings in a less permeable formation at 1156 m in RN9 (table 6). The high-Fe^{3+} prehnite was probably deposited between temperatures of 200° and 250°C, which is below the reservoir temperature of 295°C. The temperature of deposition of the low-Fe^{3+} prehnite is less well-constrained (fig. 7 in Rose and Bird, 1987).

Compositional Zoning

Some of the zoning in epidote is produced by plagioclase hydrolysis, where pH and $a_{Fe(OH)_3^0}/a_{Al(OH)_4^-}$ decrease during plagioclase replacement resulting in an Al-rich rim on epidote (Arnason and Bird, 1990). Other zoning trends in epidote are more sensitive to f_{H_2} variations such as Fe^{3+}-rich rims in epidote mantled by hematite. Compositional zoning in other silicates occurs only in SG12 near the margin of the Svartsengi system, where evidence presented above indicates an episodic history of

incursions of waters with different temperatures and salinities. The composition of sphalerite at 1204 m in RN9 is not in equilibrium with the reservoir fluid (fig. 16B). This sphalerite is compositionally zoned with a Fe-rich rim indicating a rim-to-core trend of increasing f_{H_2S}, decreasing f_{H_2}, decreasing temperature, or some combination. The Fe-rich sphalerite may have been undersaturated in the high temperature fluid ($> 300°C$) and was replaced by less soluble chalcopyrite.

Garnet

The presence of andradite-rich garnet at temperatures less than 350°C indicates a low CO_2- content in the fluid ($X_{CO_2} < 0.05$) (Taylor and Liou, 1978). Andradite-rich garnet could certainly be stable in the Reykjanes and Svartsengi reservoir fluid, where X_{CO_2} is less than 0.01. Most of the Reykjanes and Svartsengi garnet compositions are not in equilibrium with the reservoir fluid compositions (fig. 16A–C). Minimum stability temperatures for the analyzed garnet compositions are calculated with the thermochemical data and activity models in tables 7 and 8 by simultaneous solution of hydrolysis reactions (Ep-Grt or Prh-Grt), Fe^{3+}-Al intercrystalline exchange reactions (Ep-Grt or Prh-Grt), and the Fe^{3+}-Al intracrystalline exchange in epidote. The calculations are carried out until log $(a_{Ca^{2+}}/a^2_{H^+})$ converges to the reservoir composition. There is little variation in garnet composition in most Reykjanes and Svartsengi samples even in complex vesicle sequences of chlorite-rich and garnet-rich layers. Hence, minimum stability temperatures derived from garnet compositions are nearly constant and exceed the measured temperatures by up to 20°C (fig. 19A–D). Garnet from 1462 m in SG4, however, is in equilibrium with the reservoir fluid (fig. 16C). The minimum stability temperatures derived from garnet compositions are higher than the temperatures derived from chlorite compositions in the Reykjanes wells but overlap the temperatures derived from chlorite compositions in the Svartsengi wells. The composition of these garnets remains unchanged in response to varying temperatures, salinities, and permeabilities probably due to slow dissolution and precipitation rates.

Early Alteration

Oxygen isotope and fluid inclusion studies in RN8 and SG12, respectively, indicate that some of the quartz in RN8 and some of the anhydrite, calcite, and quartz in SG12 grew when the fluid was hotter (up to 40°C in SG12) and meteoric, possibly even glacial-melt water (Sveinbjörnsdóttir, Coleman, and Yardley, 1986; Franzson, 1990). Cooling could be due to heat source decay, cooler water incursions, or both.

CONCLUSIONS

This paper has shown how mineral and textural features can be correlated with fluid composition, processes of fluid flow and mixing, and formation permeability, and can provide insight into the important variables that control the evolution of hydrothermal systems. Abundance of fracture and vesicle fillings, alteration intensity, compositional hetero-

geneity in epidote and titanite, and physical observations such as circulation losses and temperature and pressure profiles in static wells were used to identify more permeable formations. Widespread mineral-mineral and mineral-fluid disequilibrium is due in part to mixing of drill cuttings within a depth interval and to nonequilibrium processes. Some chlorite grains, however, are in local equilibrium with the reservoir fluid compositions, even though there are rapid changes in the physico-chemical conditions of fluid-rock interaction. The short duration of chlorite-fluid reaction and the close approach to chlorite-fluid equilibrium are probably due to larger values of $(4D_h k_\varphi/v^2)$ in eq 7C, linear kinetic rate laws, or both, where D_h is the coefficient of hydrodynamic dispersion, k_φ is the reaction rate constant, and v is the fluid velocity. Most epidote, garnet, and titanite compositions are not sensitive to the rapid changes in the physico-chemical conditions probably due to smaller values of $(4D_h k_\varphi/v^2)$, non-linear kinetics, or both. Chlorite geothermometry was used to map out temperature patterns in the two hydrothermal systems and to show that some temperature gradients are maintained at a steady state during alteration. The temperature patterns derived from chlorite compositions are then used to interpret permeability variations, mixing and boiling processes, and incursions of cooler waters. There is a systematic correlation of temperatures derived from chlorite compositions with formation permeability in RN9 indicative of a more anisotropic permeability compared to the Svartsengi wells. Chlorite grains in the RN9 aquifers precipitated from a more reduced, lower pH fluid (?brine) compared to chlorite coexisting with the reservoir fluid composition. Experimental studies and computer models of seawater-basalt reaction indicate that the occurrence of chalcopyrite and lower temperature, Mg- and Si-rich chlorite grains in the Reykjanes wells and chlorite overgrowths on resorbed calcite, epidote, and quartz probably formed during seawater incursion and seawater-basalt reaction, which was more extensive in the sampled depth intervals in the Reykjanes system. Calcite (Svartsengi), epidote, Fe-Mg chlorite, and quartz saturation were restored at lower seawater-rock ratios. Many chlorite-filled vesicles record a rim-to-core heating trend due to heating of cooler waters or late pulses of hot, reduced thermal waters. Vesicles filled with recurrent layers of secondary minerals are probably formed by nonequilibrium processes involving diffusion and precipitation. Textural and compositional evidence for early alteration is largely obliterated, but studies on oxygen isotopes and fluid inclusions indicate that some mineral grains grew at an earlier stage when the fluid was hotter and meteoric, possibly even glacial-melt water. Both hydrothermal systems are cooling due to heat source decay, cooler water incursions, or both. There is no evidence from fluid compositions, fluid densities, and alteration patterns in either system for the presence of sharp, discordant interfaces between fluids with different temperatures, oxidation states, and salinities, but with the same fluid densities, which would indicate double-diffusive convection (Fournier, 1990).

The results of this study can be used to test computer models and experimental studies of seawater-basalt reaction and to understand the

thermal, chemical, hydrodynamic, and kinetics factors that influence mineral alteration in submarine hydrothermal systems. Several features in the two saline geothermal systems bear a striking resemblance to alteration patterns in submarine hydrothermal systems: the occurrence of Fe^{2+}-enriched chlorite + epidote + quartz mineralization in discharge zones; Mg-enriched chlorites in recharge zones in the oceanic crust, in ophiolite complexes, and in base metal sulfide deposits; and the superposition of alteration from incursions of waters with different chemical and thermal properties.

ACKNOWLEDGMENTS

The research conducted by SWL was supported by an Australian Research Fellowship and an Australian Research Council grant to Dr. J.L. Walshe, who participated in the initial stages of this project. Special thanks are due to the Icelandic National Energy Authority (Orkustofnun) for supplying drill cuttings and data used in this paper and for assistance and hospitality to SWL during preparation of the manuscript, which was financially supported by the Icelandic Science Fund (Vísindasjódur Íslands). Sudurnes Regional Heating (Hitaveita Sudurnesja) is thanked for permission to publish the data. Discussions of fluid chemistry with Dr. Jón Örn Bjarnason and reviews of the manuscript by Dr. Dennis Bird, Dr. John Bowman, Dr. Jón Örn Bjarnason, and Dr. Mark Reed have substantially improved the paper. We are also grateful to Mr. Grímur Björnsson, Mr. Sverrir Thórhallsson, and Dr. Kristín Vala Ragnardóttir for helpful discussions. We would also like to thank Mr. Mieczyslaw Ciszewski and Mr. Roger Heady for help with the scanning electron microscope, Mr. Terry Mernagh for aid with the laser Raman microprobe, Mr. John Vickers for impregnation/polishing of the thin sections, Mr. Nick Ware for assisting in electron microprobe analysis, and Mr. Henryk Zapasnik for administrative services.

REFERENCES

Arnason, J. G., and Bird, D. K., 1990, Formation of zoned Al-Fe epidote in hydrothermal systems: Geological Society of America Abstracts with Programs, v. 22, p. 157–158.

Arnórsson, S., 1978, Major element chemistry of the geothermal sea-water at Reykjanes and Svartsengi, Iceland: Mineralogical Magazine, v. 42, p. 209–220.

———— 1983, Chemical equilibria in Icelandic geothermal systems—implications for chemical geothermometry investigations: Geothermics, v. 12, p. 119–128.

Arnórsson, S., Grönvold, K., and Sigurdsson, S., 1978, Aquifer chemistry of four high-temperature geothermal systems in Iceland: Geochimica et Cosmochimica Acta, v. 42, p. 523–536.

Arnórsson, S., and Gunnlaugsson, E., 1985, New gas geothermometers for geothermal exploration–calibration and application: Geochimica et Cosmochimica Acta, v. 49, p. 1307–1325.

Arnórsson, S., Gunnlaugsson, E., and Svavarsson, H., 1983a, The chemistry of geothermal waters in Iceland. II Mineral equilibria and independent variables controlling water composition: Geochimica et Cosmochimica Acta, v. 47, p. 547–566.

———— 1983b, The chemistry of geothermal waters in Iceland. III. Chemical geothermometry in geothermal investigations: Geochimica et Cosmochimica Acta, v. 47, p. 567–577.

Arnórsson, S., Sigurdsson, S., and Svavarsson, H., 1982, The chemistry of geothermal waters in Iceland. I. Calculation of aqueous speciation from 0° to 370°C: Geochimica et Cosmochimica Acta, v. 46, p. 1513–1532.

Arnórsson, S., Stefánsson, V., Sigurmundsson, S. G., Gíslason, G., and Grönvold, K., 1975, Investigation in the Svartsengi geothermal field: Orkustofnun Report OS JHD 7541, 55 p. (in Icelandic).

Ball, J. W., Nordstrom, D. K., and Jenne, E. A., 1980, Additional and reused thermochemical data and computer code for WATEQ2—a computerized chemical model for trace and major element speciation and mineral equilibria of natural waters: United States Geological Survey Water-Resources Investigation Report 78-116, 114 p.

Barker, W. W., and Parks, T. C., 1986, The thermodynamic properties of pyrrhotite and pyrite: a re-evaluation: Geochimica et Cosmochimica Acta, v. 50, p. 2185–2194.

Barton, P. B. Jr., Bethke, P. M., and Roedder, E., 1977, Environment of ore deposition in the Creede Mining District, San Juan Mountains, Colorado: Part III. Progress toward interpretation of the chemistry of the ore-forming fluid in the OH vein: Economic Geology, v. 72, p. 1–24.

Bird, D. K., and Helgeson, H. C., 1980, Chemical interaction of aqueous solutions with epidote-feldspar mineral assemblages in geologic systems, I, Thermodynamic analysis of phase relations in the system CaO-FeO-Fe_2O_3-Al_2O_3-SiO_2-H_2O-CO_2: American Journal of Science, v. 280, p. 907–941.

Bjarnason, J. Ö., 1984, Reykjanes. Chemical composition of brine and steam from well 9: Orkustofnun Report OS-84049/JHD-13 B, 14 p. (in Icelandic).

———— 1985, The subprogram library STEAM. A tool for the calculation of the thermodynamic properties of water and steam: Orkustofnun Report OS-85069/JHD-09, 129 p. (in Icelandic).

———— 1987, Reykjanes. Results of chemical analysis of a few samples: Orkustofnun Report OS-87026/JHD-17 B, 15 p. (in Icelandic).

———— 1988, Svartsengi. Chemical monitoring 1980-1987: Orkustofnun Report OS-88001/JHD-01, 98 p. (in Icelandic with English abstract).

Björnsson, S., Arnórsson, S., and Tómasson, J., 1970, Exploration of the Reykjanes thermal brine area: Geothermics, Special Issue 2, p. 1640–1650.

———— 1972, Economic evaluation of Reykjanes thermal brine area, Iceland: American Association of Petroleum Geologists Bulletin, v. 56, p. 2380–2391.

Björnsson, S., Jónsson, J., Tómasson, J., Arnórsson, S., Ólafsdóttir, B., and Sigurmundsson, S. G., 1971, Reykjanes. A comprehensive report of research in the geothermal area: Orkustofnun Report February 1971, 172 p. (in Icelandic).

Björnsson, G., and Steingrímsson, B., 1991, Temperature and pressure in the Svartsengi geothermal system. Initial conditions and changes due to production: Orkustofnun Report OS-91016/JHD-04, 69 p. (in Icelandic with English summary).

Bowers, T. S., and Taylor, H. P., Jr., 1985, An integrated chemical and stable-isotope model of the origin of midocean ridge hot spring systems: Journal of Geophysical Research, v. 90, p. 12583–12606.

Browne, P. R. L., 1978, Hydrothermal alteration in active geothermal fields: Annual Review of Earth and Planetary Sciences, v. 6, p. 229–250.

Busey, R. H., and Mesmer, R. E., 1977, Ionization equilibria of silicic acid and polysilicate formation in aqueous sodium chloride solutions to 300°C: Inorganic Chemistry, v. 16, p. 2444–2450.

Edmond, J. M., 1986, Hydrothermal activity in the North Atlantic, *in* Vogt, P. R., and Tulcholke, B. E., editors, The Geology of North America, v. M., The Western North Atlantic Region: Boulder, Colorado, Geological Society of America, p. 173–188.

Ellis, A. J., 1963, Solubility of calcite in sodium chloride solutions at high temperatures: American Journal of Science, v. 261, p. 259–267.

Fournier, R. O., 1985, The behavior of silica in hydrothermal systems, *in* Berger, B. R., and Bethke, P. M., editors, Geology and Geochemistry of Epithermal Systems: El Paso, Texas, Economic Geology Publishing Company, Reviews of Economic Geology, v. 2, p. 45–61.

———— 1990, Double-diffusive convection in geothermal systems: the Salton Sea, California, geothermal system as a likely candidate: Geothermics, v. 19, p. 481–496.

Franzson, H., 1983a, The Svartsengi high-temperature field, Iceland. Subsurface geology and alteration: Geothermal Resources Council, Transactions, v. 7, p. 141–145.

———— 1983b, Svartsengi borehole SG-12. Drilling, stratigraphy, alteration, and aquifers: Orkustofnun Report OS-83003/JHD-02, 54 p. (in Icelandic).

———— 1987, The Eldvörp high-temperature area, SW-Iceland. Geothermal geology of first exploration well: New Zealand Geothermal Workshop, 9th, Proceedings, p. 179–185.

———— 1990, Svartsengi. Geological model of a high temperature system and its surroundings: Orkustofnun Report OS-90050/JHD-08, 41 p. (in Icelandic with English summary).

Franzson, H., Gudmundsson, G., Tómasson, J., and Thorsteinsson, Th., 1983, Drilling of well RnG-9, Reykjanes: Orkustofnun Report OS-83040/JHD-12 B, 30 p. (in Icelandic).

Giggenbach, W. F., 1980, Geothermal gas equilibria: Geochimica et Cosmochimica Acta, v. 44, p. 2021–2032.

———— 1981, Geothermal mineral equilibria: Geochimica et Cosmochimica Acta, v. 45, p. 393–410.

———— 1984, Mass transfer in hydrothermal alteration systems–a conceptual approach: Geochimica et Cosmochimica Acta, v. 48, p. 2693–2711.

Gíslason, S. R., and Arnórsson, S., 1990, Saturation state of natural waters in Iceland relative to primary and secondary minerals in basalts, *in* Spencer, R. J., and Chou, I.-M., editors, Fluid-Mineral Interactions: A Tribute to H. P. Eugster: San Antonio, Texas, Geochemical Society Special Publication Number 2, p. 373–393.

Gudmundsson, J. S., Hauksson, T., Thórhallsson, S., Albertsson, A., and Thorolfsson, G., 1984, Injection and tracer testing in Svartsengi field, Iceland: New Zealand Geothermal Workshop, 6th, Proceedings, p. 175–180.

Gudmundsson, J. S., Hauksson, T., and Tómasson, J., 1981, The Reykjanes geothermal field in Iceland: Subsurface exploration and well discharge characteristics, *in* Proceedings Seventh Workshop Geothermal Reservoir Enginnering, 5–17 December, 1981: Stanford, California Stanford Geothermal Program Workshop Report SGP-TR-55, p. 61–69.

Gudmundsson, J. S., and Thórhallsson, S., 1986, The Svartsengi reservoir in Iceland: Geothermics, v. 15, p. 3–15.

Gunnlaugsson, E., and Arnórsson, S., 1982, The chemistry of iron in geothermal systems in Iceland: Journal of Volcanology and Geothermal Research, v. 14, p. 281–299.

Heinrich, C. A., 1990, The chemistry of hydrothermal tin (-tungsten) ore deposition: Economic Geology, v. 85, p. 457–481.

Heinrich, C. A., and Seward, T. M., 1990, A spectrophotometric study of aqueous iron (II) chloride complexing from 25 to 200°C: Geochimica et Cosmochimica Acta, v. 54, p. 2207–2221.

Helgeson, H. C., 1992, Effects of complex formation in flowing fluids on the hydrothermal solubilities of minerals as a function of fluid pressure and temperature in the critical and supercritical regions of the system H_2O: Geochimica et Cosmochimica Acta, v. 56, p. 3191–3207.

Helgeson, H. C., Brown, T. H., Nigrini, A., and James, T. A., 1970, Calculations of mass transfer in geochemical processes involving aqueous solutions: Geochimica et Cosmochimica Acta, v. 34, p. 569–592.

Helgeson, H. C., Delany, J. M., Nesbitt, H. W., and Bird, D. K., 1978, Summary and critique of thermodynamic properties of rock-forming minerals: American Journal of Science, v. 278A, 229 p.

Helgeson, H. C., and Kirkham, D. H., 1974, Theoretical prediction of the thermodynamic behavior of aqueous electrolytes at high pressures and temperatures: I. Summary of the thermodynamic/electrostatic properties of the solvent: American Journal of Science, v. 274, p. 1089–1198.

Helgeson, H. C., Kirkham, D. H., and Flowers, G. C., 1981, Theoretical prediction of the thermodynamic behavior of aqueous electrolytes at high pressures and temperatures: IV. Calculation of activity coefficients, osmotic coefficients, and apparent molal and standard and relative partial molal properties to 600°C and 5 kb: American Journal of Science, v. 281, p. 1249–1516.

Holland, T. J. B., and Powell, R., 1985, An internally consistent thermodynamic dataset with uncertainties and correlations: data and results: Journal of Metamorphic Geology, v. 3, p. 343–370.

Jakobsson, S. P., Jónsson, J., and Shido, F., 1978, Petrology of the western Reykjanes Peninsula, Iceland: Journal of Petrology, v. 19, p. 669–705.

James, R. S., Turnock, A. C., and Fawcett, J. J., 1976, The stability and phase relations of iron chlorite below 8.5 kb pH_2O: Contributions to Mineralogy and Petrology, v. 56, p. 1–25.

Jónsson, J., 1978, Geological map of the Reykjanes Peninsula, scale 1:25000: Orkustofnun Report OS-JHD 7831, 303 p. (in Icelandic).

Jowett, E. C., 1991, Fitting iron and magnesium into the hydrothermal chlorite geothermometer: Geological Association of Canada/Mineralogical Association of Canada/Society of Economic Geologists Program with Abstracts, v. 16, p. A62.

Keenan, J. H., Keyes, F. G., Hill, P. G., and Moore, J. G., 1978, Steam tables: thermodynamic properties of water including vapor, liquid, and solid phases: New York, John Wiley & Sons, 156 p.

Kerrick, D. M., Lasaga, A. C., and Raeburn, S. P., 1991, Kinetics of heterogeneous reactions, *in* Kerrick, D. M., editor, Contact Metamorphism: Washington, D.C., Mineralogical Society of America, v. 26, p. 582–671.

Kharaka, Y. K., Gunter, W. D., Aggarwal, P. K., Perkins, E. H., and DeBraal, J. D., 1988, SOLMNEQ.88: a computer program for geochemical modeling of water-rock interactions: United States Geological Survey Water-Resources Investigations Open-File Report 88-4227, 420 p.

Kristmannsdóttir, H., 1971, Determination of clay minerals in rocks from wells on Reykjanes: Orkustofnun Report December 1971, 23 p. (in Icelandic).

———— 1975, Clay minerals formed by hydrothermal alteration of basaltic rocks in Icelandic geothermal fields: Geologiska Föreningens Förhandlingar, v. 97, p. 289–292.

———— 1976a, Hydrothermal alteration of basaltic rocks in Icelandic geothermal areas, *in* Proceedings of the Second United Nations Symposium on Development and Use of Geothermal Resources, San Francisco, 20–29 May, 1975: Washington, D.C., United States Government Printing Office, v. 1, p. 441–445.

———— 1976b, Types of clay minerals in hydrothermally altered basaltic rocks, Reykjanes, Iceland: Jökull, v. 26, p. 30–39.

———— 1979, Alteration of basaltic rocks by hydrothermal activity at 100–300°C, *in* Mortland, M. M., and Farmer, V. C., editors, International Clay Conference 1978: Amsterdam, Elsevier Scientific Publishing Company, p. 359–367.

———— 1983, Chemical evidence from Icelandic geothermal systems as compared to submarine geothermal systems, *in* Rona, P., Bostrom, K., Laubier, L., and Smith, K. L. Jr., editors, Hydrothermal Processes at Seafloor Spreading Centers: New York, Plenum Press, p. 291–320.

———— 1986, Saline groundwater and geothermal brine on the Reykjanes Peninsula, *in* Extended Abstracts WRI-5, Fifth International Symposium on Water-Rock Interaction, 8-17 August, 1986: Reykjavík, Orkustofnun, p. 337–340.

———— 1989, Types of scaling occurring by geothermal utilization in Iceland: Geothermics, v. 18, p. 183–190.

Kristmannsdóttir, H., and Tómasson, J., 1978, Zeolite zones in geothermal areas in Iceland: *in* Sand, L. B., and Mumpton, F. A., editors, Natural Zeolites: Occurrence, Properties, Use: Elmsford, New York, Pergamon Press, p. 277–284.

Lasaga, A. C., 1981a, Rate laws of chemical reactions, *in* A. C. Lasaga and R. J. Kirkpatrick, editors, Kinetics of Geochemical Processes: Washington, D.C., Mineralogical Society of America, v. 8, p. 1–68.

———— 1981b, Transition state theory, *in* A. C. Lasaga and R. J. Kirkpatrick, editors, Kinetics of Geochemical Processes: Washington, D.C., Mineralogical Society of America, v. 8, p. 135–169.

———— 1984, Chemical kinetics of water-rock interactions: Journal of Geophysical Research, v. 89, p. 4009–4025.

Lichtner, P. C., 1988, The quasi-stationary state approximation to coupled mass transport and fluid-rock interaction in a porous medium: Geochimica et Cosmochimica Acta, v. 52, p. 143–165.

Líndal, B., 1989, Solids deposition in view of geothermal applications in Reykjanes and Svartsengi, south western Iceland: Geothermics, v. 18, p. 207–216.

Lonker, S. W., Fitz Gerald J. D., Hedenquist, J. W., and Walshe, J. L., 1990, Mineral-fluid interactions in the Broadlands-Ohaaki geothermal system, New Zealand: American Journal of Science, v. 290, p. 995–1068.

Magonthier, M.-C., Petit, J.-C., and Dran, J.-C., 1992, Rhyolitic glasses as natural analogues of nuclear waste glasses: behaviour of an Icelandic glass upon natural aqueous corrosion: Applied Geochemistry, Supplemental Issue 1, p. 83–93.

Mesmer, R. E., Baes, C. F., and Sweeton, F. H., 1971, Acidity measurements at elevated temperatures, V. Boric acid equilibria: Inorganic Chemistry, v. 11, p. 537–543.

Mottl, M. J., 1983, Metabasalts, axial hot springs, and the structure of hydrothermal systems at mid-ocean ridges: Geological Society of America Bulletin, v. 94, p. 161–180.

Mottl, M. J., Holland, H. D., and Corr, R. F., 1979, Chemical exchange during hydrothermal alteration of basalt by seawater—II. Experimental results for Fe, Mn, and sulfur species: Geochimica et Cosmochimica Acta, v. 43, p. 869–884.

Ohmoto, H., and Lasaga, A. C., 1982, Kinetics of reactions between aqueous sulfates and sulfides in hydrothermal systems: Geochimica et Cosmochimica Acta, v. 46, p. 1727–1745.

Ólafsson, J., and Riley, J. P., 1978, Geochemical studies on the thermal brine from Reykjanes (Iceland): Chemical Geology, v. 21, p. 219–237.

Ortoleva, P., Merino, E., Moore, G., and Chadam, J., 1987, Geochemical self-organization I: reaction-transport feedbacks and modeling approach: American Journal of Science, v. 287, p. 979–1007.

Pálmason, G., Arnórsson, S., Fridleifsson, I. B., Kristmannsdóttir, H., Saemundsson, K., Stefánsson, V., Steingrímsson, B., and Tómasson, J., 1979, The Iceland crust: Evidence from drillhole data on structure and processes, *in* Talwani, M., Harrison, C. G., and Hayes, D. E., editors, Deep Drilling Results in the Atlantic Ocean: Ocean Crust: Washington, D.C., American Geophysical Union, Maurice Ewing Series 2, p. 43–65.

Papike, J. J., 1987, Chemistry of the rock-forming silicates: ortho, ring, and single-chain structures: Reviews of Geophysics, v. 25, p. 1483–1526.

Ragnarsdóttir, K. V., Walther, J. V., and Arnórsson, S., 1984, Description and interpretation of the composition of fluid and alteration mineralogy in the geothermal system, at Svartsengi, Iceland: Geochimica et Cosmochimica Acta, v. 48, p. 1535–1553.

Read, A. J., 1975, The first ionization constant of carbonic acid from 25 to 250°C and to 2000 bars: Journal of Solution Chemistry, v. 4, p. 53–70.

Reed, M. H., 1982, Calculation of multicomponent chemical equilibria and reaction processes in systems involving minerals, gases, and an aqueous phase: Geochimica et Cosmochimica Acta, v. 46, p. 513–528.

———— 1983, Seawater-basalt reaction and the origin of greenstones and related ore deposits: Economic Geology, v. 78, p. 466–485.

Reed, M. H., and Spycher, N., 1984, Calculation of pH and mineral equilibria in hydrothermal waters with application to geothermometry and studies of boiling and dilution: Geochimica et Cosmochimica Acta, v. 48, p. 1479–1492.

———— 1990, SOLTHERM: Data base of equilibrium constants for aqueous-mineral-gas equilibria: Eugene, Oregon, University of Oregon, 64 p.

Robie, R. A., Hemingway, B. S., and Fisher, J. R., 1978, Thermodynamic properties of minerals and related substances at 298.15 K and 1 bar (10^5 pascals) pressure and at higher temperatures: United States Geological Survey Bulletin 1452, 456 p.

Rose, N. M., and Bird, D. K., 1987, Prehnite-epidote phase relations in the Nordre Aputitêq and Kruuse Fjord layered gabbros, East Greenland: Journal of Petrology, v. 28, p. 1193–1218.

Ruaya, J. R., and Seward, T. M., 1987, The ion-pair constant and other thermodynamic properties of HCl up to 350°C: Geochimica et Cosmochimica Acta, v. 51, p. 121–130.

Saemundsson, K., 1979, Outline of the geology of Iceland: Jökull, v. 29, p. 7–28.

———— 1986, Subaerial volcanism in the western North Atlantic, *in* Vogt, P. R., and Tucholke, B. E., editors, The Geology of North America, v. M, The Western North Atlantic Region: Boulder, Colorado, Geological Society of America, p. 69–86.

Sakai, H., Gunnlaugsson, E., Tómasson, J., and Rouse, J. E., 1980, Sulfur isotope systematics in Icelandic geothermal systems and influence of seawater circulation at Reykjanes: Geochimica et Cosmochimica Acta, v. 44, p. 1223–1231.

Schneeberg, E. P., 1973, Sulfur fugacity measurements with the electrochemical cell $Ag/AgI/Ag_{2+x}S, f_{S_2}$: Economic Geology, v. 68, p. 507–517.

Scott, S. D., and Barnes, H. L., 1971, Sphalerite geothermometry and geobarometry: Economic Geology, v. 66, p. 653–669.

Seward, T. M., 1974, Determination of the first ionization constant of silicic acid from quartz solubility in borate buffer solutions: Geochimica et Cosmochimica Acta, v. 38, p. 1651–1664.

Shock, E. L., and Helgeson, H. C., 1988, Calculation of the thermodynamic and transport properties of aqueous species at high pressures and temperatures: correlation algorithms for ionic aqueous species and equation of state predictions to 5 kb and 1000°C: Geochimica et Cosmochimica Acta, v. 52, p. 2009–2036.

———— 1989, Corrections to Shock and Helgeson (1988) Geochimica et Cosmochimica Acta *52*: 2009–2036: Geochimica et Cosmochimica Acta, v. 53, p. 215.

Shock, E. L., Helgeson, H. C., and Sverjensky, D. A., 1989, Calculation of the thermodynamic and transport properties of aqueous species at high pressures and temperatures: standard partial molal properties of inorganic neutral species: Geochimica et Cosmochimica Acta, v. 53, p. 2157–2183.

Sigurdsson, F., 1985, Groundwater and hydrology on the outer Reykjanes Peninsula: Orkustofnun Report OS-85075/VOD-06, 51 p. (in Icelandic).

Steefel, C. I., and Van Cappellen, P., 1990, A new kinetic approach to modeling water-rock interaction: the role of nucleation, precursors, and Ostwald ripening: Geochimica et Cosmochimica Acta, v. 54, p. 2657–2677.

Stefánsson, V., 1983, Physical environment of hydrothermal systems in Iceland and on submerged oceanic ridges, *in* Rona, P. A., Boström, K. Laubier, L., and Smith, K. L., Jr., editors, Hydrothermal Processes at Seafloor Spreading Centers: New York, Plenum Press, p. 321–360.

Steinthorsson, S., Helgason, Ö., Madsen, M. B., Bender Koch, C., Bentzon, M. D., and Mørup, S., 1992, Maghemite in Icelandic basalts: Mineralogical Magazine, v. 56, p. 185–199.

Sveinbjörnsdóttir, A. E., ms, 1983a, Hydrothermal metamorphism and rock water interactions in the Krafla and Reykjanes geothermal fields, Iceland: Ph.D. thesis, University of East Anglia, 282 p.

———— 1983b, Water-rock interaction in Krafla and Reykjanes geothermal systems, Iceland: Journal of the Geological Society of London, v. 140, p. 549–550.

———— 1992, Composition of geothermal minerals from saline and dilute fluids–Krafla and Reykjanes, Iceland: Lithos, v. 27, p. 301–315.

Sveinbjörnsdóttir, A. E., Coleman, M. L., and Yardley, B. W. D., 1986, Origin and history of hydrothermal fluids of the Reykjanes and Krafla geothermal fields, Iceland. A stable isotope study: Contributions to Mineralogy and Petrology, v. 94, p. 99–109.

Sweeton, F. H., and Baes, C. F. Jr., 1970, The solubility of magnetite and hydrolysis of ferrous iron in aqueous solutions at elevated temperatures: Journal of Chemical Thermodynamics, v. 2, p. 479–500.

Sweeton, F. H., Mesmer, R. E., and Baes, C. F., 1974, Acidity measurements at elevated temperatures, VII, Dissociation of water: Journal of Solution Chemistry, v. 3, p. 191–214.

Taylor, B. E., and Liou, J. G., 1978, The low temperature stability of andradite in C-O-H fluids: American Mineralogist, v. 63, p. 378–393.

Tómasson, J., 1971, Analyses of drill cuttings from Reykjanes: Orkustofnun Report July 1971, 91 p. (in Icelandic).

Tómasson, J., and Kristmannsdóttir, H., 1972, High temperature alteration minerals and thermal brines, Reykjanes, Iceland: Contributions to Mineralogy and Petrology, v. 36, p. 123–134.

Torssander, P., 1986, Origin of volcanic sulfur in Iceland. A sulfur isotope study: Meddelanden från Stockholms Universitets Geologiska Institution, N:r 269, 164 p.

Toulmin, P. III, and Barton, P. B. Jr., 1964, A thermodynamic study of pyrite and pyrrhotite: Geochimica et Cosmochimica Acta, v. 28, p. 641–671.

Tremaine, P. R., and LeBlanc, J. C., 1980, The solubility of magnetite and the hydrolysis and oxidation of Fe^{2+} in water to 300°C: Journal of Solution Chemistry, v. 9, p. 415–442.

Truesdell, A. H., and Singers, W., 1971, Computer calculation of downhole chemistry in geothermal areas: New Zealand Division of Scientific and Industrial Research Report CD 2136, 145 p.

Vatnaskil Consulting Engineers, 1989, Svartsengi. Reservoir modeling of the high-temperature system: Orkustofnun Report OS-89031/JHD-05, 111 p. (in Icelandic).

Walshe, J. L., 1986, A six-component chlorite solid solution model and the conditions of chlorite formation in hydrothermal and geothermal systems: Economic Geology, v. 81, p. 681–703.

White, A. F., Chuma, N. J., and Goff, F., 1992, Mass transfer constraints on the chemical evolution of an active hydrothermal system, Valles caldera, New Mexico: Journal of Volcanology and Geothermal Research, v. 49, p. 233–253.